Pressure Drop and Two-Phase Heat Transfer of Pure Refrigerant (R1234yf) and Mixture Refrigerant (R454B, R454C) inside Microfin Tube

By

Afdhal Kurniawan Mainil

A dissertation submitted in partial fulfillment of the requirements for the degree of

Doctor of Engineering (Dr. Eng.)

In

Mechanical Engineering

Department of Science and Advanced Technology

Graduate School of Science and Engineering

Saga University

Japan

September 2022

ACKNOWLEDGEMENT

First, I would like to praise and thank Allah SWT, the Almighty, for the abundance of grace and gifts to carry out my studies.

With great respect, I express my deepest gratitude to my supervisor, Professor Akio Miyara, for all his knowledge, guidance, patience, and kindness. He inspired me to carry out my duties as a lecturer later in my country by being a good teacher and formidable researcher. I also thank my co-supervisor, Assoc Professor Keishi Kariya, for his help, advice, discussion, and valuable knowledge. Special thanks to Prof. Dr. Eng. Ir. Azridjal Aziz, M.T, IPU, Professor of Riau University, Indonesia, for introducing me to Professor Akio Miyara and his guidance.

I would like to thank Saga University for the SIPOP scholarship, which has supported the funding of my doctoral studies, and the Japan Copper Development Association, a sponsor of this research work, for the financial assistance.

I also want to thank all Miyara and Kariya laboratory members for being together. Especially the mini-channel group, Naoki Sakomoto, Hakimatul Ubudiyah, Kazuki Sadakata, I Wayan Sugita, and Hiroya Nagano for the help in discussing, constructing apparatus, and conducting experiments together and Miyoshi Katsuya as my Tutor in Japan.

I would like to thank Professor Yuichi Mitsutake and Professor Kenji Ishida as the thesis examination committee for their valuable time in judging my thesis and for helpful and constructive suggestions.

Thank you very much for my family, especially my beloved wife, Reni Anggraini, who has always encouraged me; my lovely Daughters, Syrenia Aleesya Afdhal and Sakura Aleesya Afdhal, whose unconditional love for me.

Finally, I am very grateful to my parents, H. Mainil and Hj. Zulhasnet, sisters, Ns. Yosi Suryarinilsih, M.Kep, SPMB, Fivi Zulfianilsih, S.T, M.T., Sri Darmawinilsih, Apt, M. farmklin, dr. Rezki Permata sari and my younger brother, Dr. Eng. Rahmat Iman Mainil, for their patience, moral support, and endless love in the long journey of my life. May God bless and appreciate them all.

This thesis is dedicated to my beloved Parents, H. Mainil and Hj Zulhasnet, my sisters and borther. My dear wife, Reni Anggraini, and lovely daughters, Syrenia Aleesya Afdhal and Sakura Aleesya Afdhal, whose love, encouragement, and prays have made me able to get such achievement and integrity

ABSTRACT

The world energy demand for running refrigeration and air conditioning (AC) systems has been growing fast in recent decades in line with improving society's living standards. However, this development is followed by several environmental problems, such as ozone depletion and climate change. International stakeholders have taken severe actions to suppress those drawbacks. The amendment of Kigali on the Montreal protocol in 2016 regulated the minimalization of hydrofluorocarbon (HFCs) production and consumption. Some AC manufacturers comply with the regulation by gradually substituting the high global warming potential (GWP) refrigerants with low GWP refrigerants.

The method for improving heat transfer performance and reducing the charge of refrigerants is carried out by employing the mini diameter tube instead of the large diameter. This study analyzes the pressure drop and two-phase heat transfer performance of pure refrigerant (R1234yf) and mixture refrigerant (R454B and R454C) inside a 3.5 mm OD microfin tube. The effects of the experimental parameters such as mass velocity, saturation temperature, diameter, heat flux, and vapor quality were observed using parametric analysis of the experimental results. Furthermore, experimentally obtained heat transfer coefficients are compared with previously correlations in available literature by considering the working conditions and the refrigerant used, then analyzed. Some data from previous research with different diameters were added to further analysis.

The experiment was carried out using test equipment at the Miyara and Kariya Laboratory Saga University, Japan. The microfin test tube specifications are equivalent diameter (d_e) is 3.18 mm, tube wall thickness (δ) is 0.15 mm, fin height (h) is 0.10 mm, helix angle (θ) is 10º, apex angle (γ) is 35º and number of fins is 25. The test microfin tube has a total length of 852 mm and an effective heat transfer length of 744 mm.

In the experiment of adiabatic pressure drop, The effects of mass velocity, vapor quality, saturation temperature, and diameter of microfin were analyzed. As a whole, the increase of frictional pressure drop was observed with the decrease of microfin diameter. The smaller diameter of the microfin tube leads to increased shear stress due to the increase of velocity gradients. Further, the increasing vapor shear stress and friction between liquid and vapor phase at higher mass velocity and vapor quality increase the pressure drop. Some existing correlations of microfin tubes were used to assess the two-phase frictional pressure drop of experimental data. The previous correlations cannot well predict the experimental data. A new correlation was developed and the proposed correlation expressed the experimental data of 3.5 mm OD and 2.5 mm OD very well with a mean deviation of 12.2 %, average deviation of -0.6 %, and 92.3 % of the data points are within the deviation of 30%. Validation of the new correlation with 699 data points from other researchers gave good agreement with approximately 17.6 % of mean deviation. The newly developed correlation could broadly be applied to the microfin tube diameter of 2.5 mm to 9.52 mm and the wide range of mass velocity and several refrigerants.

Experimental study of condensation heat transfer coefficient of refrigerant R1234yf inside 3.5 OD horizontal microfin tube has been carried out. The effect of mass velocity, vapor quality, tube diameter, and saturation on condensation heat transfer coefficient was investigated. The results show the heat transfer coefficient decreases as the wetness increases for mass velocities of 3.18 mm and 2.17 mm equivalent diameter of the test tube. Also, the findings show that as the microfin tube's diameter is decreased, the heat transfer coefficient increases. The increase of saturation temperatures resulted in decreased heat transfer coefficient due to the refrigerant's changing thermal properties. Four correlations of the heat transfer coefficients for microfin tubes from the literature were used to predict the heat transfer coefficient. Hirose et al., 2018 correlation has good agreement with experimental data than other correlation. However, slightly overestimated, especially at low mass velocity. Therefore, the development of a new correlation of microfin tubes is required. The new correlation for heat transfer condensation was developed. The proposed correlation agrees well with the measured data with average deviation and mean absolute deviation is 0.19% and 13.34%, respectively and 90.74% data points are within 30%.

The presents study also experimental flow boiling heat transfer coefficients of R1234yf inside a microfin tube with equivalent inner diameter of 3.18 mm. Generally,

the heat transfer coefficient rises slightly with vapor quality at low mass velocity. It rises with vapor quality at high mass velocity, reaches a peak, and drops at around 0.9 of vapor quality due to dry-out phenomena. In the low vapor quality region, the effect of mass velocity is not so remarkable, and the nucleate boiling dominates the heat transfer. On the other hand, forced convection is present and dominant in the heat transfer process in the high-quality region. The effect of heat flux was observed in the mass velocity 200 kg $m^{-2}s^{-1}$ and the impacts of heat flux are readily visible: nucleate boiling is the most crucial heat transfer mechanism.

This study also investigated the two-phase flow condensation and boiling heat transfer as well as adiabatic pressure drop of Mixture refrigerant R454B and R454C inside a 3.5 mm OD microfin tube. Experimental results were then compared with pure refrigerant. The frictional pressure drop of R454B is the lowest for each mass velocity, and R1234yf is the highest using the same microfin tube, where the results show that R1234yf has a frictional pressure drop value of 1.05 to 2.17 times greater than R454B and 1.06 to 1.32 times greater than 454C. A comparison between R454C and R454B shows that R454C is 1.01 to 1.64 times greater than R454B in the mass velocity range of 50 kg $m^{-2}s^{-1}$ to 300 kg $m^{-2}s^{-1}$. This phenomenon is caused by the thermo-physical difference between the three refrigerants.

Condensation and Boiling HTC's R454B is slightly larger than R1234yf, increasing 1.1 to 1.5 times enhancement in all mass velocities from 50 to 200 $kgm^{-2}s^{-1}$. With a sizeable R32 composition of about 68.9% in R454B, HTC's increase is relatively small. The condition is because of the degradation of HTC due to mass transfer resistance due to the presence of a temperature glide of zeotropic mixture refrigerant. Condensation and boiling HTC’s R454C is lower than R1234yf for all mass velocities with 1.1 to 1.7 degradation from R1234yf. The Degradation of heat transfer coefficient from this zeotropic mixture refrigerant due to mass transfer resistance during the condensation process due to the presence of a temperature glide of zeotropic mixture refrigerant.

Table of Contents

List of Figures

List of Tables

Nomenclature

A	Cross sectional area [m^2]
A_{fa}	Actual flow area [m^2]
A_{fn}	nominal flow area [m^2]
AD	average deviation [%]
Bo	Bond number [-]
C	Chisholm paremeter [-]
d	Diameter [m]
f	Friction factor [-]
Fr	Froude number [-]
G	Mass velocity [kg m^{-2} s^{-1}]
g	Gravitational acceleration [m s^{-2}]
h	Enthalpy [j kg^{-1}]
h_f	fin height [m]
m	flow rate [kg s^{-1}]
MD	Mean deviation [%]
MT	Microfin tube
N_f	Number of fin [-]
OD	outside diameter [mm]
P	Pressure [Pa]
ΔP	Pressure drop [Pa]
Re	Reynolds number [-]
T	Temperature [^oC]

v specific volume [m^3 kg^{-1}]

Δv specific volume difference between saturated vapor and saturated liquid [$m^3 kg^{-1}$]

w_t Tube wall thickness [m]

x Vapor quality [-]

Δz Measuring length [m]

Greek symbols

γ Apex angle [^{o}]

ρ Density [kg m^{-3}]

θ Helix angle [^{o}]

σ Surface tension [N m^{-1}]

λ Thermal conductivity [W $m^{-1}K^{-1}$]

Φ Two-phase pressure drop multiplier [-]

μ Viscosity [Pa-s]

ξ Void fraction [-]

δ Area ratio [-]

X_{tt} Lochart-Martinelli parameter [-]

Subcripts

c abrupt contraction

e abtupt expansion

exp experimental

eq equivalent

i inner

in inlet

l liquid

o outer

pred	predicted	
r	reduced pressure	
R	refrigerant	
sat	saturation	
T	total	
A	Cross sectional are	(m^2)
d	Diameter	(m)
G	Mass velocity	(kg m^{-2} s^{-1})
h	Enthalpy	(J kg^{-1})
m	Mass flow rate	(kg s^{-1})
Q	Heat transfer rate	(W)
T	Temperature	(^oC)
x	Vapor quality	(-)
u	Velocity	(m s^{-1})
z	Effective heat transfer length	(m)

Greek symbols

α	Heat transfer coefficient	(W m^{-2} K^{-1})
λ	Thermal conductivity	(W m^{-1} K^{-1})
ξ	Void fraction	(-)
η	Area expansion ratio	
θ	Helix angle	(deg.)
δ	Tube wall thickness	
γ	Apex angle (deg.)	

Subscripts

cal	Calculated value
eq	Equivalent
exp	Experiment
i	Inner
l	Liquid
o	Ourter

r	Refrigerant
v	Vapor
wall	Wall
wat	Water

CHAPTER

1

INTRODUCTION

1.1 Background

Presently, the world is encountering a serious problem related to the harmful effect of global warming. Air conditioning and refrigeration system is believed as one of the contributors of emission gas which have been impacted to the depleting of ozone and global warming. Therefore serious action has been considered to protect the environment from refrigeration's side effects.

International stakeholders tackled the problem by the Montreal protocol in 1987. The protocol decided the phased out of CFC refrigerants due to the high Ozone Depleting Potential (ODP). The Montreal protocol has effectively eliminated chlorofluorocarbon (CFCs) and accelerated the substitution of hydroflourocarbons (HFCs) refrigerants. Hydroflourocarbons (HFCs) have zero ozone depletion potential (ODP). However, some of them have high global warming potential (GWP) (Bolaji and Huan, 2013). This situation classifies some refrigerants such as R134a, R32 and R410 A which are currently widely used in refrigeration system as green-house gasses. Therefore, Kyoto Protocol (United Nations Framework Convention on Climate Change 1997/1998) Implemented an amendment in Kigali in October 2016 to accelerate the reduction of hydrofluorocarbon (HFCs) production and consumption (UNEP, 2016).

Concerning that, the natural refrigerants (hydrocarbon compounds HCs) and hydroflouro-olefins (HFOs) would be used as new refrigerants. However, the majority of hydrocarbon refrigerants are not environmentally feasible due to their flammability and toxicity. Currently, hydroflouro-olefins (HFOs) such as R1234ze(E) (GWP = 6), R1234yf (GWP = 4) and so like have been gaining more attention as potential replacements of HFCs due to their eco-friendly properties, such as zero ODP, low GWP, non- toxic, and midly flammability (Bellair and Hood, 2019).

Currently, R410A and R32 are widely used in residential AC and R134a is common used in automobile AC. However, the recent trend encouraged the search for lower GWP refrigerants. A comprehensive investigation of possible future refrigerants has been conducted by a research study (McLinden et al., 2014). They recommended some refrigerants such as R1234ze(E) and, R1234yf. The R1234yf has zero ODP and low GWP with thermo-physical properties close to R134a which is widely used in mobile AC. Therefore, the direct replacement of R1234yf to R134a is possible (Belman-Flores et al., 2017; Lee and Jung, 2012; Qi, 2015, 2013). Furthermore, the use of some mixture refrigerants (HFCs/HFOs) also has advantages, especially in order to mitigate the high GWP refrigerants such as R-410A, as the requirements by international regulation. One regulation such as Ban on the marketing of equipment according to the Regulation EU No. 517/2014 (Heredia-Aricapa et al., 2020). R-410A is one of the most widely used refrigerants for air conditioning applications in worldwide (Zhao et al., 2015). It has a high GWP (2088 (IPCC 2007, 2007)); therefore, it will be phased out shortly by replacing it with the low GWP refrigerant (Mota-Babiloni et al., 2017). One of promising candidate to replace R410 is R454B with a GWP of 466 (IPCC 2007, 2007) (78 % reduction from R410A) with properties nearly identical to R410A (Devecioğlu, 2017; Shen et al., 2022; Tran et al., 2021).

It is important to evaluate the pressure drop and heat transfer characteristics including heat transfer coefficient in the two-phase flow of boiling and condensation because the experimental indicator is crucial for the optimization of refrigeration cycle components (Greco, 2008). The heat transfer and pressure drop behavior of various future refrigerants has been carried out by many studies (Bashar et al., 2018; Bashar et al., 2020a; Bashar et al., 2020b; Diani et al., 2018; Hirose et al., 2018; Ichinose and Inoue, 2011). However, the evaluation of heat transfer characteristics of various refrigerants should consider the enhancement of heat transfer coefficient and efficiency of the system. It should also deal with the properties of refrigerants, in which some refrigerants were still classified as mildly flammable refrigerants. In the application of a heat exchanger that use a tube, one potential option is to use a small diameter microfin tube to reduce the amount of refrigerant charge.

Many experimental studies have reported the enhancement of the heat transfer performance by employing the micro/mini-scale diameter. Besides can reduce the charge of refrigerants, the small diameter tubes is also essential for system efficiency purposes. The use of small tubes leads to higher pressure drop. However, this problem

can be alleviated by modulating the design of tubes for example by using more parallel tubes and shorter tubes. In small diameter tubes the buoyancy effect, surface tension, shear stress, and flow regime are different from that of large diameter tubes. Moreover, the application of small diameter tubes for mobile AC, residential AC, and organic Rankine cycle, encourages the researcher to find the proper refrigerants with good thermal properties appropriated in small diameter tubes.

In this current study, experimental data on pressure drop and heat transfer in two-phase flow in microfin tubes (do = 3.5 mm) for pure refrigerant, R1234yf and mixture refrigerants, R454 B and R454C are presented. Moreover, two-phase frictional pressure drop and condesantion heat transfer correlations are developed based on the experimental data.

1.2 Literature Review

1.2.1 Classification of tube size

In two-phase flow heat transfer and pressure drop, the tube size or geometry plays an important role. Many experimental studies have reported that the enhancement of heat transfer could be achieved in small diameter tubes. However, the downsized diameter leads to an increase in the pressure drop of the systems. Moreover, small diameter tube uses less refrigerant charge, therefore it provides lighter weight that can help lower costs related to the overall packaging of a refrigeration or air conditioning system. The demand of higher energy efficiencies in residential and commercial refrigeration and air conditioning encourages the downsized of the tube size diameter.

The classification of the tube sized has been discussed based on different parameter. A most widely used classification is proposed by (Kandlikar, 2002) and (Kandlikar and Grande, 2003) according to which: Conventional or macro channels: $dh > 3$ mm, Minichannels: $3\text{mm} \geq dh > 200$ µm, Microchannels: $200\ \mu\text{m} \geq dh > 10\ \mu\text{m}$, Transitional channels: $10\ \mu\text{m} \geq dh > 1\ \mu\text{m}$, Molecular Nanochannels: $0.1\ \mu\text{m} \geq dh$. This classification was developed maninly based on the flow of gases. However, it can also be applied for two-phase flow of boiling and condensation.

According to (Mehendale et al., 2000) the classification of small channel dimensions in terms of hydraulic diameter can be classified as: Conventional or macro channels: $dh > 6$ mm, Compact passage channels: dh = 1-6 mm, Meso channels: dh

= 0.1-1 mm, Microchannels: dh = 1-100 μm. This classification is based simply on the dimensions of the channels. Although, this classification has some acceptance.

(Cheng and Mewes, 2006) explained the criteria based on an analysis considering the magnitudes of gravity and surface tension effects : Convensional or macrochannels: Bo > 3.0 (Surface tension is small in compared to gravitational force). Minichannels: 0.05 < Bo < 3.0 (surface tension effect becomes dominant and gravitational effect is small), Microchannel: Bo < 0.05 (gravity effect is neglegible)

(Ghiaasiaan, 2008) has given another classification as: Conventional channels: $dh \geq 3$ mm, Minichannels: 100 μmm $\leq dh \leq$ 1000 μm, Microchannels: 10 μm $\leq dh \leq$ 100 μm.

1.2.2 Microfin tube

The enhancement of heat exchanger performance has become popular presently which can improve the thermal efficiency and the economics of the design operation. There are two groups of the heat exchanger improvement technique, first, the active which requires external forces such as electric field, acoustic or surface vibration and second, the passive technique require special surface geometries such as rough surface or extended surface, etc.

(Bejan and Kraus, 2003) have been identified several descriptions of enhancement techniques which are : (1) Passive enhancement techniques: Treated surfaces, Rough surfaces, Extended surfaces, Displaced enhancement devices, Swirl flow devices, Coiled tubes, Surface tension devices, Additives for liquids, Additives for gases (2) Active enhancement techniques: Mechanical aids, Surface vibration. Among the heat transfer improvement techniques aforementioned, extended or finned surface are the most widely used technique (Afroz, 2008). Microfin tubes are the best example of extended surface enhancement techniques that have recently been used intensively because of their high condensation heat transfer performance and low pressure drop.

Fig 1.1 shows the microfin tube which has microfin on internal wall surface. The microfin tube was introduced firstly by (Fujie et al., 1977) of Hitachi Cable Ltd. (Kim, 2016) explained an empowered of heat transfer coefficient with relatively low pressure drop increases the microfin tubes in commercial refrigeration and air conditioning applications since the 1980s. Microfins are one of the most efficient and common heat transfer enhancement mechanism for the heat exchangers due to their

superior heat transfer performance improvement both in two-phase and single-phase applications. (Shinohara and Tobe, 1985 and Yasuda et al., 1990) developed an improved version for 9.5mm outer diameter tube. From middle of 1990s, herringbone shaped microfin tube and cross-grooved microfin tubes were developed and it was reported that their heat transfer coefficients were much higher than that of the conventional helical microfin tube.

A Further research achieved an optimum microfin configurations for different diameter tubes, as described by (Webb and Kim, 2004). (Dalkilic and Wongwises, 2009) reported that the increase of the heat transfer performance of tubes is due to the presence of microfin on the internal wall surface of horizontal tubes. The heat transfer enhancements are mainly caused by the increase in the surface heat transfer area, surface tension effect on the condensate drainage and induced turbulence by microfin. The refrigeration, air conditioning and heat pumps industry is developing very compact machinery, and this requires the use of heat exchangers with enhanced surfaces. Air cooled condensers for refrigeration and heat pumps are manufactured with enhanced surfaces both on the external and on the refrigerant side (Cavallini et al., 2000).

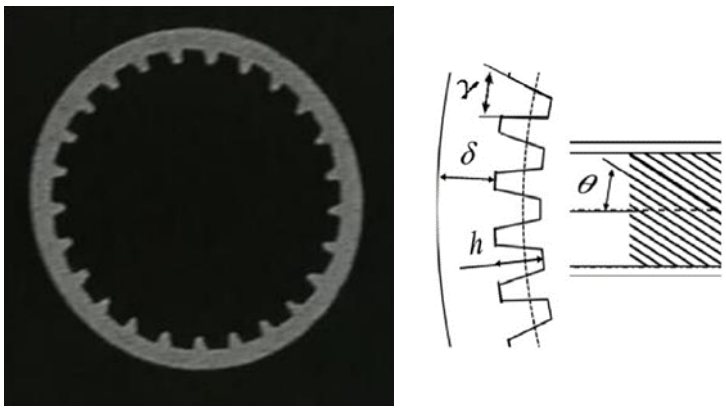

Figure 1.1 Schematic view and geometrical parameter of microfin tubes

1.2.3 Factors that enhanced the heat transfer in microfin tubes

The process of heat transfer in microfin tubes is responsible for several aspects. Firstly, the fins in microfin tube provide larger heat transfer area over that of smooth tube of the same cross-sectional flow area. The fins add roughly 50% more surface area per tube length (Bejan and Kraus, 2003). Secondly, as shown in **Fig. 1.2**, a thin liquid

film is formed at the fin tips in the case of fluid with high vapor qualities when flows through a microfin tube. The thin film will enhanced the intensity of heat transfer. The thinner this film, the better of heat transfer. Thirdly, the increase of heat transfer due to the rifling of fins trough the tube axis as the effect of swirl. Fourthly, the mixing of the flow at the wall due to the roughness of the wall, therefore the heat transfer will increase.

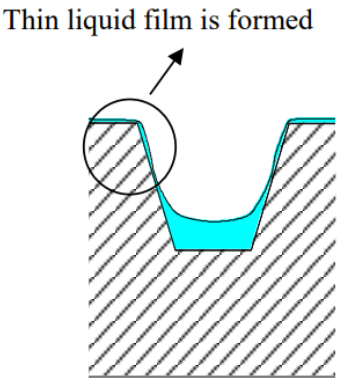

Figure 1.2 Liquid film form in microfin

Fig 1.3 illustrates the temperature and velocity profile of fluid in microfin tube during condensation process. When the fin depth is larger than the liquid film thickness, the higher heat transfer will be existed.

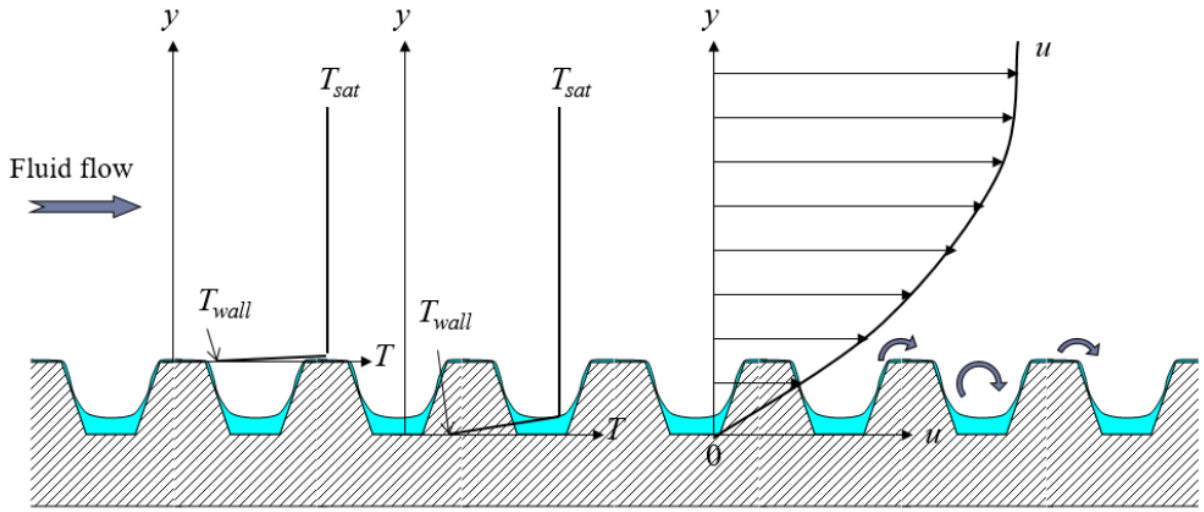

Figure 1.3 Velocity and temperature profile of fluid flow in microfin tube (Photograph courtesy of Professor Akio Miyara, Saga University)

1.2.4 History of Refrigerant

Refrigerants are the working fluid of the vapor compression cycle which transferred the heat from lower to higher temperature. The history of refrigerants are divided into four generations as shown in **Fig. 1.4**. First generation refrigerants were flammable, toxic, and highly reactive. For example NH_3, SO_2, and CO_2.

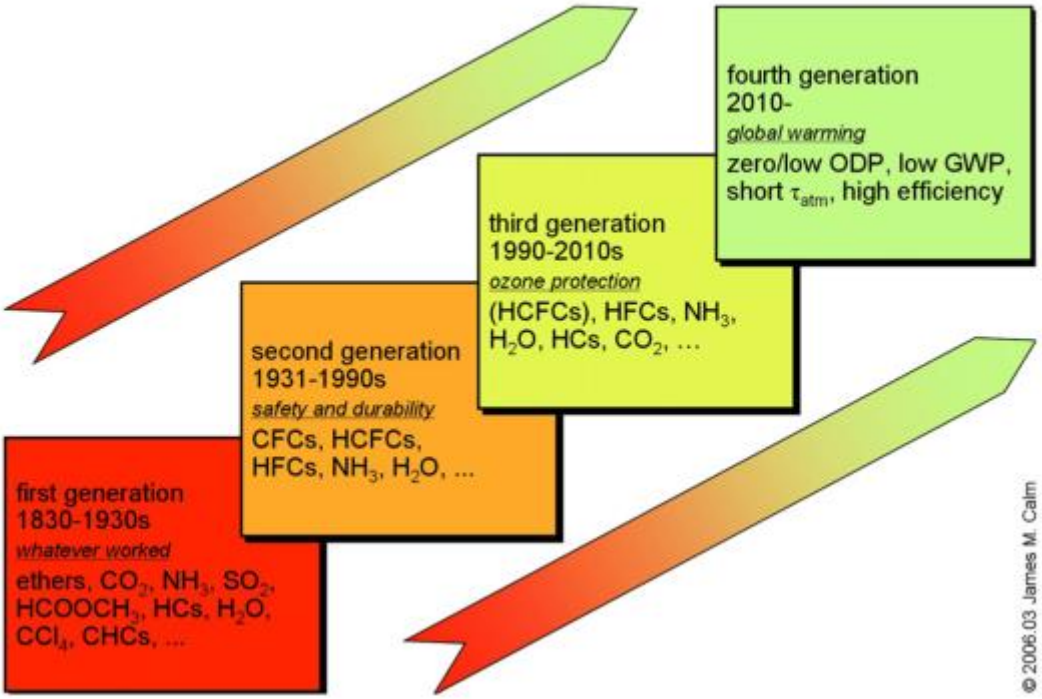

Fig 1.4 Refrigerant Progression (Calm, 2008)

From 1931-1990s, the second generation of refrigerants were available commerciallly. The production of R12 was started in 1931 followed by R-11 in 1932(Calm, 2008). However, due to the harmful effect of released CFC refrigerants to the depletion of protective ozone, the use of the third generation refrigerants with focus on stratospheric ozone protection was accelerated.

Montreal protocol resulted from Vienna Convention forced the phassed out of azone depleting substances (ODSs). HCFC was used as alternatives for CFCs in 1990s and 2000s. Montreal protocol 1987 required the phassed out of CFC refrigerants by 1996 for developed country and non developed country will do so by 2010. Moreover, the service and used of

existing equipment employing CFC refrigerants are allowed until otherwise retired. The most widely used HCFC refrigerants is R22. HCFCs such as R 22 are just marginally better than CFCs as they contain chlorine, which is harmful for the environment. To remove chlorine from the refrigerant, manufacturers created another set of refrigerants called HFCs. This refrigerants are better than HCFC as they do not deplete the ozon layer and they have better energy efficiency, eventhough they still have potential of global warming. The most common HFC used in AC is R410A. A few more HFCs are commonly used, for example R-32 in AC and R134a in refrigerators.

Hydroflourocarbons (HFCs) have zero ozone depletion potential (ODP). However, some of them have high global warming potential (GWP) (Bolaji and Huan, 2013). This situation classifies some refrigerants such as R32, R134a, and R410 A which are currently widely used in refrigeration system as green house gasses. Therefore, Kyoto Protocol (United Nations Framework Convention on Climate Change 1997/1998) Implemented an amendment in Kigali in October 2016 to accelerate the reduction of hydrofluorocarbon (HFCs) production and consumption (UNEP, 2016). Natural refrigerant such as R290 (the most natural refrigerants available in the market) comes into consideration as it is completely halogen free, has zero ODP and low GWP. However it is highly flammable.

Concerning that, the forth generation refrigerants promotes hydroflouro-olefins (HFOs) as new generation refrigerants. However, majority of hydrocarbon refrigerants are not environmentally feasible due to the flammability and toxicity. Currently, hydroflouro-olefins (HFOs) such as R1234ze(E) (GWP = 6), R1234yf (GWP = 4) and so like have been gaining more attention as potential replacements of HFCs due to their eco-friendly properties, such as zero ODP, low GWP, non- toxic, and low flammability (Bellair and Hood, 2019). Some comprehensive investigation of possible future refrigerants has been conducted by a research study (McLinden et al., 2014). They recommended some refrigerants such as R1234ze(E) and, R1234yf. The R1234yf has zero ODP and low GWP with thermophysical properties close to R134a which is widely used in mobile AC.

Therefore, the direct replacement of R1234yf to R134a is possible (Belman-Flores et al., 2017; Lee and Jung, 2012; Qi, 2015, 2013). Furthermore, the use of some mixture refrigerants (HFCs/HFOs) also have adventages especiellay in order to mitigate the high GWP refrigerants such as R-410A, as the requirements by international regulation. One regulation such as Ban on the marketing of equipment according to the

Regulation EU No. 517/2014 (Heredia-Aricapa et al., 2020). R-410A is one of the most widely used refrigerants for air conditioning applications in worldwide (Zhao et al., 2015). It has a high GWP (2088(IPCC 2007, 2007)); therefore, it will be phased out shortly by replacing it with the low GWP refrigerant (Mota-Babiloni et al., 2017). One of promising candidate to replace R410 is R454B with a GWP of 466 (IPCC 2007, 2007) (78 percent reduction from R410A) with properties nearly identical to R410A(Devecioğlu, 2017; Shen et al., 2022; Tran et al., 2021). Charachteristics of some refrigerants are shown in Table 1.1.

Table 1.1 Refrigerants characteristics used in the refrigeration and air conditioning system

Refrigerant	Chemical formula	Category	ODP	GWP	Safety*	Pressure (Mpa) at 30 °C
R404A	(R125/R143a/R134a)	HFC	0	3943	A1	1.42
R410A	(R32/R125)	HFC	0	1924	A1	1.88
R134a	CH_2FCF_3	HFC	0	1430	A1	0.77
R32	CH_2F_2	HFC	0	677	A2L	1.92
R1234yf	$CF_3CF=CH_2$	HFO	0	4	A2L	0.78
R1234ze(E)	$CH_3CH=CHF$	HFO	0	<1	A2L	0.57
R1234zd€	$CF_3CH=CC1H$	HFO	0	1	A1	0.15
R717	NH_3	Natural refrigerants	0	<1	B2L	1.16
R290	C_3H_8	Natural refrigerants	0	≤20	A3	1.07
R744	CO_2	Natural refrigerants	0	1	A1	7.21
*Nopte: A: less toxic: non flammable, 2L: very slightly flammable, 2: Slightly flammable, 3: highly flammable (Safety level are measured based on ASHRAE 31: Refrigeration safety cklassification standards)						

1.3 Objective of This Study

The objective of this study is to evaluate the pressure drop and two-phase heat transfer characteristics of pure and mixture refrigerants in small tube during condensating and boiling. The main objectives of this research are as follows:

1. To investigate the effect of parameters as mass velocity, vapor quality, saturation temperature and tube diameter on two-phase frictional pressure drop in 3.5 mm OD microfin tubes with R1234yf refrigerant and compare with available correlation in open literature.

2. To develop a new frictional pressure drop correlation for microfin tube based on the experimental data and previous data and validate it with the available data from the open literature.
3. To investigate the effects of parameters such as mass velocity, vapor quality, saturation temperature and tube diameter on condensation heat transfer coefficients in microfin tubes with with R1234yf refrigerants and compare with wellknown correlation
4. To develop a new condensation heat transfer correlation for microfin tube based on the present experimental data validate it with the available data from the open literature.
5. To investigate the effects of parameters such as mass velocity, vapor quality, heat flux on evaporation heat transfer coefficients in microfin tubes with with R1234yf refrigerants and compare with existing correlation.
6. To investigate the effect of parameters such as mass velocity, vapor quality, heat flux on two-phase frictional pressure drop, condensation heat transfer, and evaporation heat transfer in microfin tubes with mixtured refrigerants (R454B and R454C).

1.4 Thesis Outline

This thesis is organized as follows.

Chapter 1: Introduction: This chapter presents the background of the study, literature reviews including introduction on microfin tube, and the history of refrigerant progression is also presented.

Chapter 2: Experimental apparatus: This chapter describes the experimental apparatus used in this study and procedure are reported.

Chapter 3: Experimental Investigation and development general correlation for frictional pressure drop of two-phase flow inside microfin tube: This chapter presents the literature review of two-phase pressure drop in small diameter tubes. The data reduction method is presented. The experimental results of two-phase frictional pressure drop during adiabatic flow in 3.5 mm OD microfin tube with R1234yf are reported. The experimental values are compared with existing correlations obtained.

The proposed general two-phase frictional pressure drop correlation is developed. New correlation is also validated with available data from open literature and their applicable range are also reported.

Chapter 4: Experimental investigation on Condensation heat transfer of Refrigerant R1234yf in 3.5 mm OD horizontal microfin tubes and development correlation: This chapter **c**ontains the literature review of condensation heat transfer in small diameter tubes. The data reduction method is described. The experimental results of condensation heat transfer in microfin tube with R1234yf are reported. The experimental results are compared with predicted values obtained using previous condensation correlations. New correlation was proposed and validated with the available data from open literature.

Chapter 5: Experimental investigation on flow boiling heat transfer of R1234yf inside horizontal microfin tubes: This chapter presents the literature review of boiling heat transfer in small diameter tube. The data reduction method is described. The experimental results of boiling heat transfer in 3.5 mm OD microfin tube with R1234yf are reported. The experimental results are compared with predicted values obtained using existing boiling correlations.

Chapter 6: Experimental study on Pressure drop and two-phase heta transfer of mixture refrigerant (R454B and R454c) inside microfin tubes: This chapter presents the literature review of mixture refrigerant. The data reduction method is described. The experimental results of pressure drop, condensation, and boiling heat transfer in microfin tube with mixture refrigerant (R 454B and R454C) are reported.

Chapter 7: Conclusions and recommendation. Conclusions of this research work and recommendations for future studies are summarized in this chapter.

Reference

Afroz, 2008. Prediction Method of Single-phase and Two-phase Pressure Drop inside Microfin Tubes Hasan Mohammad Mostofa Afroz Prediction Method of Single-phase and Two-phase Pressure Drop inside Microfin Tubes.

Bashar, M.K., Nakamura, K., Kariya, K., Miyara, A., 2020a. Condensation heat transfer of R1234yf in a small diameter smooth and microfin tube and development of correlation. Int. J. Refrig. 120, 331–339. https://doi.org/10.1016/j.ijrefrig.2020.09.002

Bashar, M.K., Nakamura, K., Kariya, K., Miyara, A., 2020b. Development of a correlation for pressure drop of two-phase flow inside horizontal small diameter smooth and microfin tubes. Int. J. Refrig. 119, 80–91. https://doi.org/10.1016/j.ijrefrig.2020.08.013

Bashar, M.K., Nakamura, K., Kariya, K., Miyara, A., 2018. Experimental study of condensation heat transfer and pressure drop inside a small diameter microfin and smooth tube at low mass flux condition. Appl. Sci. 8. https://doi.org/10.3390/app8112146

Bejan, A., Kraus, A.D., 2003. Heat Transfer Handbook- Heat Exchangers, Heat Transfer Handbook.

Bellair, R.J., Hood, L., 2019. ur na. Process Saf. Environ. Prot. https://doi.org/10.1016/j.psep.2019.09.033

Belman-Flores, J.M., Rodríguez-Muñoz, A.P., Pérez-Reguera, C.G., Mota-Babiloni, A., 2017. Experimental study of R1234yf as a drop-in replacement for R134a in a domestic refrigerator. Int. J. Refrig. 81, 1–11. https://doi.org/10.1016/j.ijrefrig.2017.05.003

Bolaji, B.O., Huan, Z., 2013. Ozone depletion and global warming: Case for the use of natural refrigerant - A review. Renew. Sustain. Energy Rev. 18, 49–54. https://doi.org/10.1016/j.rser.2012.10.008

Calm, J.M., 2008. The next generation of refrigerants - Historical review, considerations, and outlook. Int. J. Refrig. 31, 1123–1133. https://doi.org/10.1016/j.ijrefrig.2008.01.013

Cavallini, A., Del Col, D., Doretti, L., Longo, G.A., Rossetto, L., 2000. Heat transfer and pressure drop during condensation of refrigerants inside horizontal enhanced tubes. Int. J. Refrig. 23, 4–25. https://doi.org/10.1016/S0140-7007(99)00032-8

Cheng, L., Mewes, D., 2006. Review of two-phase flow and flow boiling of mixtures in small and mini channels. Int. J. Multiph. Flow 32, 183–207. https://doi.org/10.1016/j.ijmultiphaseflow.2005.10.001

Dalkilic, A.S., Wongwises, S., 2009. Intensive literature review of condensation inside smooth and enhanced tubes. Int. J. Heat Mass Transf. 52, 3409–3426.

https://doi.org/10.1016/j.ijheatmasstransfer.2009.01.011

Devecioğlu, A.G., 2017. Seasonal performance assessment of refrigerants with low GWP as substitutes for R410A in heat pump air conditioning devices. Appl. Therm. Eng. 125, 401–411. https://doi.org/10.1016/j.applthermaleng.2017.07.034

Diani, A., Campanale, M., Cavallini, A., Rossetto, L., 2018. Low GWP refrigerants condensation inside a 2.4 mm ID microfin tube. Int. J. Refrig. 86, 312–321. https://doi.org/10.1016/j.ijrefrig.2017.11.011

Fujie, K., Itoh, M., Kimura, H., Application, F., Data, P., 1977. United States Patent [19].

Ghiaasiaan, 2008. Two-Phase Flow, Boiling, and Condensation IN CONVENTIONAL AND MINIATURE SYSTEMS. Production 2.

Greco, A., 2008. Convective boiling of pure and mixed refrigerants: An experimental study of the major parameters affecting heat transfer. Int. J. Heat Mass Transf. 51, 896–909. https://doi.org/10.1016/j.ijheatmasstransfer.2007.11.002

Heredia-Aricapa, Y., Belman-Flores, J.M., Mota-Babiloni, A., Serrano-Arellano, J., García-Pabón, J.J., 2020. Overview of low GWP mixtures for the replacement of HFC refrigerants: R134a, R404A and R410A. Int. J. Refrig. 111, 113–123. https://doi.org/10.1016/j.ijrefrig.2019.11.012

Hirose, M., Ichinose, J., Inoue, N., 2018. Development of the general correlation for condensation heat transfer and pressure drop inside horizontal 4 mm small-diameter smooth and microfin tubes. Int. J. Refrig. 90, 238–248. https://doi.org/10.1016/j.ijrefrig.2018.04.014

Ichinose, J., Inoue, N., 2011. The condensation heat transfer and pressure drop of R410A and R32 inside horizontal small-diameter tubes – 2nd report: empirical correlation for condensation heat transfer and pressure drop. Trans. JSRAE 28, 479–490.

IPCC 2007, 2007. Climate Change 2007: The Physical Science Basis. Contribution of Working Group I to the Fourth Assessment Report of the Intergovernmental Panel on Climate Change. Summary for Policymakers. (Edited by Solomon, S. DQin MManning ZChen MMarquis KAveryt MHL MS. p. 996.

Kandlikar, S.G., 2002. Two-phase flow patterns, pressure drop, and heat transfer during boiling in minichannel flow passages of compact evaporators. Heat Transf. Eng. 23, 5–23. https://doi.org/10.1080/014576302753249570

Kandlikar, S.G., Grande, W.J., 2003. Evolution of microchannel flow passages-

thermohydraulic performance and fabrication technology. Heat Transf. Eng. 24, 3–17. https://doi.org/10.1080/01457630304040

Kim, N.H., 2016. Condensation heat transfer and pressure drop of R-410A in a 7.0 mm O.D. microfin tube at low mass fluxes. Heat Mass Transf. und Stoffuebertragung 52, 2833–2847. https://doi.org/10.1007/s00231-016-1789-2

Lee, Y., Jung, D., 2012. A brief performance comparison of R1234yf and R134a in a bench tester for automobile applications. Appl. Therm. Eng. 35, 240–242. https://doi.org/10.1016/j.applthermaleng.2011.09.004

McLinden, M.O., Kazakov, A.F., Steven Brown, J., Domanski, P.A., 2014. A thermodynamic analysis of refrigerants: Possibilities and tradeoffs for Low-GWP refrigerants. Int. J. Refrig. 38, 80–92. https://doi.org/10.1016/j.ijrefrig.2013.09.032

Mehendale, S.S., Jacobi, A.M., Shah, R.K., 2000. Fluid flow and heat transfer at micro- and meso-scales with application to heat exchanger design. Appl. Mech. Rev. 53, 175–193. https://doi.org/10.1115/1.3097347

Mota-Babiloni, A., Makhnatch, P., Khodabandeh, R., 2017. Recent investigations in HFCs substitution with lower GWP synthetic alternatives: Focus on energetic performance and environmental impact Adrián. Int. J. Refrig. 82, 288–301. https://doi.org/10.1016/j.ijrefrig.2017.06.026

Qi, Z., 2015. Performance improvement potentials of R1234yf mobile air conditioning system. Int. J. Refrig. 58, 35–40. https://doi.org/10.1016/j.ijrefrig.2015.03.019

Qi, Z., 2013. Experimental study on evaporator performance in mobile air conditioning system using HFO-1234yf as working fluid. Appl. Therm. Eng. 53, 124–130. https://doi.org/10.1016/j.applthermaleng.2013.01.019

Shen, B., Li, Z., Gluesenkamp, K.R., 2022. Experimental study of R452B and R454B as drop-in replacement for R410A in split heat pumps having tube-fin and microchannel heat exchangers. Appl. Therm. Eng. 204, 117930. https://doi.org/10.1016/j.applthermaleng.2021.117930

Shinohara, Y., Tobe, M., 1985. Development of an improved thermofin tube. Hitachi Cable Rev. 4 pp. 47–50.

Tran, N., Kasireddy, R.V., Wang, C.C., 2021. An experimental investigation on convective boiling heat transfer of R-454B with lubricant oil of POE-32 or POE-68 mixture in a horizontal smooth tube. Int. J. Heat Mass Transf. 181, 121990. https://doi.org/10.1016/j.ijheatmasstransfer.2021.121990

UNEP, 2016. The Kigali Amendment to the Montreal Protocol: HFC Phase-down.

OzonAction Fact Sheet 1–7.

Webb, R.L., Kim, N.-H., 2004. Principles of enhanced heat transfer. https://doi.org/10.1016/0301-9322(95)90005-5

Yasuda, K., Ohizumi, K., Hori, M., Kawamata, O., 1990. Development of condensing thermofinn HEX-C tube, Hitachi Cable Rev. 9, pp. 27–30.

Zhao, L., Zeng, W., Yuan, Z., 2015. Reduction of potential greenhouse gas emissions of room air-conditioner refrigerants: A life cycle carbon footprint analysis. J. Clean. Prod. 100, 262–268. https://doi.org/10.1016/j.jclepro.2015.03.063

CHAPTER

2

EXPERIMENTAL APPARATUS

2.1 Experimental Apparatus

In order to investigate the pressure drop, condensation, and boiling of two-phase heat transfer of various refrigerants in microfin tubes, a test facility is set up and provided in Miyara and Kariya Laboratory in Saga University, Japan. **Figure 2.1** describes the detailed schematic diagram of the experimental apparatus used in this study. The experimental apparatus consisted of three mixing chambers, two preheaters, test sections, a cooler, an accumulator, a Coriolis mass flow meter, a water loop (cooling/heating), and a data logger. First, liquid-phase refrigerant was stored in the refrigerant tank to begin the experiment. Subsequently, the refrigerant pumps into the system to flow through the mixing chamber, preheaters, sight glass, test section, cooler, and accumulator. The refrigerant is recirculated from the cooler after being cooled in an accumulator and returned to the pump to maintain the cycle.

To control the vapor quality in the test section, the refrigerant is heated by the first and second preheaters. A tube in tube heat exchanger is used to transfer heat from refrigerant to water in the condensation process case and water to refrigerant in the boiling case. After the flow boiling process or condensation process in the test section and leaves test section. Then, the refrigerant flows through the accumulator and is cooled in the cooler, therefore it is completely subcooled. The accumulator is set to control the experimental apparatus pressure.

The mass flow of refrigerant was quantified by a Coriolis mass flow meter. Three mixing chambers were located in different places to measure the refrigerant bulk temperature. To observe the quality of refrigerant, two sight glasses are placed at the inlet and outlet of the test section. The absolute pressure transducer is used to measure the refrigerant pressure. K type and T type thermocouple is used to measure the temperature

of refrigerant and tube wall, respectively. A data logger was used to collect all measurement signals of measuring devices.

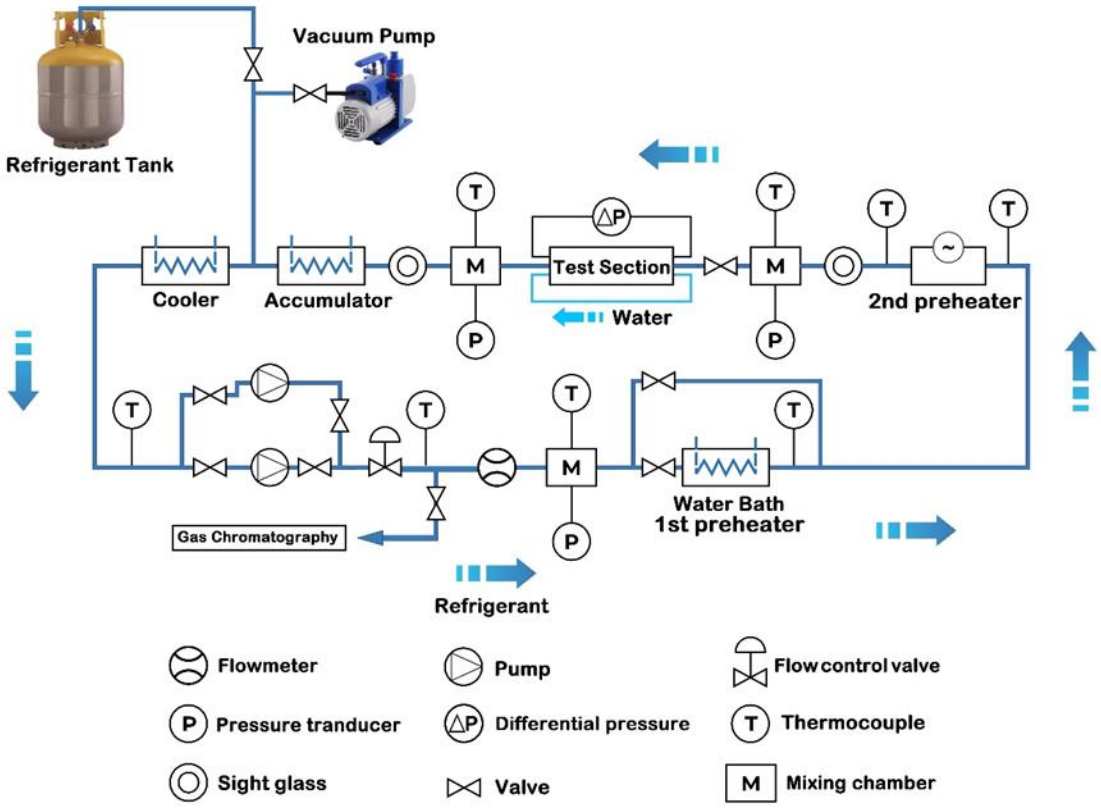

Figure 2.1 Experimental apparatus

2.2 Test section and microfin tubes

The details of the test section was presented in **Figure 2.2.** The test section consisted of a horizontally installed copper tube, headers, three water channels, and three sub-sections. In total, the test section is 852 mm in length, while it has 248 mm in length for each subsection, with the effective cooling/heating length being 744 mm. The refrigerant passes through the test tube, while water flows (counter-current) through the water loop. A differential pressure transducer is located in the test section header to measure the pressure difference. As shown in **Figure 2.3**, T-type thermocouples are installed at various points to detect the temperature of the test tube's outer wall.

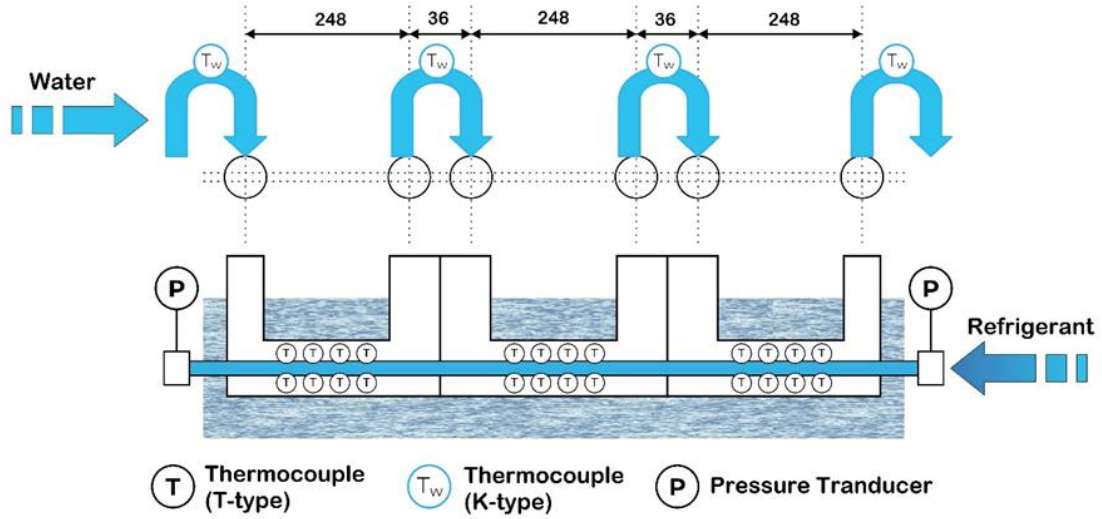

Figure 2.2. The test section details

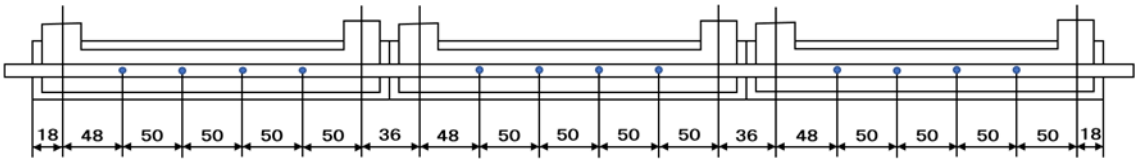

Figure 2.3. The test section details

There are three components to build the test section, which are a test tube, a rubber gasket, and an acrylic block, as shown in **Figure 2.4**. The acrylic block, rubber gasket, and test section formed a double tube fluid flow path, as described in **Figure 2.5**. **Figure 2.6** shows a schematic diagram of the connection between the heat source water and the sub-section. The temperatures of the inlet and outlet of the heat source are measured in each subsection, and the calculation of heat exchange at each subsection is conducted. The K-type thermocouples are placed in the heat source water mixer between each subsection to measure the heat source water inlet and outlet. The heat source water mixer consists of a polyurethane hose, a one-touch joint, and a spiral baffle plate as shown in **Figure 2.6**. In this present study, the type of test tube used is microfin tubes as shown in **Figure 2.7**. The dimension is listed in **Table 2.1**.

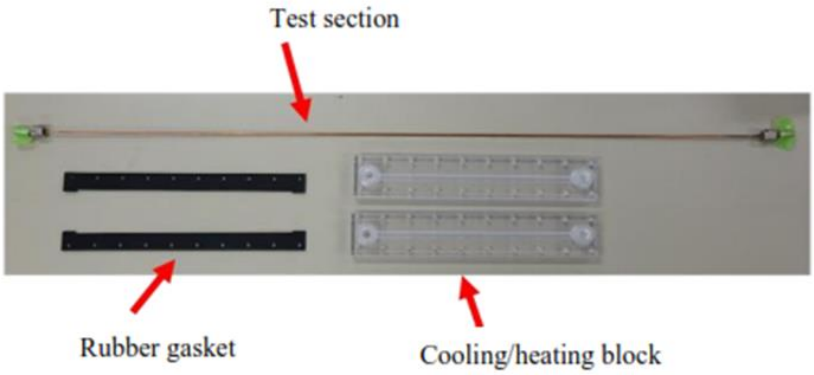

Figure 2.4. Component of the test section

Figure 2.5. Position of test section

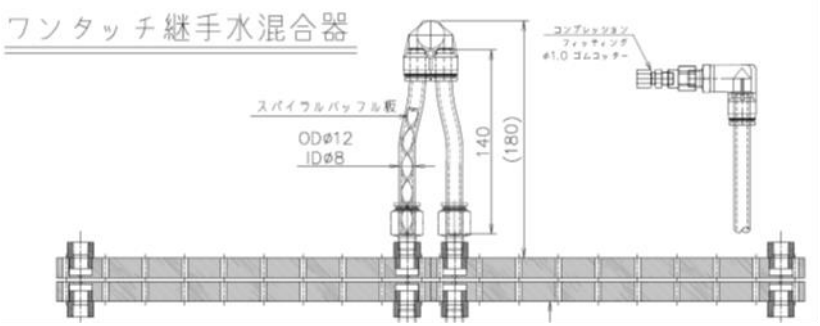

Figure 2.6. Heat source water mixture

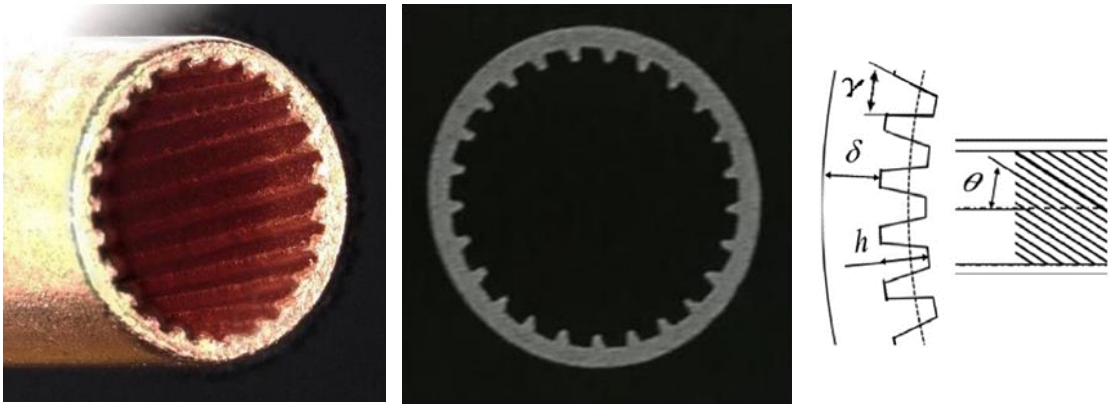

Figure 2.7. Photography and schematic view of a microfin tube

2.3 The method for ccalculating the parameters of the microfin tubes

Consider that the fin form of a microfin tube is about triangular, as illustrated in **Figure 2.8**, for a better understanding. The microfin tube's specifications are listed in **Table 2.1**.

- Fin bottom circumference = Fin root inner diameter × π
  = 3.2 × π
  = 10.05 mm
- Distance between fin = (Fin bottom circumference/ Number of fin) - l_2
  = (10.05/25)-0.063
  = 0.34 mm

- Wetted length with considering fin = (l_1 × 2+Distance between fin) × Number of fin
  = (0.1×2+0.34) ×25
  = 13.5 mm
- Wetted length without considering fin = Fin root inner diameter × π
  = 3.2 × π
  = 10.05 mm
- Pitch (*Pf*) = Fin bottom circumference/Number of fin
  = 10.05/25
  = 0.4 mm
- Area per fin = l_2 × (Fin height/2)
  = 0.063 × (0.1/2)
  = 3.15×10^{-3} mm^2
- Cross sectional area (*AC*) = $\frac{\pi}{4}$ × (fin bottom inner diameter)^2 – (Area per Fin x Number of Fin)
  = 7.96 mm^2
- Equivalent diameter (d_{eq}) = $\sqrt{\frac{4A_c}{\pi}}$
  = 3.18 mm
- Area Augmentation ratio (η) = 1+2 [sec(γ/2)-tan(γ/2)] ×(h_f / P_f)
  = 1.36 [-]

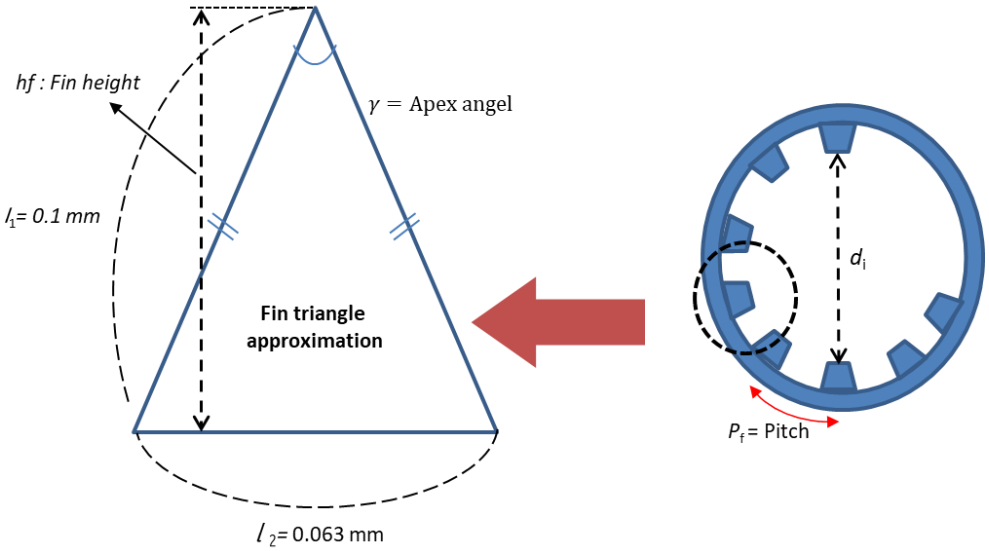

Figure 2.8. Fin shape of a microfin tube

Table 2.1 Specification of the Microfin tube

Tubes configuration	Microfin
Outside diameter, d_o [mm]	3.5
Fin root inner diameter [mm]	3.2
Inner diameter (fin tip) [mm]	3.0
Equivalent diameter, d_{eq} [mm]	3.18
Number of fin, N_f	25
Helix angle, θ [º]	10
Wall thickness, w_t [mm]	0.15
Fin height, h_f [mm]	0.1
Apex angle, γ [º]	35
Cross-sectional area [mm^2]	7.96
Area Augmentation ratio, η	1.36

2.4 Experimental Equipments

2.4.1 Absolute pressure transducer

The type of pressure transducer is PG-50KU. It is used to measure pressure with high accuracy because of its hermetically-sealed structure filled with inert gas. The working temperature ranges from -20 to 70 °C, the rated capacity is 5 Mpa and the uncertainty is ± 0.1 kPa. **Figure 2.9** shows the photograph and dimension.

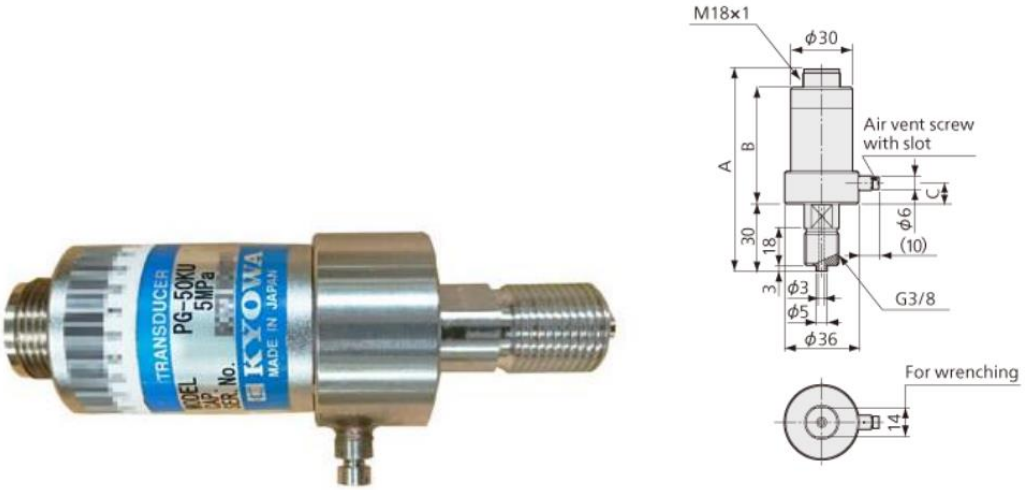

Figure 2.9 Pressure Transducer PG 50KU and its dimension

2.4.2 Differential pressure transducer

The *PDU-A-50kPa* is a stainless steel differential pressure transducer used in this experiment. It is used for measuring differential pressure. Its rated capacity is 50 kPa, the safe working temperature range is -30 to 90 °C, and the uncertainty is ±0.053 kPa. **Figure 2.10** shows the photograph and dimension.

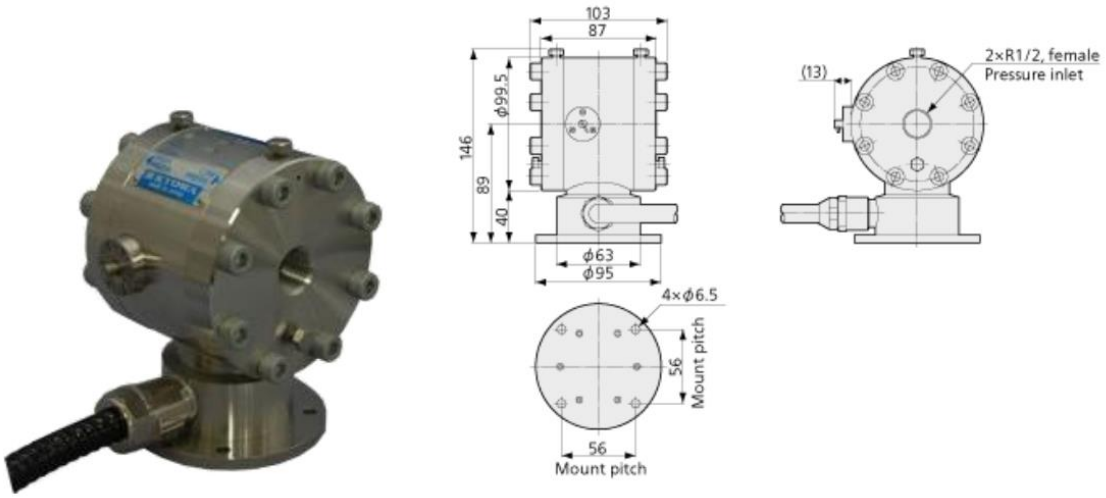

Figure 2.10. Differential pressure transducer (PDU-A-50kPa) and its dimensions

2.4.3 Coriolis mass flowmeter

The Coriolis mass flowmeter in this study consists of a single Z-shaped measuring tube, which can measure tiny flow measurements. The type is MMM 3300C (Tokyo KEISO Co., LTD.) It measures the flow according to the principle of Coriolis force. It is Using **Eq. 2.1** calculates the mass velocity flowing in the test tube.

Figure 2.11 shows the photograph of the Coriolis flowmeter.

$$G = \frac{m}{A_c} \tag{2.1}$$

Where G is the mass velocity, m is the mass flow rate, and A_C is the actual cross-sectional flow area of the test tube. The mass flow m is calculated as **Eq. 2.2**. Where, m_{max} is the full scale of the mass flow meter and E is the output voltage of the flow meter. The mass flowmeter used output 1 V with no load and 5 V with full scale. The flow rate range of the mass flowmeter used in the experiment is 0 to 20 kg/h and the measurement accuracy is ± 0.024% (Full scale).

$$m = \frac{m_{\max}}{4} \times (E - 1) \tag{2.2}$$

Figure 2.11. Coriolis mass flowmeter

2.4.4 Water flow controller and flow meter

A small size, light weight (approximately 800g) water controller (*FLC605*) is used for water flow control. It possible to manually control the flow rate by pressing buttons. Its range is 0.5 to 5 L/min and flow accuracy is ±5% of F.S. Its operating temperature is 0 to 60 °C. However, an electromagnetic flow meter (*VN05*) is used to measure the flow rate of water. **Figure 2.12** and **figure 2.13** show the photograph of water flow controller and water flowmweter, respectively. The following equations are used to calculate the flow rate of water.

$$FLC605: m_{wat} = \frac{5}{4} \times (E - 1) \tag{2.3}$$

$$VN05: m_{wat} = \frac{1}{4} \times (E - 1) \tag{2.4}$$

Where, E is the output voltage of the flowmeter. The flowmeter used output 1 V with no load and 5 V with full scale. The flow rate accuracy of the *FLC605* and *VN05* flowmeter is ± 5% FS (±0.25 L/min) at full scale of 5L/min and ±0.4% FS (±0.004 L/min) at full scale of 1 L/min, respectively.

Figure 2.12. Water flow controller

Figure 2.13. Water flow controller

2.4.5 Power supply

Figure 2. 14 shows the power meter PW3336 that is used to measure the power with high accuracy.The measurement frequensy ia 0.1 Hz to 100 kHz with basic accuracy of 0.15 %. The AC/DC direct input is up to 1000V/65 A. Its current sensor input terminal allows connection of optional current sensor to measure up to 5000A AC. Other important equipment are DC stabilized power supply (**Figure 2.15**), Power controller (**Figure 2.16**). A heating thermostat (LAUDA Alpha) is used to control the temperature of water bath as shown in **Figure 2.17**. Its temperature range is -25 to 85 °C and temperature stability is ± 0.05 °K.

Figure 2.14. Power meter

Figure 2.15. DC stabilized power supply

Figure 2.16. Power controller

Figure 2.17. LAUDA Alpha heating thermostats

2.4.6 Heat source water supply and cooler

As shown in **Figure 2.18**, in order to supply water at constant temperature in the test section, a heat source water supply model TBF320DC is used. The operating temperature is from -20 to 90 °C with the range of accuracy is ±0.01 to ±0.1 °C. For cooling purpose, a cooler (model: NCC-3000B) is utilized that show in **Figure 2.19**. The cooler consists of brine as a cooling agent with operating temperature range from -10 to 80 °C and temperature adjustment accuracy is ± 0.1°C.

Figure 2.18. Heat source water supplier

Figure 2.19. Cooler

2.5 Single phase test in Microfin tube

Single-phase R1234yf experiments are carried out inside a microfin tube (d_{eq}=3.18 mm) at mass velocities ranges from 100 to 300 kg $m^{-2}s^{-1}$. To ensure fully subcooled conditions along the test section, the inlet condition is kept subcooled. **Figure 2.20** illustrates Single-phase heat transfer coefficient R1234yf vs mass velocity. The heat transfer coefficient is defined as **Eq. 2.5**. The heat transfer coefficient increases with mass velocity, and it nearly doubles when mass velocity is increased from 100 kg $m^{-2}s^{-1}$ to 300 kg $m^{-2}s^{-1}$, as shown in **Figure 2.20**

$$\alpha_{exp} = \frac{q}{A_c\left(T_{ref} - T_{wall}\right)} \tag{2.5}$$

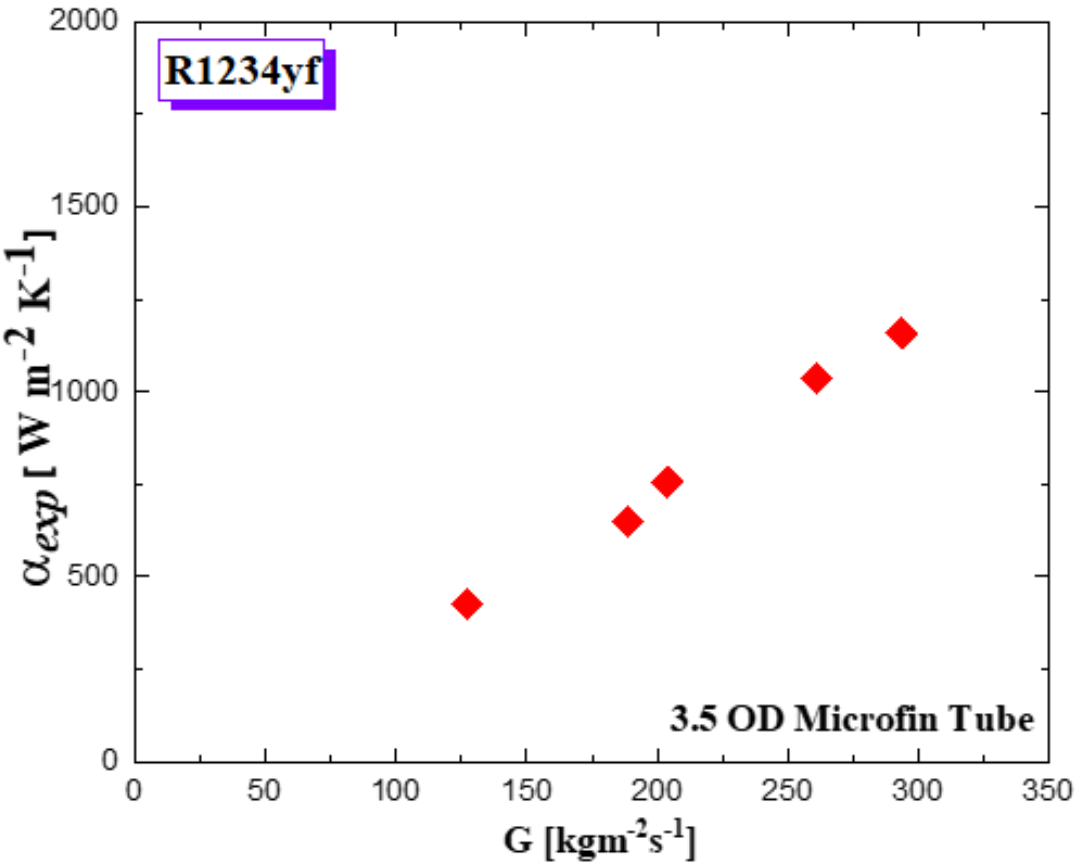

Figure 2.20. R1234yf single-phase heat transfer coefficient versus mass velocity in microfin tube

Because the correlation developed by was developed for smooth tubes, the experimental heat transfer coefficients are compared to the values predicted by the correlation developed by (Gnielinski, 2013) multiplied by the area enlargement ratio (η) of the microfin tube under investigation in **Figure 2.21**. The modified correlation of (Gnielinski, 2013) is the **Eq. (2.6)** to **Eq (2.9)**

$$\alpha_{\text{microfin, pred}} = \alpha_{\text{Gnieliski}} \cdot \eta \tag{2.6}$$

$$\alpha_{\text{Gnieliski}} = \frac{\lambda}{d_{eq}} \cdot \frac{\left(\frac{\xi}{8}\right)(\text{Re}-1000)\,\text{Pr}}{1+12.7\sqrt{\frac{\xi}{8}}\left(\text{Pr}^{2/3}-1\right)}\left[1+\left(\frac{d_{eq}}{L}\right)^{2/3}\right]\cdot K \tag{2.7}$$

Where, ξ and K expressed as follows:

$$\xi = \left(1.8\log_{10}\text{Re}-1.5\right)^{-2} \tag{2.8}$$

$$K = (Pr_{ref} / Pr_{w})^{0.11} \tag{2.9}$$

Where Pr_{w} is the prandtl number calculated at the wall temperature and the enlargement or augmentation ratio (η) is calculated as :

$$\eta = 1+2\left[\sec\left(\frac{\gamma}{2}\right)-\tan\left(\frac{\gamma}{2}\right)\right]\left(\frac{h_f}{P_f}\right) \tag{2.10}$$

$$P_f = \frac{Fin\ bottom\ circumference}{N_f} \tag{2.11}$$

The modified correlation well predicts the experimental data with the all data points capture within 15% as seen in **Figure 2.21**.

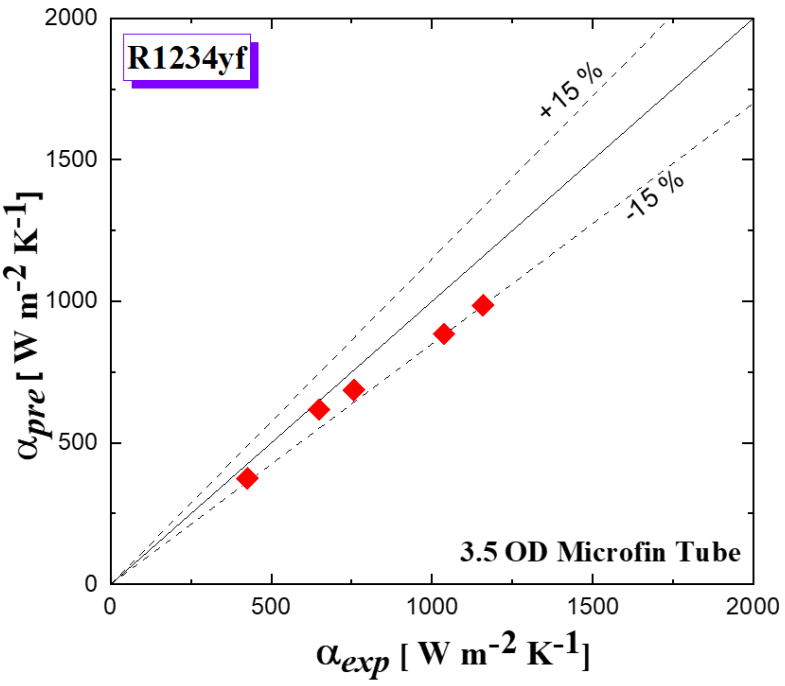

Figure 2.21. Comparison between experimental and calculated R1234yf single-phase heat transfer coefficient. Correlation by Gnielinski (2013) multiplied by the area enlargement ratio.

2.6 Coefficient of local heat transfer estimation

The heat transfer coefficient of each virtual sub-section is calculated after the inside of the test section with heat transfer length Z is divided into four virtual sub-sections as indicated in **Figure 2.22.** To estimate the local hat transfer coefficient the test section is divide into four virtual sub-sections as illustrated in **Figure 2.22.**

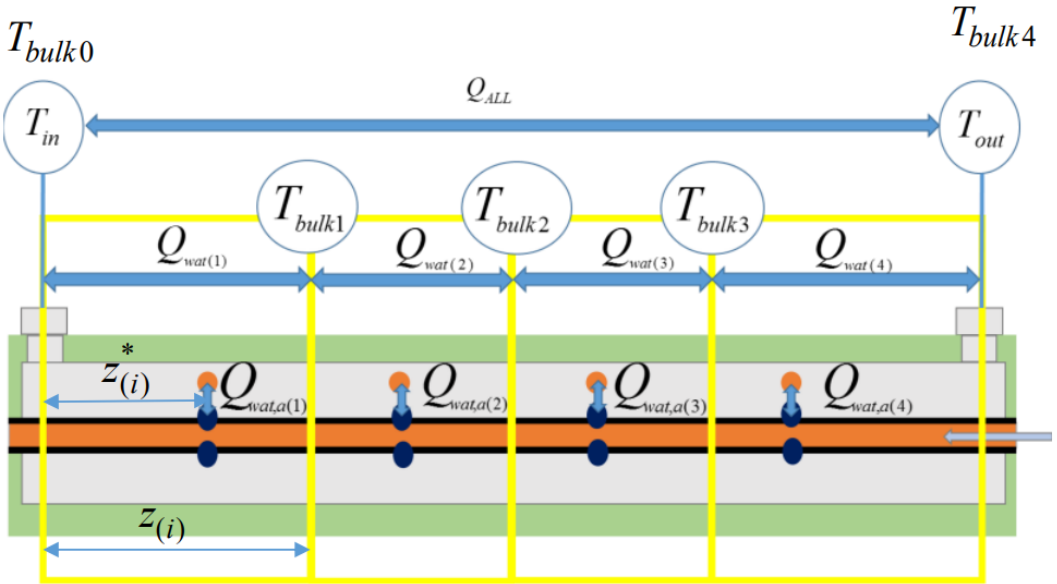

Figure 2.22. Virtual sub-sections

The rate of heat transfer of virtual sub-sections is calculated as follows:

$$Q_{wat(i)} = m_{wat}\, Cp_{wat} \left(T_{bulk(i)} - T_{bulk\,(i-1)}\right) \tag{2.12}$$

If the water side heat transfer coefficient α_{wat} is known and in the virtual sub-section is assumed to be constant, the heat transfer amount in the virtual sub-section is calculated as:

$$Q_{wat\,(i)} = \pi d_o Z_{(i)} \alpha_{wat} \left(T_{wall\,(i)} - T^*_{bulk\,(i)}\right) \tag{2.13}$$

$$T^*_{bulk\,(i)} = T_{bulk\,(i-1)} + \left(T_{bulk(i)} - T_{bulk\,(i-1)}\right) \frac{z^*_{(i)}}{z_{(i)}} \tag{2.14}$$

The sum of the heat exchanges of the four virtual sub-sections is equal to the heat exchange of the total test sections as Eq. 2.15.

$$Q_{all} = \sum_{i=1}^{4} Q_{wat\,(i)} \tag{2.15}$$

If the value of α_{wat} is given, each subsection's heat transfer can be calculated. As a result, the internal heat transfer coefficient is determined as:

$$\alpha_{ref\,(i)} = \frac{Q_{wat\,(i)}}{\pi d_e z_{(i)} \left(T_{ref(i)} - T_{wall(i),i}\right)} \tag{2.16}$$

Where $T_{ref(i)}$ is temperature of refrigerant, $T_{wall(i),i}$ is wall surface tube temperature, and d_{eq} is the equivalent diameter. The specific enthalpy of the refrigerant at the virtual sub-section outlet and the wall temperature measurement point *i* is estimated as follows:

$$h_{(i)} = h_{(i-1)} - \frac{Q_{wat(i)}}{m_{ref}} \tag{2.17}$$

$$h^*_{bulk\,(i)} = h_{(i-1)} + \left(h_{(i)} - h_{(i-1)}\right) \frac{z^*_{(i)}}{z_{(i)}} \tag{2.18}$$

Reference

Gnielinski, V., 2013. On heat transfer in tubes. Int. J. Heat Mass Transf. 63, 134–140. https://doi.org/10.1016/j.ijheatmasstransfer.2013.04.015

CHAPTER

3

EXPERIMENTAL INVESTIGATION AND DEVELOPMENT GENERAL CORRELATION FOR FRICTIONAL PRESSURE DROP OF TWO-PHASE FLOW INSIDE MICROFIN TUBE

Publications of this chapter

(1) Mainil, A.K.; Sakamoto, N,; Hakimatul, U.; Kariya, K.; Miyara, A. Experimental study and general correlation for frictional pressure drop of two-phase flow inside microfin tubes, International Journal of Refrigeration. https://doi.org/10.1016/j.ijrefrig.2022.07.017

3.1 Introduction

The increase in global warming has triggered a rise in the use of renewable energy sources. The global demand for air conditioning (AC) in 2018 was estimated to expand 110.97 million units, including both residential and commercial units (JRAIA, 2019). The growth of air conditioning causes the escalation of world energy consumption. However, it certainly impacts global environmental problems such as the depletion of the ozone layer and global warming. Authorities are increasing the pressure on the AC manufacturers regarding energy efficiency enhancement and environmental protection by establishing the regulations of the refrigerant used to suppress those environmental degradations. Currently, the high global warming potential (GWP) refrigerants such as R134a are still widely used in automobiles, which has been encouraged to be replaced by other alternative refrigerants. Some nationalities, such as European Union (EU), issued a policy to accelerate the prohibition of utilization

refrigerant with GWP >150. In this context, R134a (GWP=1430) will be eliminated shortly (Heredia-Aricapa et al., 2020).

Several researches have examined the drop-in replacement of R134a with lower GWP refrigerants regarding operating characteristics, cycle performance, heat transfer, and pressure drop performance in tube and others applications (Illán-Gómez et al., 2015; Illán-Gómez and García-Cascales, 2019; Kærn et al., 2021; Kedzierski and Kang, 2018; Li et al., 2019; López-Belchí, 2019; Morales-Fuentes et al., 2021; Pereira et al., 2019; Rangel-Hernández et al., 2019; Sieres and Santos, 2018; Tian et al., 2020). Some of those studies highlighted the potential of R1234yf as a future refrigerant in AC systems since its thermal and physical properties are remarkably similar to R134a (Akasaka et al., 2010; Lee and Jung, 2012; Qi, 2015, 2013; Zilio et al., 2011). Furthermore, R1234yf has zero ODP and a GWP of less than 1 (IPCC, 2013), making it legal to use in mobile air conditioners under current EU regulation.

However, R1234yf is a mild flammability refrigerant classified as A2L by the ANSI/ASHRAE standard (ANSI/ASHRAE Addenda 2015 Supplement, 2015; ANSI/ASHRAE Standard 34-2013, 2013), and this issue has attracted the attention of various researchers. Reducing charge amount refrigerants is particularly significant in refrigeration systems to improve the safety of flammable refrigerants and address environmental concerns. One of the solutions in heat exchanger applications is to use small diameter microfin tubes instead of the large ones, which is currently being developed and researched.

The study of microfin tubes with an outer diameter less than 5 or 4 mm continues, since the benefits offered by the smaller diameter of microfin. Small diameter microfin tubes have numerous advantages, including increased heat transfer, reduced weight, reduced air side pressure drop, significant refrigerant amount charge reduction, and the possibility for reduction space, energy, and cost - savings. Although the microfin tube has many advantages, reducing the diameter of the tube and adding fins, obviously contributes to higher pressure drop. Thus, the pressure drop characteristics in the small diameter microfin tubes at various conditions are needed to be investigated.

Since the microfin tubes with diameters 4 and 5 mm are already being used in AC in Japan and other places, the effort to obtain the smaller diameter's experimental data is still ongoing. Several studies have carried out the experimental research of R1234yf in a small diameter of microfin tubes (Diani et al., 2018a, 2017, 2015; Bashar

et al., 2020). They concluded that the small diameter microfin tubes lead to the increase of pressure drop. Although the correlations for small microfin tubes have been developed by some researchers, such as (Hirose et al., 2018; Bashar et al., 2020), the correlations are only limited to specific diameters and a short diameter range. Therefore, an accurate predictive tool for two-phase pressure drop in a wide range of the tubes diameter and experimental conditions is essential to develop.

This study investigates the two-phase flow frictional pressure drop of R1234yf inside a microfin tube with an outside diameter of 3.5 mm. Effects of various experimental conditions such as mass velocity, vapor quality, saturation temperature, and tube diameter on the frictional pressure drop were investigated with the present and previous data. The experimental data were also compared with some existing correlations. Herein, we attempted to develop a new correlation of two-phase pressure drop by using the present experimental data of microfin tube and the previous data with diameters from 2.5 mm to 9.52 mm.

3.2 Experimental Apparatus and Data Reduction

3.2.1 Experimental Appratus

Fig. 2.1 depicts the test equipment used to collect pressure drop data. Although this experimental apparatus is used to investigate boiling and condensation heat transfer processes, the pressure drop was measured in the adiabatic two-phase flow condition. Two pumps, a Coriolis flowmeter (Model: MMM3300C, 0.024%), two preheaters, three mixing chambers, a test section, an accumulator, and a cooler were all part of this facility. Two pumps operate the refrigerant; the difference between the two pumps is in the test conditions, with the first pump used for mass velocities equal and less than 50 kg $m^{-2}s^{-1}$ and the second pump used for mass velocities higher than 50 kg $m^{-2}s^{-1}$. The liquid refrigerant is pumped through a flow meter, mixing chamber, two preheaters, test section, sight glass, the accumulator, the cooler. The refrigerant is subcooled in the cooler. Vapor quality that enters the test section is set using a preheater in the vapor quality range of 0.1–0.9. The test section is a tube-in-tube heat exchanger where water flows in annular space and heats or cools the refrigerant flowing in the test tube for experiments of boiling or condensation. However, in the present experiment, the water

temperature is adjusted to the saturation temperature of the refrigerant so that the refrigerant flow is maintained adiabatic.

Three mixing chambers are installed at the inlet of the first preheater and the inlet and outlet of the test section to obtain specific enthalpy from the measured pressure and bulk temperature of the refrigerant. The accumulator controls the system pressure of the test apparatus. And, the cooler cools the refrigerant to ensure the refrigerant is in subcooled liquid. The pressure drop in the test section is measured by a differential pressure transducer where the pressure tapes are set at the inlet and outlet of the test section. An absolute pressure transducer (Model: PG-50KU, ±0.1kPa), a differential pressure transducer (Model: PDU-A-5KPa, ±0.053 kPa), and K-type thermocouple (±0.05°C) are placed at various locations, and a sight glass at the inlet and outlet of the test section to monitor the refrigerant's state. A data logger collects all signals from the pressure transducer and thermocouples. The test equipment is well insulated to maintain the system temperature.

Fig. 2.2 depicts a schematic of the test section, where a copper tube is horizontally placed in the test section, which is equipped with two headers, three subsections, and a water channel, as shown in figure. Type K thermocouples are installed at the inlet and outlet subsections of the water line to measure the temperature of the water, and the water flow rate is also measured using a flow meter. The flow rate of the water is adjusted according to the conditions to be achieved.

The Photography and schematic view of the tested microfin tube are shown in **Fig. 2.7** And the summary of the microfin tube specifications is recorded in **Table 3.1**. The outside and equivalent diameters are 3.5 mm and 3.18 mm, respectively. The 25 microfins with the helix angle of 10° and fin height of 0.1 mm are formed inner surface. The test section length that the pressure drop was measured is 852 mm. 24 pieces of T-type thermocouples (±0.05°C) are placed at several points on the surface of the test tube.

Table 3.1. The microfin tube specifications

Tubes configuration	Microfin
Outside diameter, d_o [mm]	3.5
Equivalent diameter, d_{eq} [mm]	3.18
Number of fin, N_f	25
Helix angle, θ [º]	10
Wall thickness, w_t [mm]	0.15
Fin height, h_f [mm]	0.1
Apex angle, γ [º]	35

The experiments were conducted at the range of mass velocity 50- 300 kg $m^{-2}s^{-1}$, vapor quality 0.1-0.9, and saturation temperature 20 ºC and 30 ºC. R1234yf was used as the test refrigerant. The thermophysical properties of R1234yf for all experimental conditions in this study were obtained from REFPROP 10.0a (Lemmon et al., 2018) and are listed in **Table 3.2**.

Table 3.2. Thermophysical properties of R1234yf (Lemmon et al., 2018)

Properties [Unit]	T_{sat} 20 ºC	T_{sat} 30ºC
P [Mpa]	0.591	0.783
Pr [-]	0.175	0.231
ρ_l [kg m^{-3}]	1109.9	1073.3
ρ_v [kg m^{-3}]	32.796	43.729
μ_l [µPa s]	162.26	143.97
μ_v [µPa s]	11.173	11.686
ρ_l/ρ_v [-]	33.84254	24.54435
μ_l/μ_v [-]	14.523	12.320
σ [mN m^{-1}]	6.798	5.564
λ_l [mW m^{-1} K^{-1}]	65.079	62.019

3.2.2 Data Reduction

The total adiabatic pressure drop ΔP_T is expressed using **Eq. (3.1)** as the sum of frictional pressure drop ΔP_F and pressure drop due to abrupt contraction ΔP_c and expansion ΔP_e at the inlet and outlet of the test section, respectively.

$$\Delta P_T = \Delta P_F + \Delta P_c + \Delta P_e \tag{3.1}$$

The gravity and momentum pressure drop are not needed to consider in this study since the test section is horizontal and the test mode is adiabatic. The pressure drop because of the abrupt contraction and expansion were estimated by **Eq. (3.2)** and **Eq. (3.3)**, according to the Collier and Thome method (Collier and Thome, 1994).

$$\Delta P_c = \frac{G^2 v_l}{2}\left[\left(\frac{1}{C_c}-1\right)^2+\left(1-\frac{1}{\delta^2}\right)\right]\left[1+\left(\frac{\Delta v_v}{v_l}\right)x\right] \tag{3.2}$$

$$\Delta P_e = G^2\delta_e\left(1-\delta_e\right)v_l\left[\frac{(1-x)^2}{(1-\xi)}+\left(\frac{v_v}{v_l}\right)\frac{x^2}{\xi}\right] \tag{3.3}$$

Where G is mass velocity, δ is the area ratio, and C_c is the coefficient of contraction that is a function of δ. In addition, the relationship between C_c and δ is described by (Perry, 1963). The void function, ξ is assumed as constant and is calculated by the homogeneous model expressed by **Eq. (3.4)**.

$$\xi = \frac{1}{1+\left[\frac{1-x}{x}\right]\frac{\rho_v}{\rho_l}} \tag{3.4}$$

The vapor quality at the test section inlet is expressed with enthalpies as **Eq. (5)**:

$$x = \frac{h_{in}-h_l}{h_v-h_l} \tag{3.5}$$

The enthalpies of saturation liquid and vapor, h_l and h_v, are obtained with the measured pressure. The enthalpy at the test section inlet, h_{in}, is calculate from the amount of heat in the preheater (*W)* as **Eq. (3.6)**.

$$h_{in} = h_{in,\,preheater} + \left(\frac{W}{G}\right) \tag{3.6}$$

Where, $h_{in,preheater}$ is the enthalpy at preheater inlet obtained with the measured pressure and temperature of subcooled liquid. The amount of heat (*W*) was transferred by the

electricity in the direct heating method. The experiments were conducted in the adiabatic setting by keeping the refrigerant and water with the same temperature. The vapor quality does not change because no additional heat is applied to the refrigerant flowing in the test section.

The mass velocity, *G*, is determined by **Eq. (3.7),** where A_c is the cross-sectional flow area of the microfin tube, which is determined by **Eq. (3.8)** while m_R is the flow rate of the refrigerant.

$$G = \frac{m_R}{A_c} \tag{3.7}$$

$$A_c = \pi\left(\frac{d_i}{2}\right)^2 - \left(A_{fin} \times N_f\right) \tag{3.8}$$

Where d_i is the fin bottom inner diameter, A_{fin} is the total area of 1 fin, and N_f is the number of the fin. In the present study, the equivalent diameter, d_{eq}, determined by **Eq. (3.9)** is used as the representative length.

$$d_{eq} = \sqrt{\frac{4A_c}{\pi}} \tag{3.9}$$

The uncertainty of frictional pressure drop was assessed in this investigation using the procedure outlined in (JCGM 100, 2008). It is possible to estimate the frictional pressure drop uncertainty using **Eq. (3.10)**. The frictional pressure drop's mean, minimum, and maximum uncertainty are 5.5 percent, 2.0 percent, and 22.4 percent, respectively. When the mass velocity and vapor quality are low, the uncertainty increases because the differential pressure transducer's sensitivity is not sufficiently high, resulting in decreased accuracy.

$$U\left(\Delta P_F\right) = \left\{\left(U\left(\Delta P_T\right)\frac{\partial \Delta P_F}{\partial \Delta P_T}\right)^2 + \left(U\left(\Delta P_c\right)\frac{\partial \Delta P_F}{\partial \Delta P_c}\right)^2 + \left(U\left(\Delta P_e\right)\frac{\partial \Delta P_F}{\partial \Delta P_e}\right)^2\right\}^{0.5} \tag{3.10}$$

3.3. Result and Discussion

3.3.1. Frictional Pressure Drop

The experimental investigation of the two-phase pressure drop at the adiabatic condition of R1234yf in microfin tubes is carried out in this study. The effect of mass

velocity, saturation temperature, tube diameter, and vapor quality on the frictional pressure drop is deliberate in this study.

Fig. 3.1 shows the plot of experimental frictional pressure drop against the vapor quality at saturation temperature of 20 ºC for the mass velocity of 50 - 300 kg $m^{-2}s^{-1}$ in 3.5 mm outer diameter of microfin tube. The higher pressure drop is at the mass velocity of 300 kg $m^{-2}s^{-1}$. Here, the frictional pressure of R1234yf increased with increasing mass velocity and vapor quality. The effect of mass velocity and vapor quality on the increase of pressure drop due to increasing vapor shear stress and increased interfacial friction between vapor-liquid two-phase flow in the tube. This result agrees with other studies by (Bashar et al., 2020; Diani et al., 2017; Jige and Inoue, 2019; Singh and Kukreja, 2018).

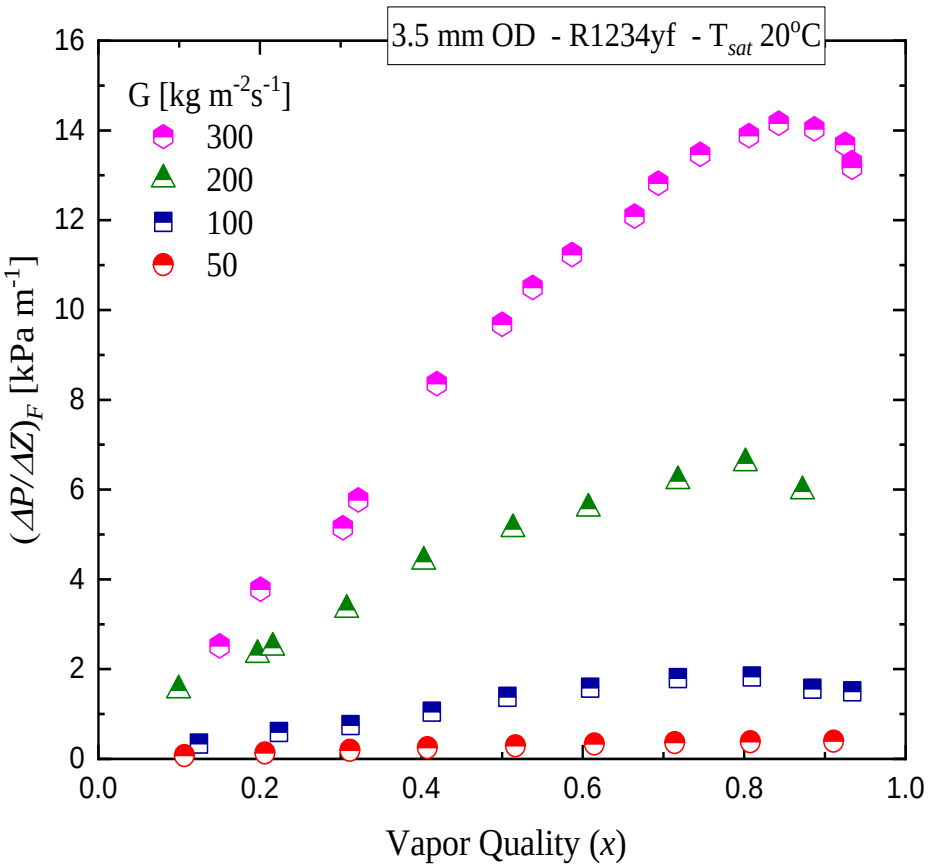

Fig. 3.1 Effect of mass velocity and vapor quality on frictional pressure drop

The saturation temperature has a role in decreasing the pressure drop, as shown in **Fig. 3.2**. Two saturation temperatures of 20 ºC and 30 ºC are employed to evaluate the pressure gradient with a variation of mass fluxes of 100 and 200 kg $m^{-2}s^{-1}$. The

result shows that the pressure drop decrease at higher saturation temperature for all mass velocity range. It indicated that the fluid properties such as viscosity, density are shifted by changing saturation temperature, as shown in **Table 3.2**. Specifically, the higher the saturation temperature, the higher the vapor density (ρ_v). As a result, the vapor velocity is lower at fixed mass velocity, with less heat transfer coefficients than at lower saturation temperature. Similar results are also obtained by (Diani et al., 2018b, 2018a; Rahman et al., 2017; Revellin and Thome, 2007). The gradient of pressure drop at each mass velocities for both saturation temperatures increases with the increase of vapor quality until it reaches the maximum value, after which it slightly decreases.

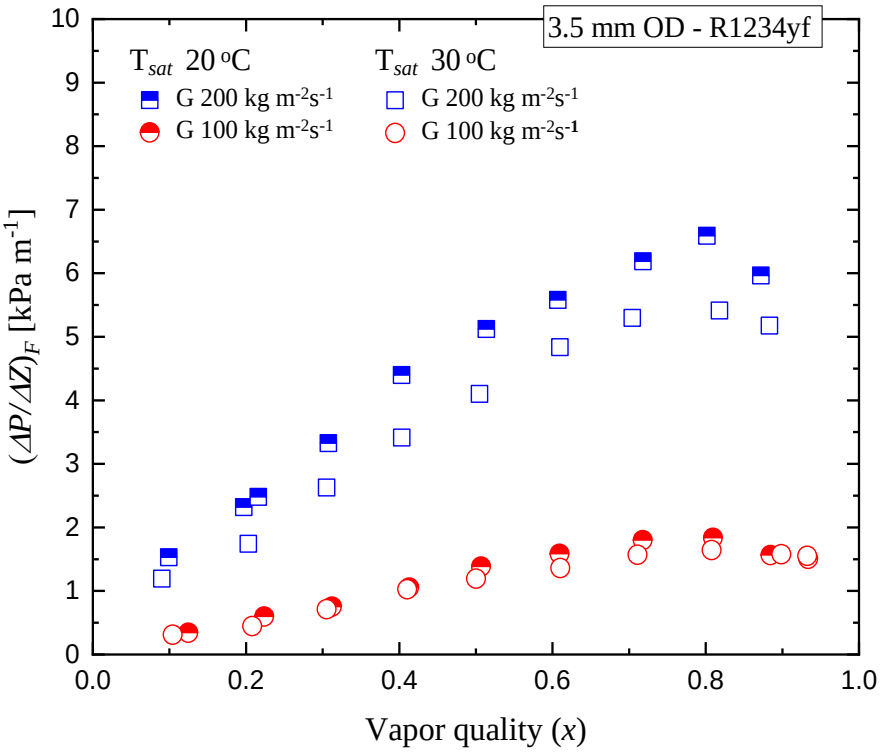

Figure 3.2. Effect of saturation temperature on frictional pressure drop

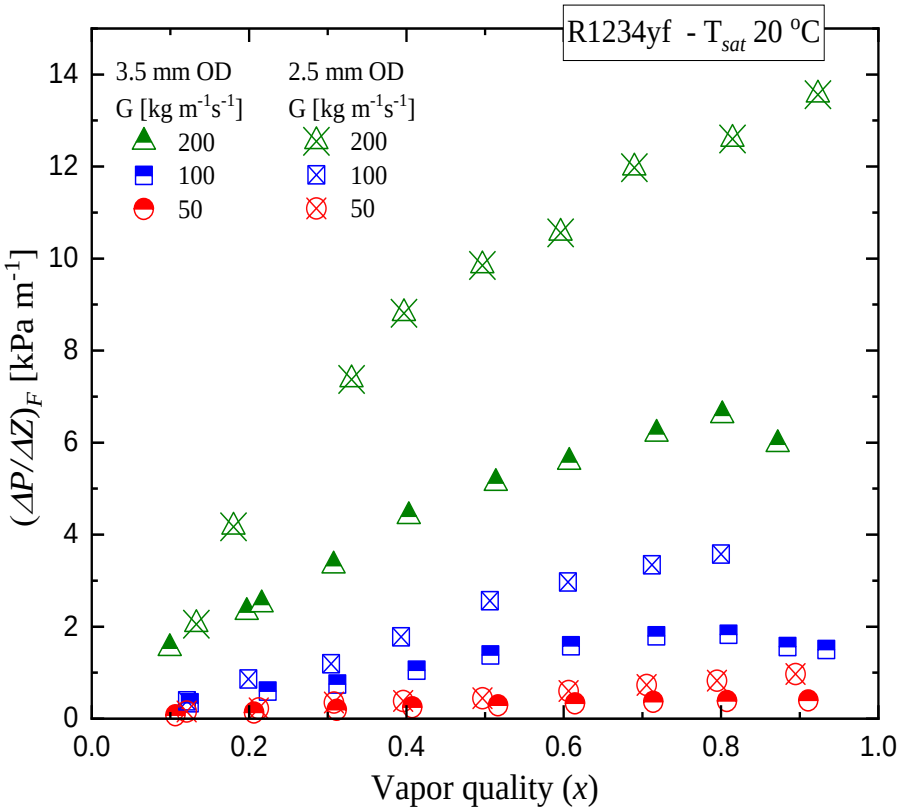

Fig. 3.3. Effect of microfin tubes diameter on frictional pressure drop

In order to investigate the effect of tube diameter on frictional pressure drop, the pressure drop data of microfin tubes with an outer diameter of 2.5 mm (Bashar et al., 2020) are compared with the present data. **Fig. 3.3** illustrates the comparison of frictional pressure drop in microfin tubes with outer diameters of 2.5 mm and 3.5 mm where the equivalent diameters are 2.17 mm and 3.18 mm. The trends show that, on average, the frictional pressure drop of microfin tube with an outer diameter of 2.5 mm is higher than that of 3.5 mm. The smaller diameter of the microfin tube leads to the increase of shear stress due to the increase of velocity gradients. The same results are observed in other studies (Jige et al., 2016).

3.3.2 Comparison with the well-known correlation

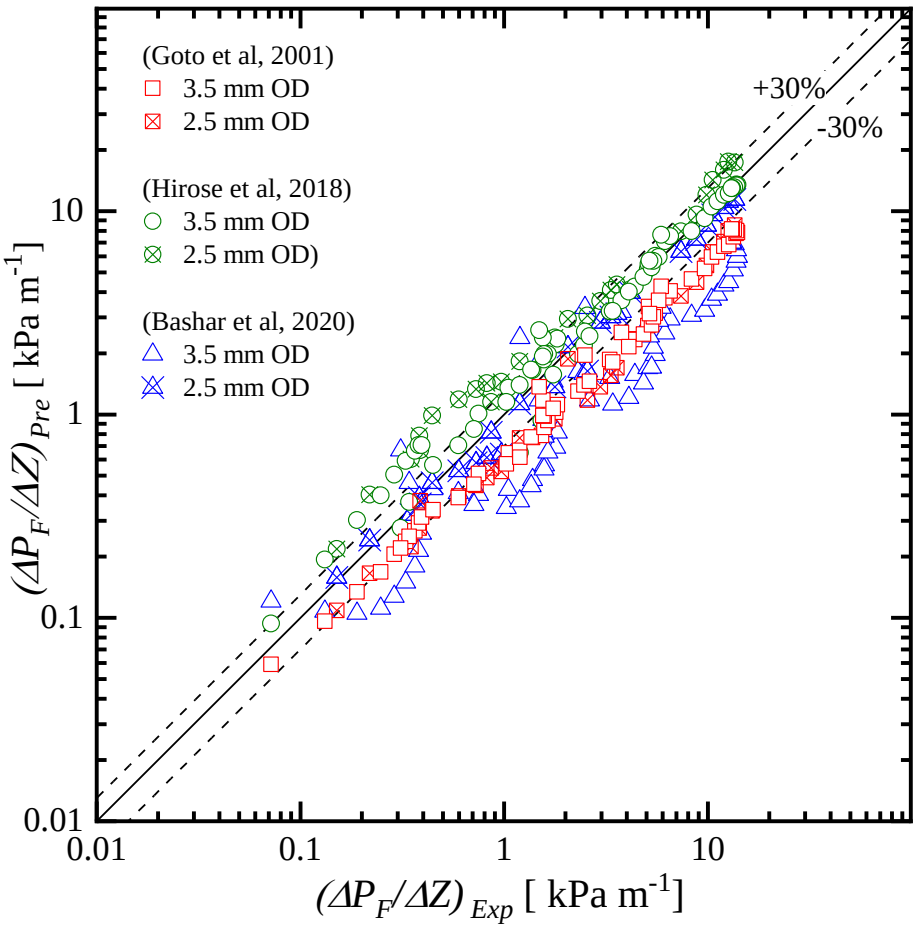

Fig. 3.4. Comparison of two-phase frictional pressured drop with some existing correlation of microfin tubes.

The experimental two-phase flow pressure drop of R1234yf in microfin tubes with outer diameter 2.5 mm and 3.5 mm were compared with existing correlations to predict the experimental data. **Fig. 3.4** shows three correlations used in this study (Bashar et al., 2020; Goto et al., 2001; Hirose et al., 2018). All existing correlations used here are listed in **Table 3.3.** In total, 91 data points are used for comparison with the existing correlation. The mean deviation (MD), average deviation (AD) and R30 are applied as an evaluation criterion for those correlations. The R30 is the parameter to represent the proportion of data points that has a deviation within 30% of the total predicted data. **Table 3.4** lists the AD and MD, which are calculated by **Eq. ((3.11)-(3.12))**.

$$AD = \frac{1}{n}\sum_{i=n}^{n}\left(\frac{\Delta P_{F,pre} - \Delta P_{F,Exp}}{\Delta P_{F,Exp}}\right)\times 100 \quad (3.11)$$

$$MD = \frac{1}{n}\sum_{i=n}^{n}\left|\frac{\Delta P_{F,pre} - \Delta P_{F,Exp}}{\Delta P_{F,Exp}}\right|\times 100 \quad (3.12)$$

Table 3.3. Existing correlations for frictional pressure drop of microfin tube

Authors	Correlation	Experimental conditions
(Goto et al., 2001)	$\left(\frac{\Delta P}{\Delta Z}\right)_F = \Phi_v^2\left(\frac{\Delta P}{\Delta Z}\right)_v$, $\left(\frac{\Delta P}{\Delta Z}\right)_v = 2f_v\frac{G^2x^2}{d\rho_v}$ $\Phi_v = 1+1.64X_{tt}^{0.79}$ $X_{tt} = \{(1-x)/x\}^{0.9}(\rho_v/\rho_l)^{0.5}(\mu_l/\mu_v)^{0.1}$	Helical and herringbone microfin tubes. Fluid: R410A, R22 G: 200-340 kg $m^{-2}s^{-1}$ Test Mode: Condensation
(Hirose et al., 2018)	$\left(\frac{\Delta P}{\Delta Z}\right)_F = \Phi_v^2\left(\frac{\Delta P}{\Delta Z}\right)_v$, $\left(\frac{\Delta P}{\Delta Z}\right)_v = 2f_vG^2x^2/(\rho_v d)$ $f_v = 0.26\,\mathrm{Re}_v^{-0.38}\eta^{0.95}(\cos\theta)^{-2.8}$ $\Phi_v = 1+1.55X_{tt}^{0.4}$ $X_{tt} = \{(1-x)/x\}^{0.9}(\rho_v/\rho_l)^{0.5}(\mu_l/\mu_v)^{0.1}$	Microfin Tube. Fluids: R32, R152a, R410A G: 100 -400 kg $m^{-2}s^{-1}$ Test mode: condensation
(Bashar et al., 2020)	$\left(\frac{\Delta P}{\Delta Z}\right)_F = \Phi_v^2\left(\frac{\Delta P}{\Delta Z}\right)_v$, $\left(\frac{\Delta P}{\Delta Z}\right)_v = \frac{2f_vG^2x^2}{d\rho_v}$ $\Phi_v^2 = 1+CX_{tt}^n+X_{tt}^2$ $n = \{1-0.87\exp(-0.001Fr)\}Bo$ $C = 21\{1-\exp(-0.28Bo^{0.5})\}\{1-0.45\exp(-0.02Fr^{1.2})\}$	Smooth and Microfin Tubes Fluids: R134a, R1234yf G: 50 – 200 kg $m^{-2}s^{-1}$ Test Mode : Adiabatic

The correlation of (Goto et al., 2001) majority underestimates the experimental data with a mean deviation of 37.7 %. For (Hirose et al., 2018), correlation is well predicted in some parts of experimental data, however still over-estimated in others parts, especially in low mass velocity by 28.8 % of mean deviation. (Bashar et al., 2020) correlation cannot be applied to the microfin tubes with an outer diameter of 3.5 because it is not well predicted in experimental data of 3.5 mm OD with a mean deviation of 41.6 %. The number of data points within ±30% deviation to the total

number of are data points is 23.1 %, 65.9 %, and 34.1 % from (Goto et al., 2001), (Hirose et al., 2018) and (Bashar et al., 2020) correlations, respectively.

Table 3.4. Deviations of frictional pressure drops determined by existing and proposed correlations

Correlation	AD (%)	MD (%)	R 30(%)
(Goto et al., 2001)	-37.7	37.7	23.1
(Hirose et al., 2018)	24.8	28.8	65.93
(Bashar et al., 2020)	-32.7	41.6	34.1
Proposed Correlation Eq. (13)-(23)	-0.6	12.2	92.3

3.4. Development of New General Correlation

Overall, the calculated pressure drop data from the above correlations show the discrepancy from the present frictional pressure drop for majority experimental data. Therefore, to improve the accuracy of the predicted two-phase pressure drop, the development of a new correlation for microfin is reported herein. The new correlation for a frictional pressure drop of two-phase flow is as follows:

The two-phase frictional pressure drop equation (**Eq. (3.13)**) is:

$$\left(\frac{\Delta P}{\Delta Z}\right)_F = \Phi_v^2 \left(\frac{\Delta P}{\Delta Z}\right)_v \tag{3.13}$$

The term of $\left(\frac{\Delta P}{\Delta Z}\right)_F$ indicates the two-phase flow of frictional pressure drop, and $\left(\frac{\Delta P}{\Delta Z}\right)_v$ is the frictional pressure drop for the vapor flows inside the tube. **Eq. (3.14)** is the equation for the $\left(\frac{\Delta P}{\Delta Z}\right)_v$ as follows:

$$\left(\frac{\Delta P}{\Delta Z}\right)_v = \frac{2 f_v G^2 x^2}{d_{eq} \rho_v} \tag{3.14}$$

Where f_v is the friction factor, G is mass velocity, x is vapor quality, ρ_v is vapor density, and d is tube diameter.

The diameter used in the case of microfin tubes is the equivalent diameter (d_{eq}). The friction factor (f_v) can be calculated by (Carnavos, 1980) equation (**Eq. ((3.15) - (3.16))** that proposed friction factor for single-phase inside microfin tubes.

$$f_v = \frac{0.046}{Re_v^2 F^*} \tag{3.15}$$

$$F^* = \left(\frac{A_{fa}}{A_{fn}} \right)^{0.5} \left(\sec\theta \right)^{0.75} \tag{3.16}$$

The terms of A_{fa} , A_{fn} , and θ are actual flow area, nominal flow area on based tube ID as if the fin structure were not present, and helix angle of microfin tubes, respectively.

Eq. (3.17) describes the two-phase pressure drop multiplier, which is similar to the analysis of (Chisholm and Laird, 1958):

$$\Phi_v^2 = 1 + C\,\mathrm{X}_{tt}^n + \mathrm{X}_{tt}^2 \tag{3.17}$$

The Martinelli parameter, X_{tt} , can be determined by **Eq. (3.18)**:

$$\mathrm{X}_{tt} = \sqrt{\left(\frac{\Delta P}{\Delta Z} \right)_l \Big/ \left(\frac{\Delta P}{\Delta Z} \right)_v} = \left(\frac{1-x}{x} \right)^{0.9} \left(\frac{\rho_v}{\rho_l} \right)^{0.5} \left(\frac{\mu_l}{\mu_v} \right)^{0.1} \tag{3.18}$$

The value of C and n in **Eq. (3.17)** can be generated by the curve fitting method from the experimental data as shown in **Fig. 3.5.** The 91 present and previous experimental data points of 3.5 mm and 2.5 mm OD in the figure show the relationship between X_{tt} and Φ_v . 25 data points taken from (Kuo and Wang, 1996) with a larger tube diameter are also plotted. The solid lines are the two-phase pressure drop multipliers Φ_v as a function of X_{tt} with constant parameters C and n that are adjusted to fit the experimental data. The dash-dot lines indicating the previous correlations (Chisholm and Laird, 1958; Hirose et al., 2018) cannot predict the data well with different diameters. This comparison shows that the correlation of Φ_v with particular C and n is only applied to specific diameters. As well known, the parameter C has different values depending on the flow conditions. Therefore, to obtain a general correlation, it is necessary to develop functions for C and n, considering the effect of tube diameter, mass velocities, and physical property values.

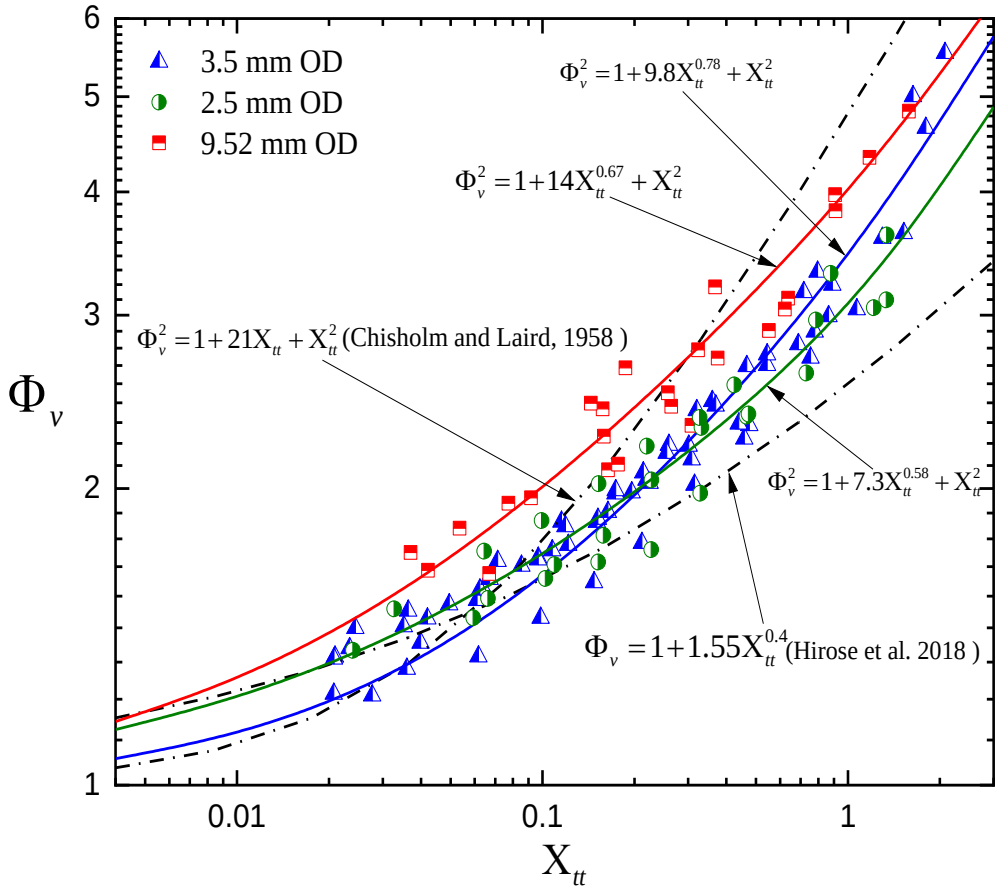

Fig. 3.5. Relation between X_{tt} and Φ_v

Following the Miyara's method (Miyara et al., 2004), the coefficient C approximately correlated in terms of Bond number (Bo) and Froude number (Fr) as expressed in **Eq. (3.19)**.

$$C = 21 f_1(Bo)\, f_2(Fr) \tag{3.19}$$

The function of $f_1(Bo)$ was employed the same equation as in the previous study (Afroz and Miyara, 2011; Miyara et al., 2004)

$$f_1(Bo) = \left\{1 - \exp\left(-0.28 Bo^{0.5}\right)\right\} \tag{3.20}$$

The curve fitting method obtained several values of C and n at each group of data points with the same Fr number. Then, the function of $f_2(Fr)$ was obtained by curve fitting method with plotting the values of $C/(21 f_1(Bo))$ versus Fr as described in **Fig. 3.6.** Equation of C is expressed in **Eq. (3.21)**.

$$C = 21\left\{1-\exp\left(-0.28Bo^{0.5}\right)\right\}\left\{1-0.7\exp\left(-0.36Fr^{0.65}\right)\right\} \quad (3.21)$$

An equation of n as the function Fr was obtained by solving the mathematical solutions, as follows.

$$n = 1-0.4\exp\left(-0.08Fr\right) \quad (3.22)$$

Where Bond and Froude number are defined as **Eq. (3.23)** and **Eq. (3.24).**

$$Bo = \frac{gd^2\left(\rho_l-\rho_v\right)}{\sigma} \quad (3.23)$$

$$Fr = \frac{G}{\sqrt{\rho_v\left(\rho_l-\rho_v\right)gd}} \quad (3.24)$$

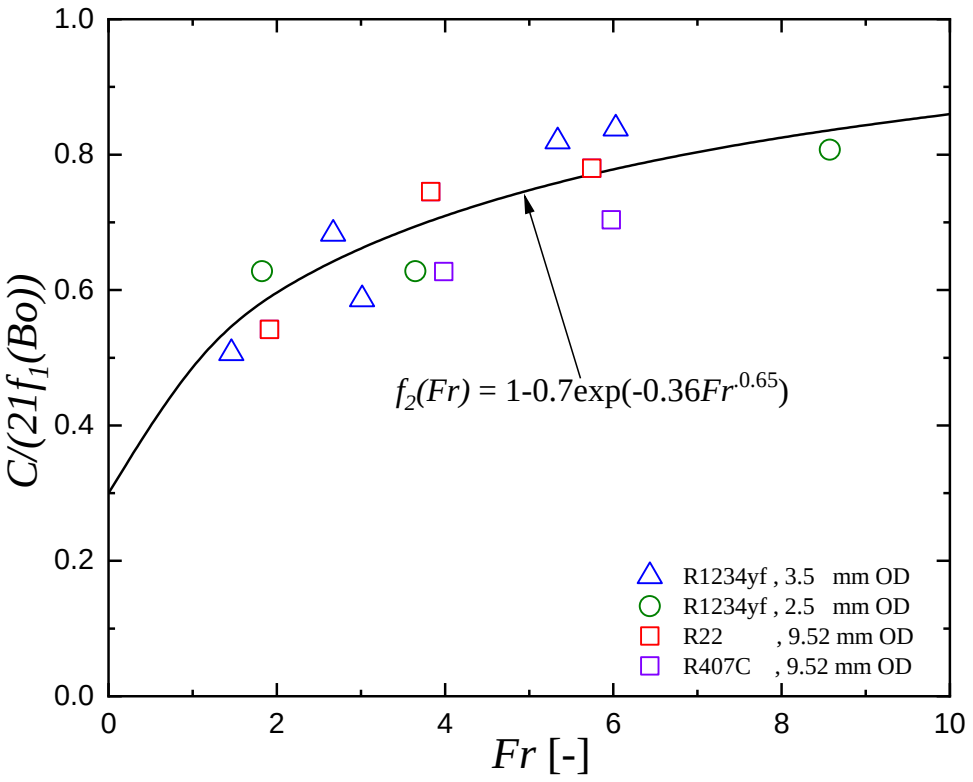

Fig. 3.6. Approximate correlation of the C obtained from experimental value of the C, Bo versus Fr of two-phase frictional pressure drop

In the same way, as in **Fig. 3.6**, a plot is performed using the new obtained function by plotting the values of $C/(21f_2(Fr))$ versus Bo, as described in **Fig. 3.7.** Furthermore, the function of Bo in **Eq. (3.20)** is also included.

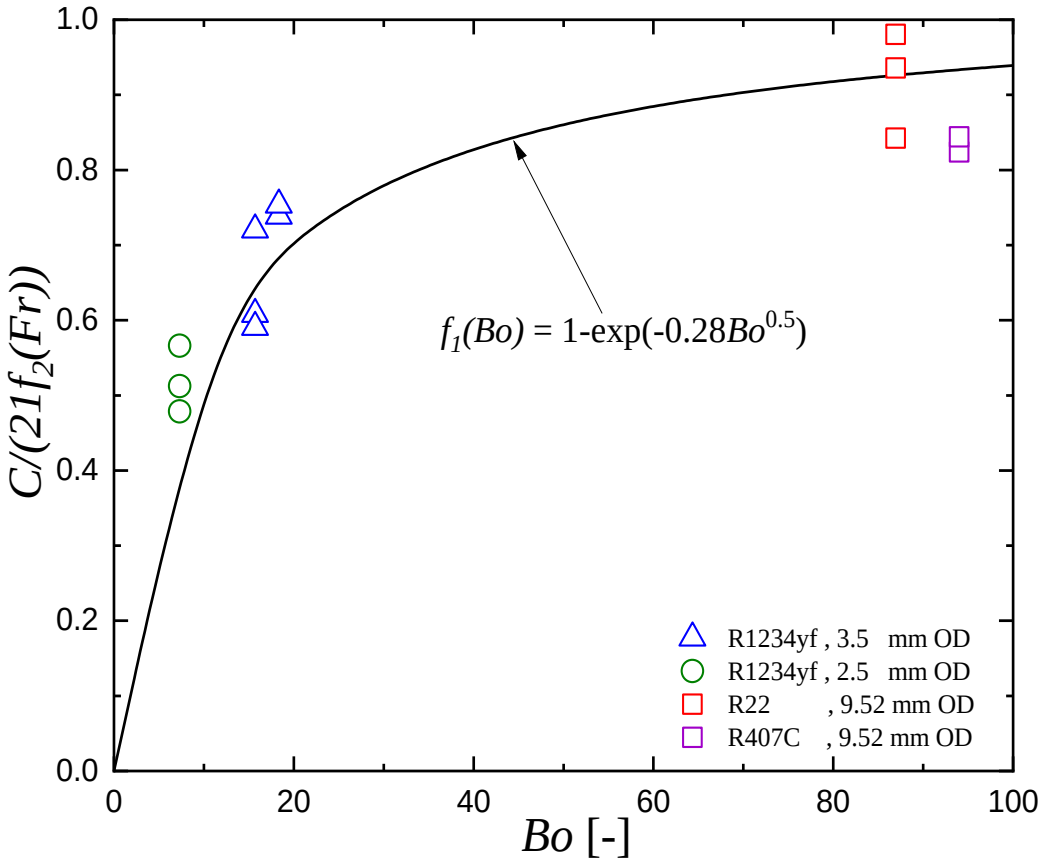

Fig. 3.7. Approximate correlation of the C obtained from experimental value of the C, Fr versus Bo of two-phase frictional pressure drop

The new prediction correlation is summarized in **Table 3.5**. The presently developed correlation can also fit the present and previous data with a mean deviation of 12.2 %, average deviation of -0.6 %, and 92.3 % of the data points are within the deviation of 30%, as shown in **Fig. 3.8** and **Table 3.4**.

Table 3.5. The proposed of two-phase flow frictional pressure drop correlation

$$\left(\frac{\Delta P}{\Delta Z}\right)_F = \Phi_v^2 \left(\frac{\Delta P}{\Delta Z}\right)_v, \quad \left(\frac{\Delta P}{\Delta Z}\right)_v = \frac{2 f_v G^2 x^2}{d \rho_v}, \quad f_v = \frac{0.046}{\mathrm{Re}_v^2 F^*}, \quad F^* = \left(\frac{A_{fa}}{A_{fn}}\right)^{0.5} (\sec\theta)^{0.75}$$

$$\Phi_v^2 = 1 + C\,\mathrm{X}_{tt}^n + \mathrm{X}_{tt}^2$$

$$C = 21\left\{1 - \exp\left(-0.28 Bo^{0.5}\right)\right\}\left\{1 - 0.7\exp\left(-0.36 Fr^{0.65}\right)\right\}$$

$$n = 1 - 0.4\exp\left(-0.08 Fr\right)$$

$$\mathrm{X}_{tt} = \sqrt{\left(\frac{\Delta P}{\Delta Z}\right)_l \Big/ \left(\frac{\Delta P}{\Delta Z}\right)_v} = \left(\frac{1-x}{x}\right)^{0.9} \left(\frac{\rho_v}{\rho_l}\right)^{0.5} \left(\frac{\mu_l}{\mu_v}\right)^{0.1}$$

$$Bo = \frac{g d^2 \left(\rho_l - \rho_v\right)}{\sigma}, \quad Fr = \frac{G}{\sqrt{\rho_v \left(\rho_l - \rho_v\right) g d}}$$

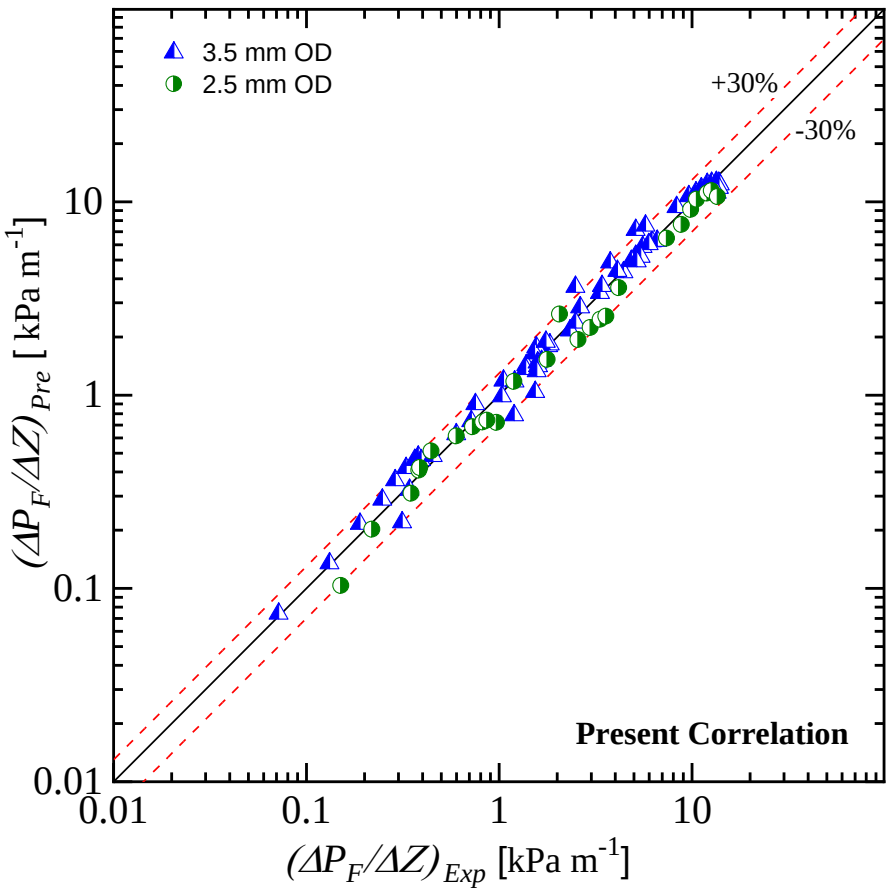

Fig. 3.8. Comparison of frictional pressure drop present and previous experimental data with present correlation

Furthermore, the newly developed frictional pressure drop correlation was also validated with other available data from other studies (Diani et al., 2018b, 2018a, 2015; Ding et al., 2009; Jige and Inoue, 2019; Kuo and Wang, 1996; Mancin et al., 2014; Singh and Kukreja, 2018) with a total of 699 data points. The comparison of developed correlation with two-phase frictional drop experimental data of microfin tubes from other researchers was shown in **Fig. 3.9** and **Table 3.6**. The data used for validation has been conducted for various working fluids R1234yf, R1234ze(E), R410A, R32, R22, R407C and R134a, the mass velocity range of 100 kg $m^{-2}s^{-1}$ to 1000 kg $m^{-2}s^{-1}$ with covered the microfin tube outside diameter of 2.5 mm to 9.52 mm. The proposed correlation shows good agreement with the present experimental data and data from other researchers aforementioned previously.

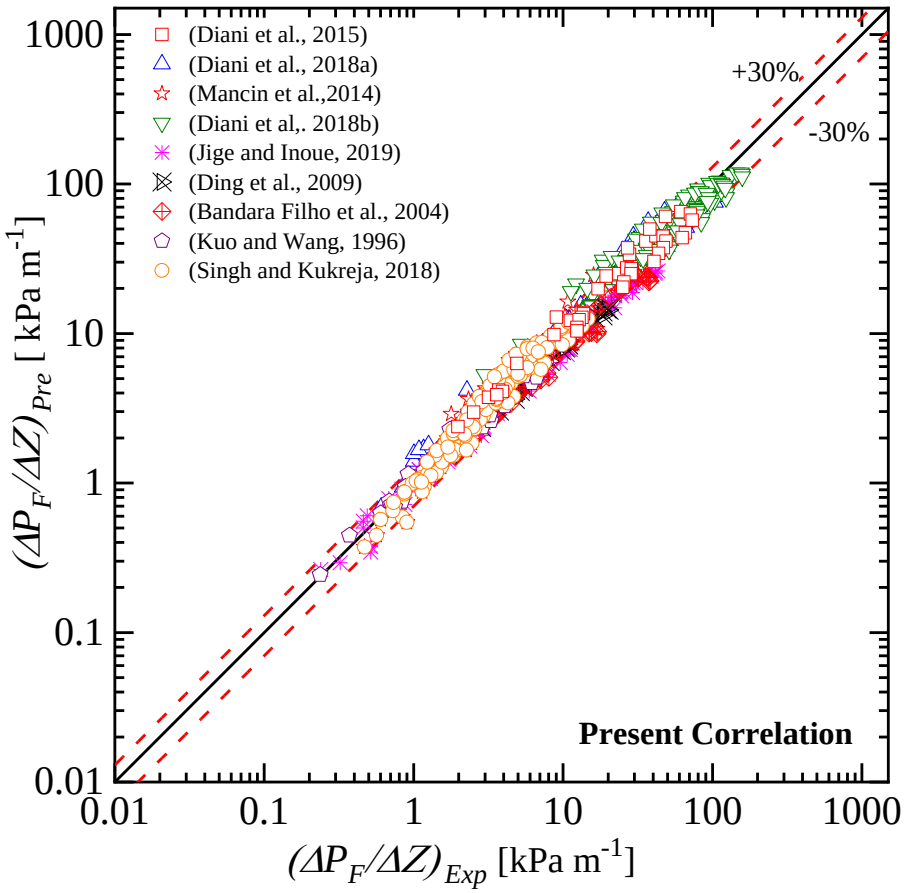

Figure 3.9. Comparison of present correlation with other researcher's data.

Table 3.6. Two-phase frictional pressure data for the proposed correlation validation.

Author (s)	d_o [mm]	Fluids	G [kgm^{-2}s^{-1}] /T_{sat} [^{o}C]	Test mode / test data	AD [%]	MD [%]	R30 [%]
(Diani et al., 2015)	4.0	R1234yf	190-940 / 30	Boiling/ 41	2.6	15.5	90.2
(Diani et al., 2018b)	4.0	R1234ze(E)	100-1000 / 30, 40	Condensation /121	9.9	17.1	85.1
(Mancin et al., 2014)	4.0	R134a	190-755 /30	Boiling /34	4.8	21.1	82.4
(Diani et al., 2018a)	3.0	R1234yf, R1234ze(E), R134a	300-1000 / 30, 40	Condensation / 180	0.5	15.9	88.9
(Jige and Inoue, 2019)	2.5, 3.0, 3.5	R32	100-400 / 15	Adiabatic / 93	-13.2	17.0	86.0
(Ding et al., 2009)	5.0	R410A	200-400 / 5	Boiling / 24	-18.8	18.8	100
(Bandarra Filho et al., 2004)	7.0	R134a	200-500 / 5	Boiling / 42	-23.9	23.9	71.4
(Kuo and Wang, 1996)	9.52	R22, R407C	100-300/ P 0.6 MPa	Adiabatic / 25	-0.9	12.8	96.0
(Singh and Kukreja, 2018)	9.52	R134a, R410A	200-600 /35, 40	Condensation / 139	5.3	14.6	88.5

3.5. Conclusion

The two-phase frictional pressure drop experiments of R1234yf in microfin with outer diameter 3.5 mm have been conducted in this study at saturation temperature of 20 °C and 30 °C, mass velocity from 50 kg m^{-2}s^{-1} to 300 kg m^{-2}s^{-1}, and vapor quality 0.1-0.9. The previous data with the 2.5 mm outer diameter microfin tube was added for further analysis.

The effects of mass velocity, vapor quality, saturation temperature, and diameter of microfin were analyzed. As a whole, the increase of frictional pressure drop was

observed with the decrease of microfin diameter. The smaller diameter of the microfin tube leads to the increase of shear stress due to the increase of velocity gradients. Further, the increasing vapor shear stress and friction between liquid and vapor phase at higher mass velocity and vapor quality increase the pressure drop.

Some existing correlations of microfin tubes were used to assess the two-phase frictional pressure drop of experimental data. The previous correlations cannot well predict the experimental data. A new correlation was developed and the proposed correlation expressed the experimental data of 3.5 mm OD and 2.5 mm OD very well with a mean deviation of 12.2 %, average deviation of -0.6 %, and 92.3 % of the data points are within the deviation of 30%. Validation of the new correlation with 699 data points from other researchers gave good agreement with approximately 17.6 % of mean deviation. The newly developed correlation could broadly be applied to the microfin tube diameter of 2.5 mm to 9.52 mm and the wide range of mass velocity and several refrigerants.

Reference

Afroz, 2008. Prediction Method of Single-phase and Two-phase Pressure Drop inside Microfin Tubes Hasan Mohammad Mostofa Afroz Prediction Method of Single-phase and Two-phase Pressure Drop inside Microfin Tubes.

Baker, O., 1953. Design of pipelines for the simultaneous flow of oil and gas. Soc. Pet. Eng. - Fall Meet. Pet. Branch AIME, FM 1953. https://doi.org/10.2118/323-g

Barnea, D., Luninski, Y., Taitel, Y., 1983. Flow pattern in horizontal and vertical two phase flow in small diameter pipes. Can. J. Chem. Eng. 61, 617–620. https://doi.org/10.1002/cjce.5450610501

Bashar, M.K., Nakamura, K., Kariya, K., Miyara, A., 2020a. Condensation heat transfer of R1234yf in a small diameter smooth and microfin tube and development of correlation. Int. J. Refrig. 120, 331–339. https://doi.org/10.1016/j.ijrefrig.2020.09.002

Bashar, M.K., Nakamura, K., Kariya, K., Miyara, A., 2020b. Development of a correlation for pressure drop of two-phase flow inside horizontal small diameter smooth and microfin tubes. Int. J. Refrig. 119, 80–91.

https://doi.org/10.1016/j.ijrefrig.2020.08.013

Bashar, M.K., Nakamura, K., Kariya, K., Miyara, A., 2018. Experimental study of condensation heat transfer and pressure drop inside a small diameter microfin and smooth tube at low mass flux condition. Appl. Sci. 8. https://doi.org/10.3390/app8112146

Bejan, A., Kraus, A.D., 2003. Heat Transfer Handbook- Heat Exchangers, Heat Transfer Handbook.

Bellair, R.J., Hood, L., 2019. ur na. Process Saf. Environ. Prot. https://doi.org/10.1016/j.psep.2019.09.033

Belman-Flores, J.M., Rodríguez-Muñoz, A.P., Pérez-Reguera, C.G., Mota-Babiloni, A., 2017. Experimental study of R1234yf as a drop-in replacement for R134a in a domestic refrigerator. Int. J. Refrig. 81, 1–11. https://doi.org/10.1016/j.ijrefrig.2017.05.003

Bolaji, B.O., Huan, Z., 2013. Ozone depletion and global warming: Case for the use of natural refrigerant - A review. Renew. Sustain. Energy Rev. 18, 49–54. https://doi.org/10.1016/j.rser.2012.10.008

Calm, J.M., 2008. The next generation of refrigerants - Historical review, considerations, and outlook. Int. J. Refrig. 31, 1123–1133. https://doi.org/10.1016/j.ijrefrig.2008.01.013

Cavallini, A., Del Col, D., Doretti, L., Longo, G.A., Rossetto, L., 2000. Heat transfer and pressure drop during condensation of refrigerants inside horizontal enhanced tubes. Int. J. Refrig. 23, 4–25. https://doi.org/10.1016/S0140-7007(99)00032-8

Chen, L., Tian, Y.S., Karayiannis, T.G., 2006. The effect of tube diameter on vertical two-phase flow regimes in small tubes. Int. J. Heat Mass Transf. 49, 4220–4230. https://doi.org/10.1016/j.ijheatmasstransfer.2006.03.025

Cheng, L., Mewes, D., 2006. Review of two-phase flow and flow boiling of mixtures in small and mini channels. Int. J. Multiph. Flow 32, 183–207. https://doi.org/10.1016/j.ijmultiphaseflow.2005.10.001

Coleman, J.W., Garimella, S., 1999. Characterization of two-phase flow patterns in small diameter round and rectangular tubes. Int. J. Heat Mass Transf. 42, 2869–2881. https://doi.org/10.1016/S0017-9310(98)00362-7

Collier, J.G., Thome, J.R., 1994. (Oxford Engineering Science Series) John G. Collier, John R. Thome-Convective Boiling and Condensation-Clarendon Press (1994).pdf.

Dalkilic, A.S., Wongwises, S., 2009. Intensive literature review of condensation inside

smooth and enhanced tubes. Int. J. Heat Mass Transf. 52, 3409–3426. https://doi.org/10.1016/j.ijheatmasstransfer.2009.01.011

Devecioğlu, A.G., 2017. Seasonal performance assessment of refrigerants with low GWP as substitutes for R410A in heat pump air conditioning devices. Appl. Therm. Eng. 125, 401–411. https://doi.org/10.1016/j.applthermaleng.2017.07.034

Diani, A., Campanale, M., Cavallini, A., Rossetto, L., 2018. Low GWP refrigerants condensation inside a 2.4 mm ID microfin tube. Int. J. Refrig. 86, 312–321. https://doi.org/10.1016/j.ijrefrig.2017.11.011

Fujie, K., Itoh, M., Kimura, H., Application, F., Data, P., 1977. United States Patent [19].

Fukano, T., Kariyasaki, A., 1993. Characteristics of gas-liquid two-phase flow in a capillary tube. Nucl. Eng. Des. 141, 59–68. https://doi.org/10.1016/0029-5493(93)90092-N

Ghajar, A.J., 2005. Non-boiling heat transfer in gas-liquid flow in pipes - A tutorial. J. Brazilian Soc. Mech. Sci. Eng. 27, 46–73. https://doi.org/10.1590/S1678-58782005000100004

Ghiaasiaan, 2008. Two-Phase Flow, Boiling, and Condensation IN CONVENTIONAL AND MINIATURE SYSTEMS. Production 2.

Greco, A., 2008. Convective boiling of pure and mixed refrigerants: An experimental study of the major parameters affecting heat transfer. Int. J. Heat Mass Transf. 51, 896–909. https://doi.org/10.1016/j.ijheatmasstransfer.2007.11.002

Heredia-Aricapa, Y., Belman-Flores, J.M., Mota-Babiloni, A., Serrano-Arellano, J., García-Pabón, J.J., 2020. Overview of low GWP mixtures for the replacement of HFC refrigerants: R134a, R404A and R410A. Int. J. Refrig. 111, 113–123. https://doi.org/10.1016/j.ijrefrig.2019.11.012

Hewitt, G.F., Taylor, N.S.H., 1970. Annular two phase flow. https://doi.org/10.1016/0017-9310(72)90222-0

Hirose, M., Ichinose, J., Inoue, N., 2018. Development of the general correlation for condensation heat transfer and pressure drop inside horizontal 4 mm small-diameter smooth and microfin tubes. Int. J. Refrig. 90, 238–248. https://doi.org/10.1016/j.ijrefrig.2018.04.014

Ichinose, J., Inoue, N., 2011. The condensation heat transfer and pressure drop of R410A and R32 inside horizontal small-diameter tubes – 2nd report: empirical

correlation for condensation heat transfer and pressure drop. Trans. JSRAE 28, 479–490.

IPCC 2007, 2007. Climate Change 2007: The Physical Science Basis. Contribution of Working Group I to the Fourth Assessment Report of the Intergovernmental Panel on Climate Change. Summary for Policymakers. (Edited by Solomon, S. DQin MManning ZChen MMarquis KAveryt MHL MS. p. 996.

Kandlikar, S.G., 2002. Two-phase flow patterns, pressure drop, and heat transfer during boiling in minichannel flow passages of compact evaporators. Heat Transf. Eng. 23, 5–23. https://doi.org/10.1080/014576302753249570

Kandlikar, S.G., Grande, W.J., 2003. Evolution of microchannel flow passages-thermohydraulic performance and fabrication technology. Heat Transf. Eng. 24, 3–17. https://doi.org/10.1080/01457630304040

Kim, N.H., 2016. Condensation heat transfer and pressure drop of R-410A in a 7.0 mm O.D. microfin tube at low mass fluxes. Heat Mass Transf. und Stoffuebertragung 52, 2833–2847. https://doi.org/10.1007/s00231-016-1789-2

Lee, Y., Jung, D., 2012. A brief performance comparison of R1234yf and R134a in a bench tester for automobile applications. Appl. Therm. Eng. 35, 240–242. https://doi.org/10.1016/j.applthermaleng.2011.09.004

Lin, P.Y., Hanratty, T.J., 1987. Effect of Pipe Diameter on Flow Patterns For Air-Water Flow in Horizontal Pipes 13, 549–563.

Mandhane, J.M., Gregory, G.A., Aziz, K., 1974. A Flow Pattern Map for Gas-Liquid Flow in Horizontal Pipes. J. Multiph. Flow 1, 537–553.

Massoud, M., 2005. Engineering Thermofluids, Engineering Thermofluids. https://doi.org/10.1007/b138870

McLinden, M.O., Kazakov, A.F., Steven Brown, J., Domanski, P.A., 2014. A thermodynamic analysis of refrigerants: Possibilities and tradeoffs for Low-GWP refrigerants. Int. J. Refrig. 38, 80–92. https://doi.org/10.1016/j.ijrefrig.2013.09.032

Mehendale, S.S., Jacobi, A.M., Shah, R.K., 2000. Fluid flow and heat transfer at micro- and meso-scales with application to heat exchanger design. Appl. Mech. Rev. 53, 175–193. https://doi.org/10.1115/1.3097347

Mishima, K., Hibiki, T., 1996. Some characteristics of air-water two-phase flow in small diameter vertical tubes. Int. J. Multiph. Flow 22, 703–712. https://doi.org/10.1016/0301-9322(96)00010-9

Mota-Babiloni, A., Makhnatch, P., Khodabandeh, R., 2017. Recent investigations in

HFCs substitution with lower GWP synthetic alternatives: Focus on energetic performance and environmental impact Adrián. Int. J. Refrig. 82, 288–301. https://doi.org/10.1016/j.ijrefrig.2017.06.026

Oya, T., 1971. Upward liquid flow in small tube into which air streams (1st report, Experimental apparatus and flow patterns. Bull. JSME 14, 1320–1329.

Perez, H., 2008. Hernandez Perez, Valente (2008) Gas-liquid two-phase flow in inclined pipes. PhD thesis, University of Nottingham.

Qi, Z., 2015. Performance improvement potentials of R1234yf mobile air conditioning system. Int. J. Refrig. 58, 35–40. https://doi.org/10.1016/j.ijrefrig.2015.03.019

Qi, Z., 2013. Experimental study on evaporator performance in mobile air conditioning system using HFO-1234yf as working fluid. Appl. Therm. Eng. 53, 124–130. https://doi.org/10.1016/j.applthermaleng.2013.01.019

Shen, B., Li, Z., Gluesenkamp, K.R., 2022. Experimental study of R452B and R454B as drop-in replacement for R410A in split heat pumps having tube-fin and microchannel heat exchangers. Appl. Therm. Eng. 204, 117930. https://doi.org/10.1016/j.applthermaleng.2021.117930

Taitel, Y., Dukler, A.E., 1976. A model for predicting flow regime transitions in horizontal and near horizontal gas-liquid flow. AIChE J. 22, 47–55. https://doi.org/10.1002/aic.690220105

Tong, L.., Tang, Y.., 1997. Boiling Heat Transfer and Two-Phase.

Tran, N., Kasireddy, R.V., Wang, C.C., 2021. An experimental investigation on convective boiling heat transfer of R-454B with lubricant oil of POE-32 or POE-68 mixture in a horizontal smooth tube. Int. J. Heat Mass Transf. 181, 121990. https://doi.org/10.1016/j.ijheatmasstransfer.2021.121990

UNEP, 2016. The Kigali Amendment to the Montreal Protocol: HFC Phase-down. OzonAction Fact Sheet 1–7.

Webb, R.L., Kim, N.-H., 2004. Principles of enhanced heat transfer. https://doi.org/10.1016/0301-9322(95)90005-5

Wongwises, S., Pipathattakul, M., 2006. Flow pattern, pressure drop and void fraction of two-phase gas-liquid flow in an inclined narrow annular channel. Exp. Therm. Fluid Sci. 30, 345–354. https://doi.org/10.1016/j.expthermflusci.2005.08.002

Yang, C.Y., Shieh, C.C., 2001. Flow pattern of air-water and two-phase R-134a in small circular tubes. Int. J. Multiph. Flow 27, 1163–1177.

https://doi.org/10.1016/S0301-9322(00)00070-7

Zhao, L., Zeng, W., Yuan, Z., 2015. Reduction of potential greenhouse gas emissions of room air-conditioner refrigerants: A life cycle carbon footprint analysis. J. Clean. Prod. 100, 262–268. https://doi.org/10.1016/j.jclepro.2015.03.063

CHAPTER

4

EXPERIMENTAL INVESTIGATION ON CONDENSATION HEAT TRANSFER OF REFRIGERANT R1234YF IN HORIZONTAL MICROFIN TUBE AND DEVELOPMENT CORRELATION

Publications of this chapter

(1) Mainil, A. K., Sakamoto, N., Ubudiyah, H., Kariya, K., & Miyara, A. (2022). Experimental Investigation on Condensation Heat Transfer of Refrigerant R1234yf in Horizontal Microfin Tube. *Transaction of the Japan Society of Refrigeration and Air Conditioning Engineers*, *39*(2)

4.1Introduction

The world energy demand for running refrigeration and air conditioning (AC) systems has been growing fast in recent decades in line with improving society's living standards. However, this development is followed by several environmental problems, such as ozone depletion and climate change. International stakeholders have taken severe actions to suppress those drawbacks. The amendment of Kigali on the Montreal protocol in 2016 regulated the minimalization of hydrofluorocarbon (HFCs) production and consumption (UNEP, 2016). Some AC manufacturers comply with the regulation by gradually substituting the high global warming potential (GWP) refrigerants with low GWP refrigerants. Currently, Low GWP refrigerants R32 has broadly applied as a refrigerant for residential AC, and R1234yf with zero ODP and low GWP is a prominent alternative to replacing R134a, which is widely used as mobile AC. The

direct replacement of R1234yf to R134a is possible due to both substances similar thermo-physical properties, as proved by several experiments (Belman-Flores et al., 2017; Lee and Jung, 2012; Qi, 2015, 2013).

Moreover, the recent advanced method for improving heat transfer performance and reducing the charge of refrigerants is carried out by employing the mini diameter tube instead of the large diameter. The use of refrigerant flammability safety group of refrigerants such as R1234yf in the AC system has strict consideration for maximum charge utilization. The application of a small diameter tube is beneficial in this situation. Moreover, small diameter microfin tubes can significantly reduce the refrigerant charge. The diameter microfin tube of 4 and 5 mm has been used widely and many reports to understand some refrigerants' two-phase heat transfer behavior (Diani et al., 2018b; Hirose et al., 2018; Ichinose and Inoue, 2011; Li et al., 2012; Son and Oh, 2012; Zhang et al., 2018). However, this far, the condensation heat transfer reports in small diameter microfin tubes using R1234yf with tube diameter less than 4 mm are still limited.

Some literature evaluated the heat transfer coefficient of R1234yf using microfin tubes in small diameter tubes, (Diani et al., 2017) reported an experimental result of R1234yf condensation inside a 3.4 mm ID horizontal microfin tube. The experiment showed that the heat transfer coefficient increases when mass velocity and vapor quality increase. The condensation behavior in the smaller tube (2.4 mm ID) has been carried out (Diani et al., 2018a) using a low GWP refrigerant including R1234yf. The experimental heat transfer coefficient and pressure drop were also compared against calculated values predicted by existing empirical correlations besides investigating the heat transfer characteristics. Our research group (Bashar et al., 2020) investigated the condensation heat transfer coefficient of R1234yf in a 2.5 mm outer diameter smooth and microfin tube and developed new correlations for the smooth tube.

In this present research, condensation heat transfer characteristics of R1234yf were investigated experimentally in 3.5 mm OD of microfin tubes. The experiments were carried out at saturation temperatures of 20°C and 30°C, and mass velocity was varied from 50, 100, and 200 kg $m^{-2}s^{-1}$. The effect of mass velocity, vapor quality, and saturation temperature on condensation heat transfer coefficient was investigated. Besides, experimental data of 3.5 mm OD was compared with published data of 2.5 mm OD to determine the effect of microfin tube diameter. The existing empirical correlations of the heat transfer coefficients for microfin tubes from the literature were

used to predict the heat transfer coefficient's value, which was then compared with the experimental data obtained.

4.2 Experimental Apparatus And Data Reduction

4.2.1. Experimental Apparatus

The experiments were carried out using an experimental facility to investigate the condensation heat transfer of R1234yf in microfin tubes. The detail of the test facility is illustrated in Fig.2.1 A Coriolis mass flow meter, a cooler, an accumulator, a cooling/heating water loop, three mixing chambers, two preheaters, test sections, and a data logger were all part of the experimental setup.

The liquid refrigerant will flow through the mixing chamber, preheaters, sight glass, test section, accumulator, and cooler on its way to the cooler. The refrigerant is continuously pumped from the cooler into the device to keep the process cycle running. Refrigerant enthalpy was controlled in the first and second preheaters, respectively. After crossing the test section, the refrigerant flows through the cooler and is completely subcooled by brine. An accumulator is employed to maintain the system pressure. The mass flow rate is determined in the Coriolis mass flow meter. Three mixing chambers are placed in different locations to measure the pressure and temperature of the refrigerant. Thermocouples are used to measure the temperature of the refrigerant and the tube wall. A data logger records all measurement variables. All refrigerant lines in the test section are insulated to maintain the system temperatures. The thermophysical properties of refrigerant are obtained from REFPROP 10.0a (Lemmon et al., 2018)[j].

Fig. 2.2 displays the test section in detail. It has a total length of 852 mm and an effective heat transfer length of 744 mm and is composed of two headers, three cooling water channels, and three sub-sections. The wall temperature is measured using 12 T-type thermocouples installed on the test section's wall. The outside diameter of microfin test tube is 3.5 mm.

Fig. 2.7 shows the photography and schematic view of the microfin tube. The microfin test tube parameters are equivalent diameter (d_{eq}) is 3.18 mm, tube wall thickness (δ) is 0.15 mm, fin height (h) is 0.10 mm, helix angle (θ) is 10º, apex angle (γ) is 35º, the number of fins (n_f) is 25 and expansion ratio (η) is 1.36. The diameter indicates the equivalent diameter (d_{eq}) in the figure with the help of the dashed line. The

expansion ratio (η) is the ratio of wet edge length and wet edge length (without fins). The experiments are conducted by varying the mass velocity from 50 kg $m^{-2}s^{-1}$ to 200 kg $m^{-2}s^{-1}$. Heat fluxes range from 7 to 20 kW m^{-2}, vapor quality varies from 0 to 1 at saturation temperature of 20 ºC and 30 ºC, as shown in Table 4.1. The thermophysical properties of R1234yf used in the experiment are shown in Table 4.2.

Table 4.1. Experimental conditions.

Parameter	Condition
Refrigerant	R1234yf
Mass velocity [kg m^{-2} s^{-1}]	50 – 200
Vapor quality [-]	0 – 1
Heat flux [kW m^{-2}]	7 – 20
Saturation Temperature [ºC]	20, 30

Table 4.2. Thermophysical properties of R1234yf (Lemmon et al., 2018)

T_{sat} [ºC]	ρ_l [kg m^{-3}]	ρ_v [kg m^{-3}]	$\frac{\rho_l}{\rho_v}$	μ_l [μPa-s]	μ_v [μPa-s]	$\frac{\mu_l}{\mu_v}$	λ_l [mW $m^{-1}K^{-1}$]	σ [mN m^{-1}]
20	1109.9	32.80	33.84	162.26	11.17	14.52	65.08	6.80
30	1073.3	43.73	24.54	143.97	11.67	12.32	62.02	5.56

4.2.2. Data Reduction

The local condensation heat transfer coefficient during condensation is determine by the Eq. (4.1).

$$\alpha = \frac{Q_{\text{wat(i)}}}{\pi d_{\text{eq}} Z_{\text{(i)}} \left(T_{r\text{(i)}} - T_{\text{wi(i)}} \right)} \tag{4.1}$$

Where Q_{wat}, d_{eq}, and $Z_{\text{(n)}}$ are the heat transfer rate of the water side of each sub-section, the equivalent diameter of the test tube (microfin) and the length of local point, respectively.

T_{r} is refrigerant temperature that estimated from the measure refrigerant pressure, and T_{wi} is temperature of the inner wall of the test tube. The heat transfer rate amount of water side of each sub section can be calculated by Eq. (4.2).

$$Q_{\mathrm{wat(i)}} = m_{\mathrm{wat}} \left(h_{\mathrm{wat(i)}} - h_{\mathrm{wat(i)}} \right) \tag{4.2}$$

In this case, the calculation of the microfin tube uses an equivalent diameter. The equivalent diameter (d_{eq}) is determined by Eq. (4.3).

$$d_{\mathrm{eq}} = \sqrt{\frac{4A_{\mathrm{c}}}{\pi}} \tag{4.3}$$

The test tube's inner wall temperature is calculated from the measured temperature of the test tube is outside the wall surface by the one-dimensional equation of heat conduction Eq. (4.4).

$$T_{\mathrm{wi(i)}} = T_{\mathrm{wo(n)}} + \frac{Q_{\mathrm{wat(i)}} \ln\left(\frac{d_{\mathrm{o}}}{d_{\mathrm{eq}}} \right)}{2\pi Z_{\mathrm{(i)}} \lambda_{\mathrm{tube}}} \tag{4.4}$$

Where, T_{wo} is the outside wall surface temperature, d_{o} is the outside diameter of the test tube, and λ is the thermal conductivity.

Local enthalphy is calculated by Eq. (4.5), and the vapor quality of refrigerant is calculated by Eq. (4.6).

$$h_{\mathrm{(i)}} = h_{\mathrm{(i\text{-}1)}} - \left(\frac{Q_{\mathrm{wat(i)}}}{m_{\mathrm{r}}} \right) \tag{4.5}$$

$$x_{\mathrm{(i)}} = \frac{h_{\mathrm{(i)}} - h_{\mathrm{l}}}{h_{\mathrm{v}} - h_{\mathrm{l}}} \tag{4.6}$$

Where $h_{\mathrm{(n)}}$ is the local enthalpy of refrigerant at each wall thermocouple point of the test tube, h_{l} and h_{v} are the saturated liquid and vapor enthalpy of refrigerant, respectively.

Specific measurement instruments, such as a thermocouple, are necessary to determine the heat transfer coefficient. The uncertainty analysis of the heat transfer coefficient is carried out using the fundamental equation of condensation heat transfer and the JCGM 100 method (JCGM 100, 2008), which considers measuring instruments' accuracy. Eq. (4.7) determines the condensation heat transfer coefficient's uncertainty,

varying from 1.05% to 26.22%.

$$U\alpha_{\exp} = \left\{ \left(Uq \frac{\partial \alpha_{\exp}}{\partial q} \right)^2 + \left(UT_{\mathrm{r}} \frac{\partial \alpha_{\exp}}{\partial T_{\mathrm{r}}} \right)^2 + \left(UT_{\mathrm{wi}} \frac{\partial \alpha_{\exp}}{\partial T_{\mathrm{wi}}} \right)^2 \right\}^{0.5} \tag{4.7}$$

4.3Heat Transfer Coeffecient Models Used in the Present Study

4.3.1. Kedzierski and Goncalves (1999) Correlation

Kedzierski and Goncalves (Kedzierski and Goncalves, 1999) was presented local convective-condensation measurements using four refrigerants: R134a, R410A (R32/R125, 50%/50% of mass), R32 and R125 in a microfin tube. For this geometry, the cross-sectional area was 60.8 mm^2 with an equivalent diameter of 8.8 mm. The hydraulic diameter (D_{h}) of the microfin tube was estimated to be 5.45 mm. The experimental condition of mass velocity are 57 – 552 kg m^{-2}s^{-1}. The expansion ratio of microfin tube (η) is 1.6, h = 0.2 mm, n_{f} = 60, θ = 18$^{\mathrm{o}}$, γ = 50$^{\mathrm{o}}$. The specification of tube is also summarized in table 4.3

Kedzierski and Goncalves used hydraulic diameter to improve the correlation prediction accuracy of heat transfer microfin tube in Eq. (4.8).

$$Nu = \frac{h_{2\phi} D_{\mathrm{h}}}{k_{\mathrm{l}}} = 4.94 Re^{0.235} Pr^{0.308} \left(\frac{P}{P\mathrm{c}} \right)^{-1.16x^2} \left(-\log 10 \frac{P}{P\mathrm{c}} \right)^{-0.887x^2} Sv^{2.708x} \tag{4.8}$$

Where the Reynold number (*Re*), the Prandtl number (*Pr*), the reduced pressure (*P*/*P*c), the dimensionless specific volume (*S*v) and the quality (*x*) are all evaluated locally at the saturated condition. Hydraulic diameter of the microfin tubes is defined as:

$$D_{\mathrm{h}} = \frac{4A_{\mathrm{c}} \cos \alpha}{N_{\mathrm{f}} S} \tag{4.9}$$

Where S is the one fin perimeter, N_{f} is the number of fins, A_{c} is the cross-sectional flow area and α is the helix angle of the fin. The convective condensation heat transfer coefficient ($h_{2\phi}$) is defined as:

$$h_{2\phi} = \frac{q''}{T_{\mathrm{r}} - T_{\mathrm{w}}} \tag{4.10}$$

Where $q^{"}$ is the heat flux to microfin tube, T_r is the refrigerant temperature, and T_w is the measured wall temperature.

4.3.2. Koyama and Yonemoto (2006) Correlation

Koyama and Yonemoto (Koyama and Yonemoto, 2006) developed a new correlation for heat transfer coefficient of pure refrigerant in microfin tube using experimental data and supplemented with from other researchers' data. The correlation is developed by modifying the void fraction and friction coefficient by Yu and Koyama(Yu and Koyama, 1998)). The experimental conditions are d_o = 7.0 -10.0 mm, d_{eq}= 6.25-8.37 mm, h = 0.16-0.24 mm, n_f = 30-85, θ = 7-30 °, γ = 24-58 °, η = 1.5-2.27, G=100-500 kg $m^{-2}s^{-1}$ and refrigerant which is used are R22, R123 and R134a. The specification of tube is also summarized in table 4.3. The correlation for heat transfer coefficient in the microfin tube is defined in the following equation:

$$Nu = \sqrt{Nu_F{}^2 + Nu_N{}^2} \tag{4.11}$$

$$Nu_F = 2.12\sqrt{f_v}\,\Phi_v\left(\frac{\rho_l}{\rho_V}\right)^{0.1}\left(\frac{x}{1-x}\right)Re_l{}^{0.5}Pr_l{}^{0.5} \tag{4.12}$$

$$Nu_N = 1.98\left(\frac{H(\xi)}{\eta^{0.5}Bo^{0.1}}\right)\left(\frac{GaPr_l}{Ph_l}\right)^{0.25} \tag{4.13}$$

Where Nu_F is the forced convection condensation Nusselt number, Nu_N is the natural convection condensation Nusselt number, Re_l is the liquid Reynols number, Pr_l is the liquid Prandtl number. Bo, Ga, and Ph_l are the Bond number, the Galileo number and the phase change number, respectively. Which are defined as:

$$Re_l = \frac{G(1-x)d}{\mu_l} \tag{4.14}$$

$$Bo = \frac{(p-t)d\,g(\rho_l-\rho_v)}{\sigma} \tag{4.15}$$

$$Ga = \frac{g\rho_l^2 d^3}{\mu_l^2} \tag{4.16}$$

$$Ph_l = \frac{C_{pl}\left(T_{sat} - T_{wi}\right)}{\Delta h_{lv}} \tag{4.17}$$

Where P is the pitch of microfin, t is the width of microfin tip, σ is the surface tension, and Δh_{lv} is the latent heat

Additional assumptions are introduced to achieve the optimum correlation for the heat transfer coefficient in the microfin tube. Function of ϕ_v and f_v are given by Eq.4.18 and Carnavos Correlation(T.C. Carnavos, 1980)[j], respectively.

$$\Phi_v = 1 + 1.2\,Fr^{0.5} X_{tt}^{0.5} \tag{4.18}$$

$H(\xi)$ is a function that expresses the effect of a thick liquid film flowing at the bottom of the tube as the following equation:

$$H(\xi) = \xi + \left\{10\left(1-\xi\right)^{0.1} - 8\right\}\sqrt{\xi}\left(1-\sqrt{\xi}\right) \tag{4.19}$$

where ξ is the void fraction as proposed by koyama et al. (2001)(Koyama et al., 2001) that be estimated from following equation:

$$\xi = 0.81\xi_{smith} + 0.19x^{100(\rho_l/\rho_v)^{0.8}}\xi_{homo} \tag{4.20}$$

$$\xi_{homo} = \left[1 + \frac{\rho_v}{\rho_l}\left(\frac{1-x}{x}\right)\right]^{-1} \tag{4.21}$$

Where ξ_{smith} could be estimated from following equation that proposed by Smith(Smith, 1969)[j]

$$\xi_{smith} = \left[1 + \frac{\rho_V}{\rho_l}\left(\frac{1-x}{x}\right)\left(0.4 + 0.6\sqrt{\frac{\frac{\rho_l}{\rho_V} + 0.4\frac{1-x}{x}}{1 + 0.4\frac{1-x}{x}}}\right)\right]^{-1} \tag{4.22}$$

4.3.3. Inoue et al. (2008) Correlation

Inoue et al.(Inoue et al., 2008) developed a new correlation for heat transfer coefficient by considering Yu and Koyama method(Yu and Koyama, 1996). They used maximum diameter instead of inner diameter, and the experimental conditions are d_{max} = 5.85-8.46 mm, G = 200-300 kgm^{-2}s^{-1} and refrigerant which is used are R22, R134a, R123 and R410A. The formula for this correlation was taken in the report of Bashar et al. (2000)(Bashar et al., 2020). The Nusselt number (Nu) in their correlation is defined as the following equation:

$$Nu = \sqrt{Nu_F^{\,2} + Nu_B^{\,2}} \tag{4.23}$$

Where Nu_F is the forced convection condensation nusselt number, and Nu_B is the free convection condensation nusselt number. The Nu_F and Nu_B are defined as following equation:

$$Nu_F = 0.743\sqrt{f_V}\left(\frac{\Phi_V}{X_{tt}}\right)\left(\frac{\mu_l}{\mu_V}\right)^{0.1}\left(\frac{x}{1-x}\right)^{0.1} Re_l^{0.7} \tag{4.24}$$

$$Nu_B = \left(\frac{0.725}{\eta^{0.25}}\right) H(\xi)\left(\frac{Ga\,Pr_l}{Ph_l}\right)^{0.25} \tag{4.25}$$

4.3.4. Hirose et al. (2018) Correlation

Hirose et al.(Hirose et al., 2018) developed a new correlation to predict heat transfer coefficient based on Yu and Koyama correlation(Yu and Koyama, 1996)). The refrigerant mass velocity (G) varied from 100 to 400 kg m^{-2}s^{-1} and the test section inlet refrigerant temperature was maintained at 35 °C. The refrigerants used are R32, R152a, and R410. The spesification of microfin tube are; d_o=4.04 mm, d_{eq} = 3.62 mm, h = 0.18 mm, θ = 17^o, γ = 14^o, n_f = 40, η = 2.05. The specification is also summarized in table 4.3 The correlation that proposed are following equation:

$$Nu_F = 7.85\sqrt{f_v}\left(\frac{\Phi_v}{X_{tt}}\right)\left(\frac{\mu_l}{\mu_V}\right)^{0.1}\left(\frac{x}{1-x}\right)^{0.1} Re_l^{0.47};\ \text{for wavy flow area}\ \ (Fr_{so} < 20) \tag{4.26}$$

$$Nu_{\mathrm{F}} = 15.4\sqrt{f_{\mathrm{v}}}\left(\frac{\Phi_{\mathrm{v}}}{X_{\mathrm{tt}}}\right)\left(\frac{\mu_{\mathrm{l}}}{\mu_{\mathrm{v}}}\right)^{0.1}\left(\frac{x}{1-x}\right)^{0.1} Re_{\mathrm{l}}^{0.43};\ \text{for annular flow area}\left(Fr_{\mathrm{so}} > 20\right) \quad (4.27)$$

$$Nu_{\mathrm{B}} = 1.6\eta^{-0.25} Bo^{-0.2} H(\xi)\left(\frac{Ga\, Pr_{\mathrm{l}}}{Ph_{\mathrm{l}}}\right)^{0.25} \quad (4.28)$$

$H(\xi)$ is obtained from Eq. (4.19) and ξ is the void fraction from Eq. (4.20).

The Lockhart–Martinelli parameter, X_{tt}, and the two-phase pressure drop multiplier, ϕ_{v} are respectively defined as:

$$X_{\mathrm{tt}} = \left(\frac{1-x}{x}\right)^{0.9}\left(\frac{\rho_{\mathrm{v}}}{\rho_{\mathrm{l}}}\right)^{0.5}\left(\frac{\mu_{\mathrm{l}}}{\mu_{\mathrm{v}}}\right)^{0.1} \quad (4.29)$$

$$\Phi_{\mathrm{v}} = 1 + 1.55 X_{\mathrm{tt}}^{0.4} \quad (4.30)$$

The friction factor, f_{v} were obtained by Inoue and Ichinose(Inoue and Ichinose, 2012) as follows:

$$f_{\mathrm{v}} = 0.26 Re_{\mathrm{v}}\, \eta^{0.95}\left(\cos\theta\right)^{-2.8} \quad (4.31)$$

4.4 Result and Discussion

4.4.1 Effect of mass velocity, vapor quality, diameter of tube and saturation temperature on condensation's HTC.

To determine the effect of mass velocity, vapor quality, and diameter of microfin tube on heat transfer coefficient, the condensation heat transfer of horizontal test sections is measured. Three different mass velocities of 50, 100, and 200 $kgm^{-2}s^{-1}$ at saturation temperature of 20℃ were varied. The comparison of the results of this study with the previous report of our research group (Bashar et al., 2020) are carried out to evaluate the consequence of diameter application.

Fig 4.1 shows relation between heat transfer coefficient and wetness at different mass velocity using R1234yf inside 3.5 mm OD. Fig. 4.2 shows the heat transfer coefficient of refrigerant R1234yf in the microfin tube. For all mass velocity for both 3.18 mm and 2.17 mm equivalent diameter of test tube, the heat transfer coefficient decreases as the

wetness increase due to the heat transfer resistance of the liquid film increasing as condensation progresses. Furthermore, the forced convection condensation reduced when the refrigerant vapor velocity declined. Fig 4.1 also depicts the effect of mass velocities; increasing the mass velocity enhances the heat transfer coefficient because the vapor speed and thin liquid film raise; hence more turbulence exhibits in the flow inside the tube. The phenomena were similar to previous literature (Bashar et al., 2020; Rahman et al., 2018).

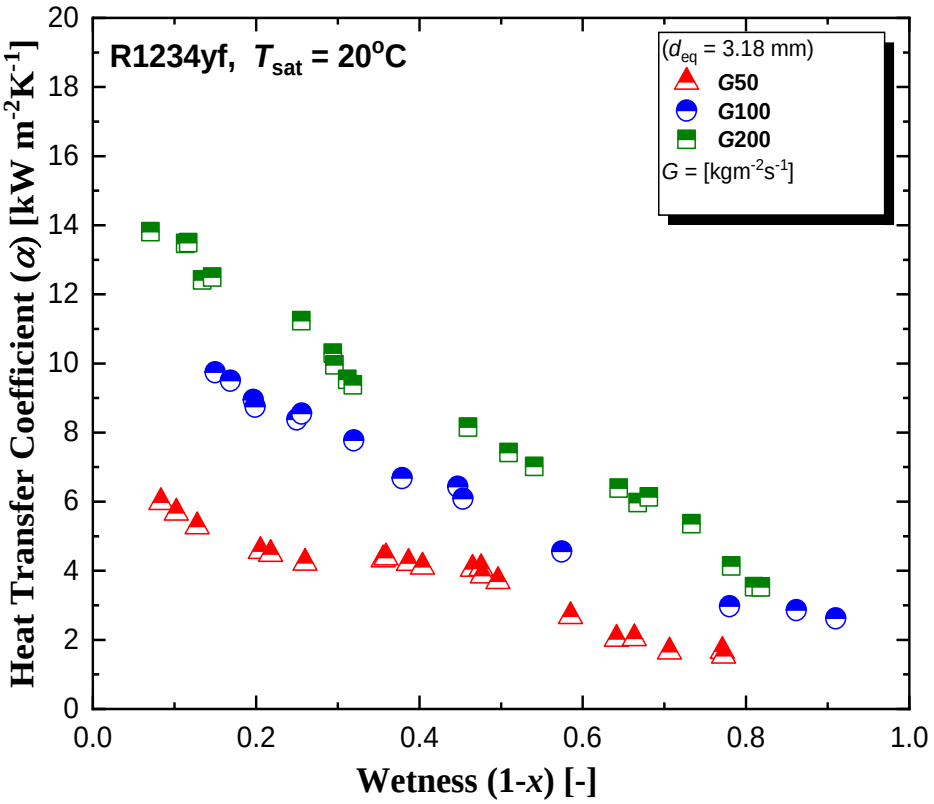

Fig. 4.1. Relation between heat transfer coefficient and wetness at different mass velocity

Fig. 4.2 also illustrates the comparison of the heat transfer coefficient trend of tube equivalent diameter of 3.18 mm to the equivalent diameter of 2.17 mm. The results show an increased heat transfer coefficient at the smaller diameter tube. The increase in the heat transfer coefficient ranges from 1.3 to 2.2 times for mass velocities ranging from 50 to 200 kg m^{-2}s^{-1}. The effects of gravity on condensation heat transfer reduce as the diameter of the test tube decreases. The effects of shear stress and surface tension become more vigorous in small diameter tubes than larger ones, making the annular

flow more probable (shear-dominated flow). A similar experimental result was also observed and confirmed by Yang et al.(Yang et al., 2019).

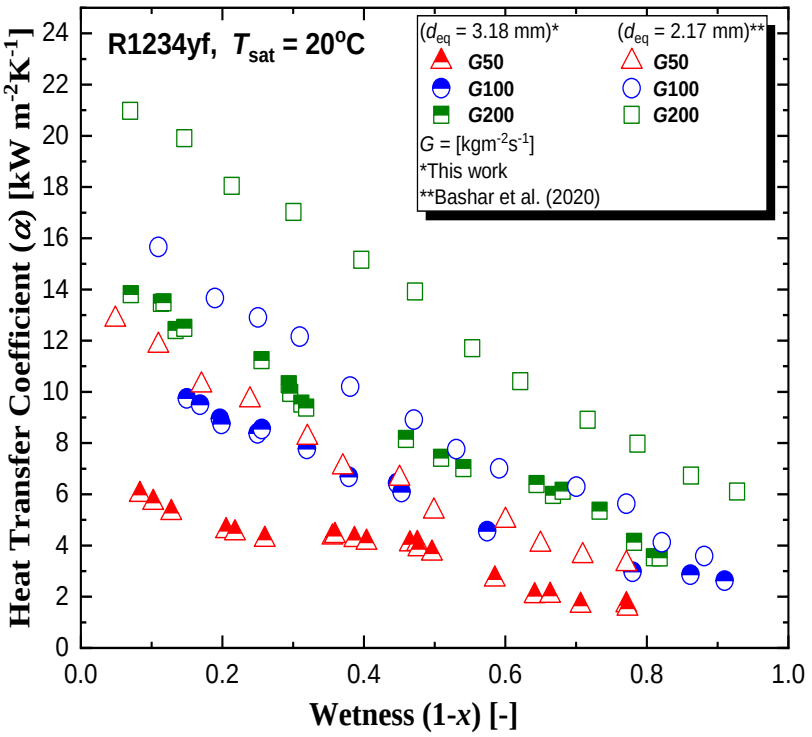

Fig. 4.2. Relation between heat transfer coefficient and wetness at different mass velocity with different tubes

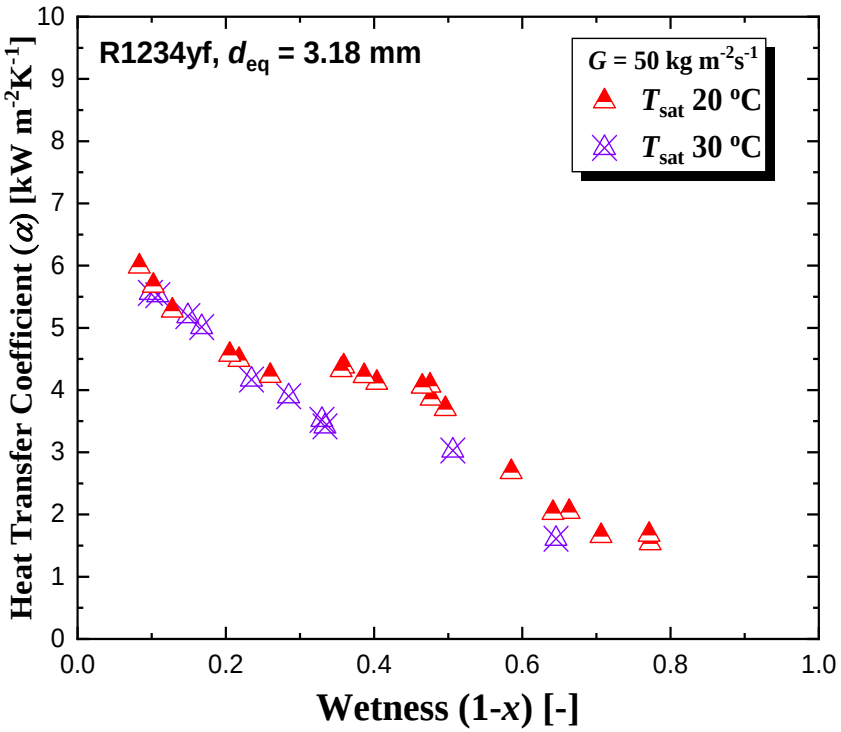

Fig. 4.3. Relation between heat transfer coefficient and wetness at different saturation temperature

The effect of saturation temperatures on heat transfer coefficient is illustrated at Fig. 4.3. Herein, two saturation temperatures were modulated at fixed mass flux of 50 kg $m^{-2}s^{-1}$. The result shows that the increase of saturation temperatures resulted in a slight decrease in heat transfer coefficient. The changing of saturation temperature leads to the shifting of thermal properties of refrigerants, as shown in Table 4.2. In details, the increase of saturation temperature resulted to the decrease viscosity and density ratio which decrease the shear stress. Moreover, the thermal conductivity and surface tension of liquid phase decrease with the increase of saturation temperature.

4.4.2. Comparison of various models for condensation HTC

Fig. 4.4 shows the comparisons of the measured heat transfer coefficient values of microfin tube and the calculated values of heat transfer coefficient by Kedzierski and Goncalves correlation(Kedzierski and Goncalves, 1999). The calculated values of heat transfer coefficient are well predicted for mass velocity 50 kg $m^{-2}s^{-1}$ within ±30%. This correlation underestimate at the high mass velocity. The average deviation (*AD*) and mean absolute deviation (*MD*) are -27.58% and 31.51%, respectively, which were calculated by Eq. (4.32) and Eq. (4.33), respectively.

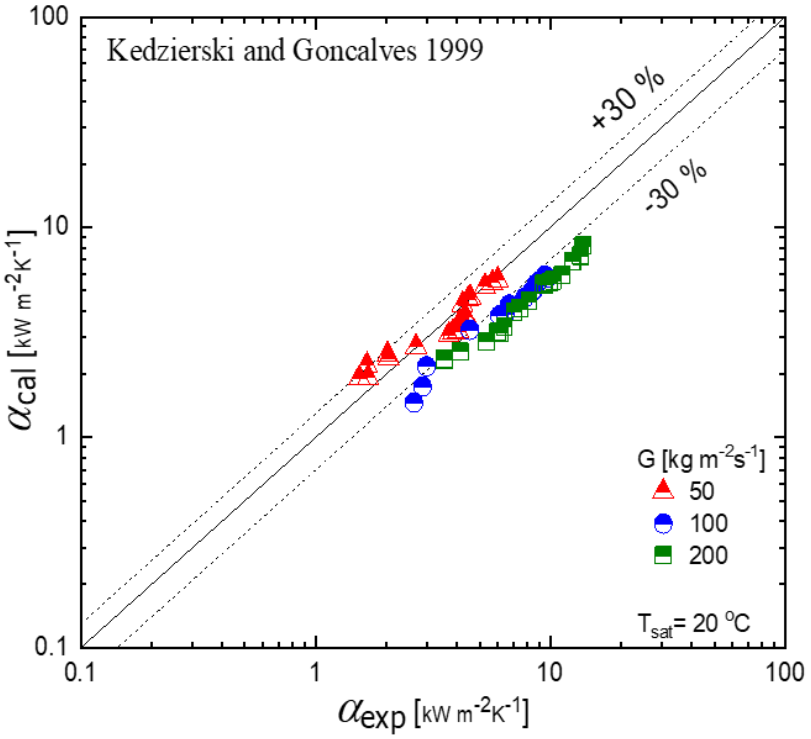

Fig. 4.4. Comparison of measured and calculated heat transfer coefficient values for the microfin tube by Kedzierski and Goncalves (1999)(Kedzierski and Goncalves, 1999)

$$AD = \frac{1}{n}\sum_{i=n}^{n}\left(\frac{\alpha_{cal}-\alpha_{exp}}{\alpha_{exp}}\right)\times 100 \tag{4.32}$$

$$MD = \frac{1}{n}\sum_{i=n}^{n}\left|\frac{\alpha_{cal}-\alpha_{exp}}{\alpha_{exp}}\right|\times 100 \tag{4.33}$$

Fig. 4.5 shows the comparisons of the measured heat transfer coefficient values of microfin tube and the calculated values of heat transfer coefficient by Koyama and Yonemoto correlation(Koyama and Yonemoto, 2006). The calculated values of heat transfer coefficient are majority not well predicted for low mass velocity 50 kg $m^{-2}s^{-1}$ with measured value. This correlation overestimate at low vapor quality of mass velocity 100 kg $m^{-2}s^{-1}$ and slightly underestimate at high vapor quality of high mass velocity 200 kg $m^{-2}s^{-1}$, while the average deviation (*AD*) and mean absolute deviation (*MD*) are 21.38% and 42.15%, respectively.

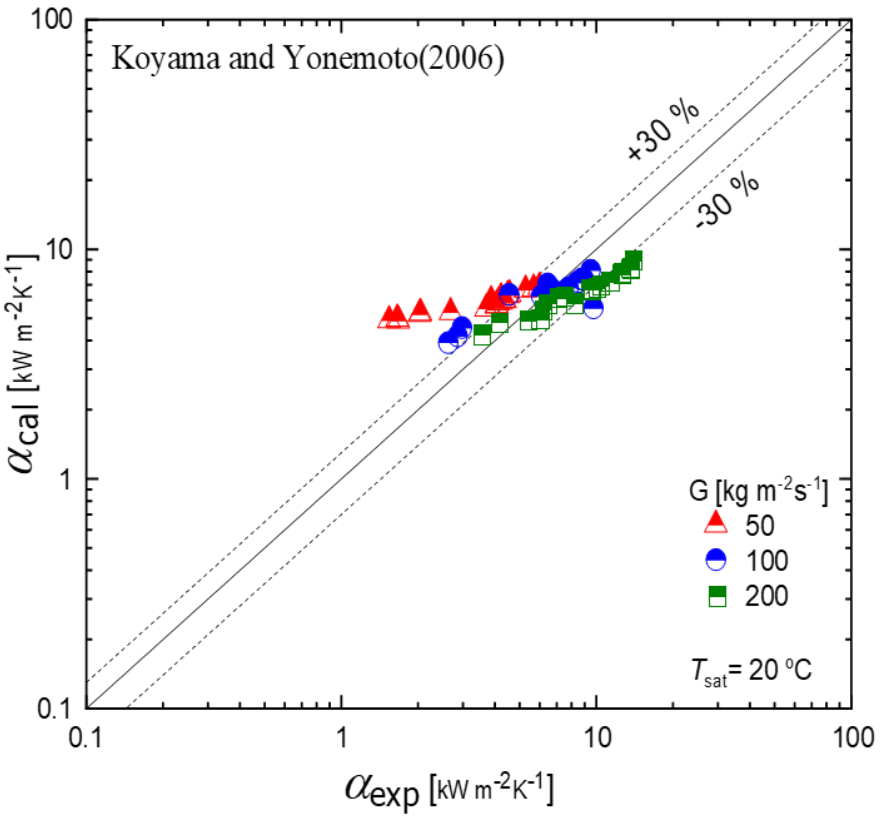

Fig. 4.5. Comparison of measured and calculated heat transfer coefficient values for the microfin tube by Koyama and Yonemoto (2006)(Koyama and Yonemoto, 2006)

The comparisons of the measured heat transfer coefficient values of microfin tube with the calculated values of heat transfer coefficient by Inoue et al. correlation (Inoue et al., 2008) is shown in Fig.4.6. The calculated values of heat transfer coefficient are not well predicted and underestimate for all mass velocity with measured value however this correlation slightly predicted and correlates within ±30% in low vapor quality of mass velocity 50 $kgm^{-2}s^{-1}$ and 100 $kgm^{-2}s^{-1}$. The average deviation (*AD*) and mean absolute deviation (*MD*) are -33.83% and 39.72%, respectively.

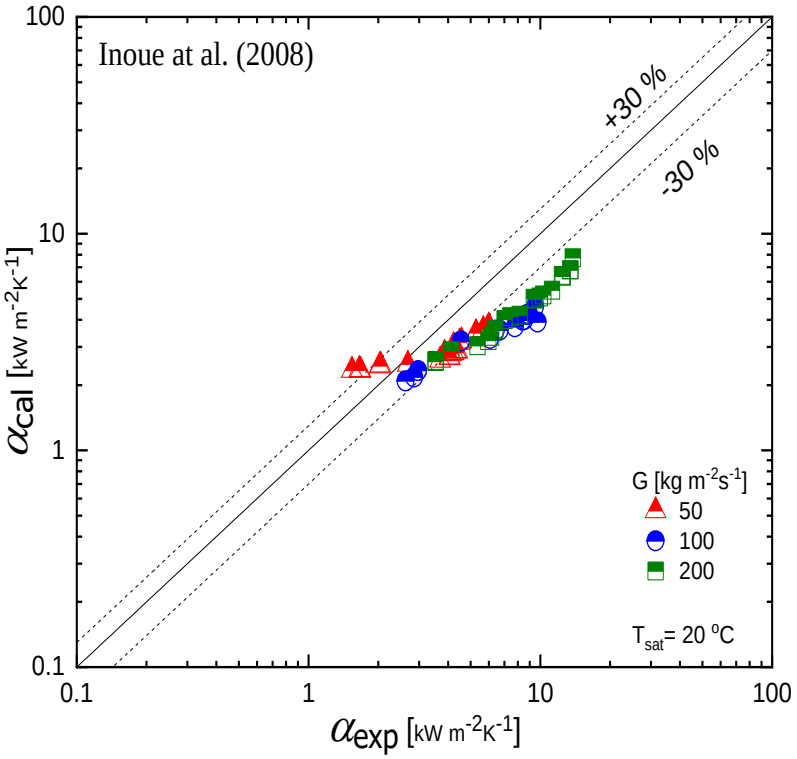

Fig. 4.6 Comparison of measured and calculated heat transfer coefficient values for the microfin tube by Inoue et al. (2008)

The comparisons of the measured heat transfer coefficient values of microfin tube with the calculated values of heat transfer coefficient by Inoue et al. correlation (Inoue et al., 2008) is shown in Fig.4.6. The calculated values of heat transfer coefficient are not well predicted and underestimate for all mass velocity with measured value however this correlation slightly predicted and correlates within ±30% in low vapor quality of mass velocity 50 $kgm^{-2}s^{-1}$ and 100 $kgm^{-2}s^{-1}$. The average deviation (*AD*) and mean absolute deviation (*MD*) are -33.83% and 39.72%, respectively.

Fig. 4.7 shows the comparisons of the measured heat transfer coefficient values of microfin tube and the calculated values of heat transfer coefficient by Hirose et al. correlation (Hirose et al., 2018). The calculated values of heat transfer coefficient are well predicted for all data of mass velocity 100 kg $m^{-2}s^{-1}$ and majority from 200$kgm^{-2}s^{-1}$ with the measured value, however, it is not well predicted as overestimate for low mass velocity 50 $kgm^{-2}s^{-1}$ and slightly overestimate at high vapor quality of mass velocity 200 $kgm^{-2}s^{-1}$. The average deviation (*AD*) and mean absolute deviation (*MD*) are 23.18% and 30.84% respectively that calculated by Eq. (4.32) and Eq. (4.33).

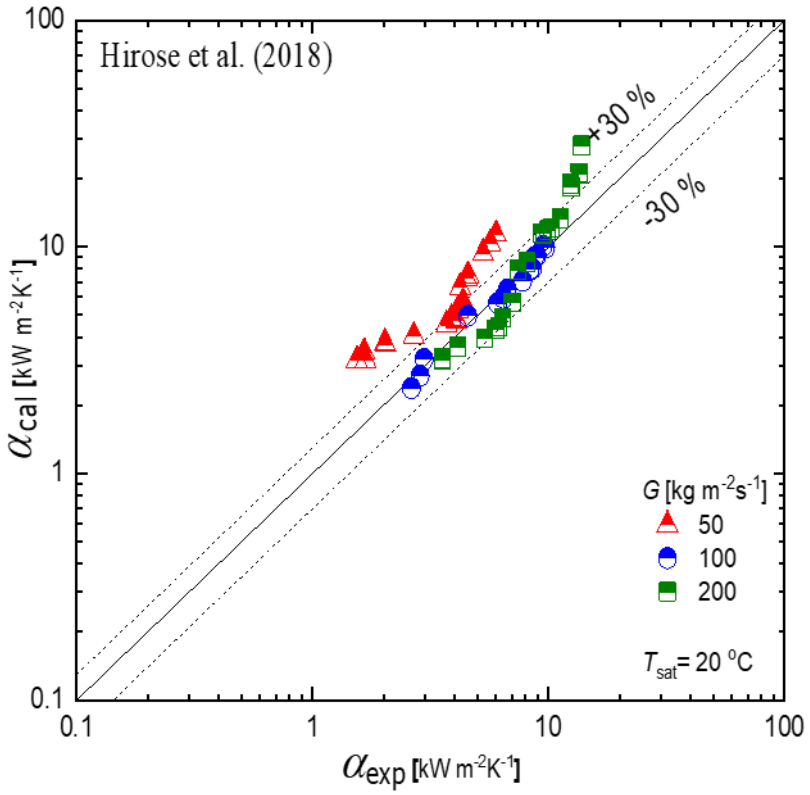

Fig. 4.7. Comparison of measured and calculated heat transfer coefficient values for the microfin tube by Hirose et al. (2018)(Hirose et al., 2018)

Fig. 4.8 shows the comparisons of the experimental heat transfer values of microfin tubes and the calculated values calculated by four correlations(Hirose et al., 2018; Inoue et al., 2008; Kedzierski and Goncalves, 1999; Koyama and Yonemoto, 2006). The correlation of Hirose et al. (2018)(Hirose et al., 2018) gives well predicted than other correlations with mean absolute deviation (*MD*) are 30.84% as shown in Table 4.4. Hirose et al. (2018) correlation is more good agreement with experimental data than other correlation.

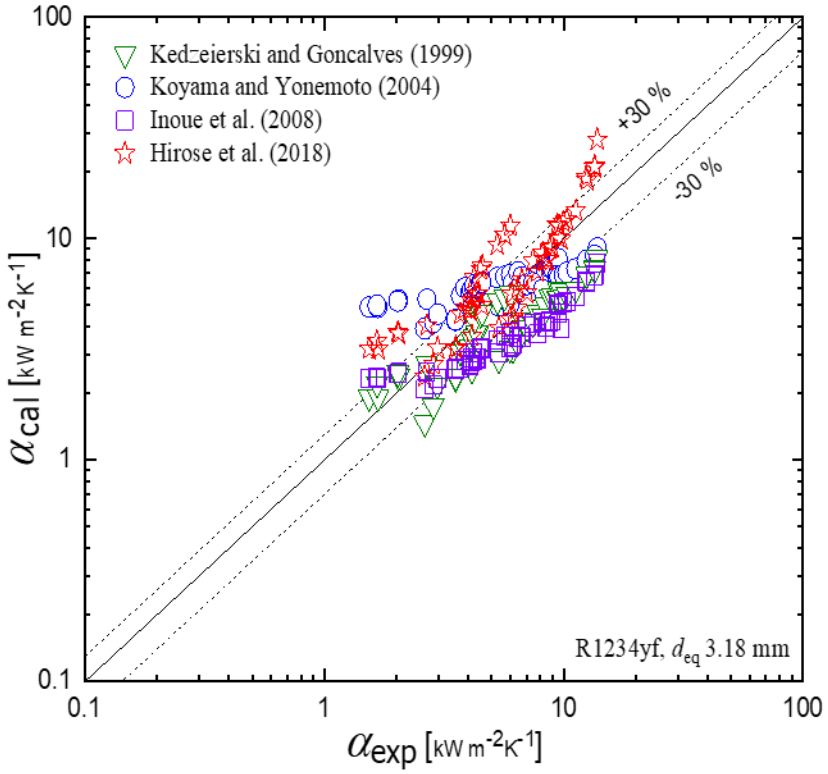

Fig. 4.8. Comparison of values of heat transfer coefficient calculated by previous correlations for microfin tubes, from Kedzierski and Goncalves (1999)(Kedzierski and Goncalves, 1999), Koyama and Yonemoto (2006)(Koyama and Yonemoto, 2006), Inoue et al. (2008)(Inoue et al., 2008)) and Hirose et al. (2018)(Hirose et al., 2018).

It uses a microfin tube whose diameter is closer to the diameter used in this study than the others. Besides, this correlation divides the forced convection calculation formula into two based on the flow regime, namely wavy flow area and annular flow area, with different formulas, respectively. However, this correlation is slightly overestimated, especially at low mass velocity. Therefore, it necessarily requires the development of new correlations of microfin tube. The considerations in developing the correlation in the future are that the Hirose et al. (2018) (Hirose et al., 2018) correlation is limited to a tube with outside diameter of 4 mm. Thus, it needs to be developed for a wide range of experimental conditions, diameter, mass velocity, and thermophysical properties that are more varied and add fin shape parameters into the correlation, such as, the fin height and the pitch or distance between the fins.

Table 4.3 Comparison specification of microfin tube

	Present study	**A**	**B**	**C**
d_{eq} **[mm]**	3.18	6.25~8.37	8.8	3.62
θ **(º)**	10	7~30	18	17
h **[mm]**	0.10	0.16~0.24	0.2	0.18
γ **[º]**	35	24~58	50	14
n_f **[-]**	25	30~85	60	40
η **[-]**	1.36	1.5~2.27	1.6	2.05

A= (Koyama and Yonemoto, 2006)

B= (Kedzierski and Goncalves, 1999)

C= (Hirose et al., 2018)

Table 4.4. Deviations of condensation heat transfer coefficient

Correlation	***AD* (%)**	***MD* (%)**
Kedzierski and Goncalves (1999)	-27.58	31.51
Koyama and Yonemoto (2006)	21.38	42.15
Inoue et al. (2008)	-33.83	39.72
Hirose et al. (2018)	23.18	30.84

4.5 Development Correlation

We tried to derive an empirical correlation to predict the heat transfer coefficients, for many kinds of refrigerants, based on (Yu and Koyama, 1996) the correlation. In their correlation, Yu and Koyama defined the Nu number as :

$$Nu = \sqrt{Nu_F^{\,2} + Nu_B^{\,2}} \tag{4.34}$$

Nu_F is the forced convection condensation Nusselt number and Nu_B is the free convection condensation Nusselt number proposed by (Yu and Koyama, 1996). Nu_B is defined as:

$$Nu_{\mathrm{B}} = \left(\frac{0.725}{\eta^{0.25}} \right) H(\xi) \left(\frac{Ga \, \mathrm{Pr_L}}{Ph_{\mathrm{L}}} \right)^{0.25} \tag{4.35}$$

Where Ga is the galileo number and Ph_L is the the phase change number.

$$Ga = \frac{g \rho_{\mathrm{L}}{}^2 d^3}{\mu_{\mathrm{L}}{}^3} \tag{4.36}$$

$$Ph_{\mathrm{L}} = \frac{Cp_{\mathrm{L}} \left(T_{\mathrm{sat}} - T_{\mathrm{wi}} \right)}{\Delta h_{\mathrm{vl}}} \tag{4.37}$$

Where $H(\xi)$ is the modification for the difference of the condensed liquid film between the inner surface of the tube and the plate wall on which the theory is suitable that proposed by (Yu and Koyama, 1996).

$$H(\xi) = \xi + \left\{ 10(1-\xi)^{0.1} - 8.9 \right\} \sqrt{\xi} - (1-\xi) \tag{4.38}$$

Where, ξ is a void fraction. In the case where microfin small-diameter tubes, ξ could be estimated from below equation, as proposed by Koyama et al. (2001).

$$\xi = 0.81 \xi_{\mathrm{smith}} + 0.19 x^{100(\rho_V/\rho_L)^{0.8}} \xi_{\mathrm{homo}} \tag{4.39}$$

$$\xi_{\mathrm{homo}} = \left[1 + \frac{\rho_{\mathrm{v}}}{\rho_{\mathrm{l}}} \left(\frac{1-x}{x} \right) \right]^{-1} \tag{4.40}$$

$\mathrm{Nu_F}$ is the forced convection condensation Nusselt number proposed by (Koyama and Yonemoto, 2006) , $\mathrm{Nu_F}$ is defined as:

$$Nu_{\mathrm{F}} = \sqrt{\frac{f_V}{2}} \, \mathrm{Re_L} \, \Phi_{\mathrm{V}} \left(\frac{\rho_{\mathrm{L}}}{\rho_{\mathrm{V}}} \right)^{0.5} \left\{ \frac{x}{1-x} \right\} \left(\frac{\mathrm{Pr_L}}{T_{\mathrm{i}}^*} \right) \tag{4.41}$$

Where Pr_{L} is the liquid Prandtl number. T_{i}^* is the dimensionless temperature difference between the vapor-liquid interface and the tube wall. Re_{L} is the liquid Reynolds number defined as:

$$\mathrm{Re_L} = G(1-x)d/\mu_\mathrm{L} \tag{4.42}$$

Where f_v is the friction factor that can be calculated by (T. C. Carnavos, 1980) equation (Eq. 4.43 – 4.44) that proposed friction factor for single-phase inside microfin tube.

$$f_\mathrm{v} = \frac{0.046}{\mathrm{Re_v^2}\, F^*} \tag{4.43}$$

$$F^* = \left(\frac{A_{fa}}{A_{fn}}\right)^{0.5} (\sec\theta)^{0.75} \tag{4.44}$$

Φ_v is two-phase pressure drop multiplier from proposed general correlation as follows:

$$\Phi_\mathrm{v}^2 = 1 + C\,\mathrm{X_{tt}^n} + \mathrm{X_{tt}^2} \tag{4.45}$$

$$C = 21\left\{1-\exp\left(-0.28Bo^{0.5}\right)\right\}\left\{1-0.7\exp\left(-0.36Fr^{0.65}\right)\right\} \tag{4.46}$$

$$n = 1-0.4\exp\left(-0.08Fr\right) \tag{4.47}$$

$\left(\mathrm{Pr}_L/T_i^*\right)$ is obtained from the following equation, by using the nusselt number Nu from Eq. 4.48. The result is Eq. 4.49

$$Nu = \frac{\alpha\, d_\mathrm{eq}}{\lambda_\mathrm{L}} \tag{4.48}$$

$$\mathrm{Pr_L}/T_\mathrm{i}^* = \frac{\left(Nu^2 - {Nu_\mathrm{B}}^2\right)^{0.5}}{\sqrt{0.5\, f_\mathrm{v}}\,\mathrm{Re_L}\,\Phi_\mathrm{v}\left(\rho_\mathrm{L}/\rho_\mathrm{V}\right)^{0.5}\left\{x/1-x\right\}} \tag{4.49}$$

It is already known that the heat transfer performance is depended on the refrigerant flow pattern. We used Solliman's modified Froude number *Fr* so to divide into the wavy flow and annular flow. (Dobson and Chato, 1998)have reported that the flow is annular when $Fr_\mathrm{so} > 20$, and wavy when $Fr_\mathrm{so} < 20$, based on experimental results

for a smooth small-diameter tube. Solliman's modified Froude number Fr_{so} is defined as follows:

$$Fr_{so} = 0.025\,\mathrm{Re}_L^{1.59}\left(\frac{1+1.09X_{tt}^{0.039}}{X_{tt}}\right)^{1.5}\frac{1}{Ga^{0.5}},\ \text{For}\ \left(Re_L \le 1250\right) \tag{4.50}$$

$$Fr_{so} = 1.26\,\mathrm{Re}_L^{1.04}\left(\frac{1+1.09X_{tt}^{0.039}}{X_{tt}}\right)^{1.5}\frac{1}{Ga^{0.5}},\ \text{For}\ \left(Re_L > 1250\right) \tag{4.51}$$

First, we obtained the correlation between ($\mathrm{Pr_L/T_i^*}$) and Re_L of the measured data at wavy flow area (Fr_{so}< 20) from (4.49), using Eqs. (4.48) and (4.35). Fig 4.9 shows the relation between ($\mathrm{Pr_L/T_i^*}$) and Re_L at wavy flow area (Fr_{so}<20). The following correlation was obtained within ±30%:

$$Pr_L/T_i^* = 1.91\mathrm{Re}_L^{-0.24} \quad \left(Fr_{so} < 20\right) \tag{4.52}$$

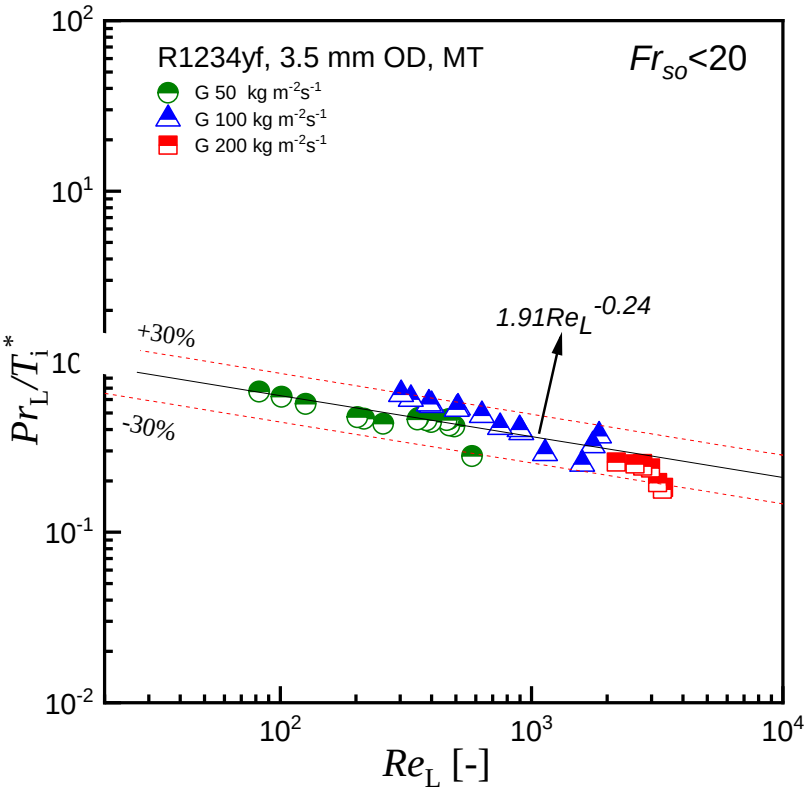

Fig 4.9. Relation between dimension less temperature difference and liquid Reynolds number for the microfin tube for *Fr*so < 20

The new correlation of forced convection Nusselt number NuF for wavy flow area (Fr_{so}< 20) was obtained from Eqs. (4.41) and (4.52) as follows:

$$Nu_F = 1.35\sqrt{f_v}\left(\Phi_V / X_{tt}\right)\left(\mu_L/\mu_V\right)^{0.1}\left\{x/1-x\right\}^{0.1}\mathrm{Re}_L^{\,0.76} \tag{4.53}$$

For small-diameter tube, it is considered that the influence of free convection condensation is large at wavy flow area, due to both buoyancy and surface tension having an effect on condensation heat transfer. Therefore, we tried to express that the effect for refrigerant using Bond number *Bo*. Nu_B is assumed by the folllowing equation:

$$Nu_B = f\left(\eta, Bo\right)H\left(\xi\right)\left(\frac{Ga\,\mathrm{Pr_L}}{Ph_L}\right)^{0.25} \tag{4.54}$$

C and n are determined by the mathematical solution, the result is as follows.

$$f\left(\eta, Bo\right) = \frac{0.5}{\eta^{0.25}Bo^{0.35}} \tag{4.55}$$

Therefore, Nu_B is express by following equation.

$$Nu_B = 0.5\eta^{-0.25}Bo^{-0.35}H\left(\xi\right)\left(Ga\,\mathrm{Pr_L}/Ph_L\right)^{0.25} \tag{4.56}$$

However, the effect of forced convection heat heat transfer is large at the annular flow area (Fr_{so}>20). Pr_L/T_i^* is obtained from Eq. (4.49), by using the Nusselt number (*Nu*) of Eq. (4.48) and the free convection condensation Nusselt number Nu_B of Eq. (4.56). Fig. 4.10 shows the relation between Pr_L/T_i^* and Re_L at the annular flow area (Fr_{so}>20). Finally, the following correlations were obtained within ±30%:

$$\mathrm{Pr}_L/T_i^* = 3.44\,\mathrm{Re}_L^{\,-0.31} \tag{4.57}$$

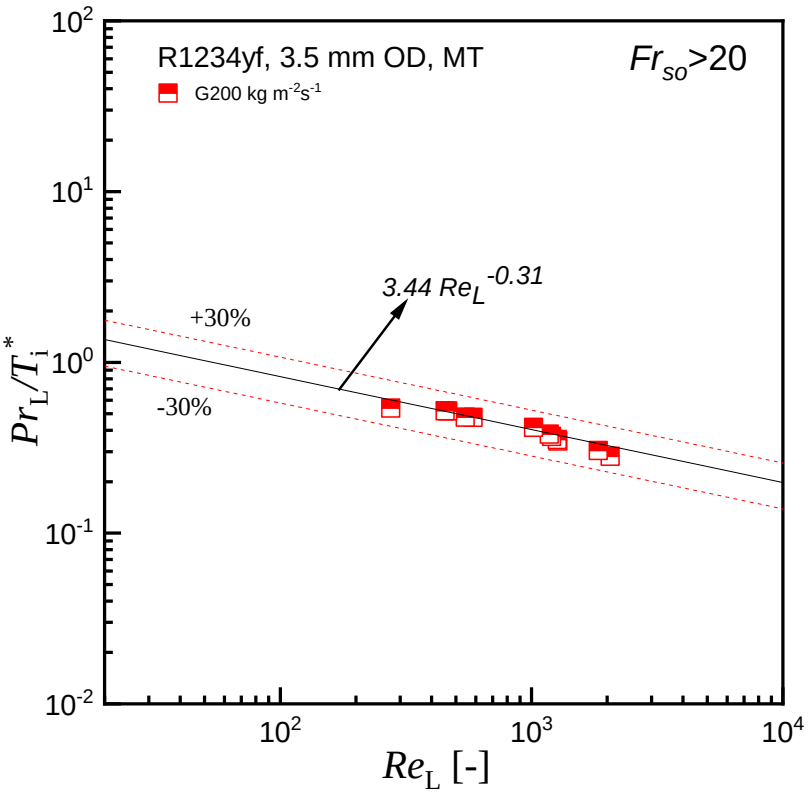

Fig. 4.10. Relation between dimension less temperature difference and liquid Reynolds number for the microfin tube for $Fr_{so} > 20$.

The new correlation of forced convection Nusselt number NuF for annular flow area ($Fr_{so} > 20$) was obtained from Eqs. (4.51) and (4.52) as follows:

$$Nu_F = 2.43\sqrt{f_v}\left(\Phi_V / X_{tt}\right)\left(\mu_L/\mu_V\right)^{0.1}\left\{x/1-x\right\}^{0.1}\mathrm{Re}_L^{\,0.69} \qquad (4.58)$$

The final form of the new correlation is presented in Table 4.5 for the sake of better understanding.

Table. 4.5 Proposed Correlation for condensation heat transfer

$$Nu = \sqrt{Nu_F^{\,2} + Nu_B^{\,2}}$$

$$Nu_F = 1.35\sqrt{f_v}\left(\Phi_V / X_{tt}\right)\left(\mu_L/\mu_V\right)^{0.1}\left\{x/1-x\right\}^{0.1}\mathrm{Re}_L^{\,0.76}, \text{ for } (Fr_{so} < 20)$$

$$Nu_F = 2.43\sqrt{f_v}\left(\Phi_V / X_{tt}\right)\left(\mu_L/\mu_V\right)^{0.1}\left\{x/1-x\right\}^{0.1}\mathrm{Re}_L^{\,0.69}, \text{ for } (Fr_{so} > 20)$$

$$Nu_B = 0.5\eta^{-0.25}Bo^{-0.35}H\left(\xi\right)\left(Ga\,\mathrm{Pr}_L/Ph_L\right)^{0.25}$$

$$\Phi_v^2 = 1 + C\,\mathrm{X}_{tt}^{n} + \mathrm{X}_{tt}^{2}$$

$$C = 21\left\{1-\exp\left(-0.28Bo^{0.5}\right)\right\}\left\{1-0.7\exp\left(-0.36Fr^{0.65}\right)\right\},\ n = 1-0.4\exp\left(-0.08Fr\right)$$

$$f_v = \frac{0.046}{\mathrm{Re}_v^2 F^*},\ F^* = \left(\frac{A_{fa}}{A_{fn}}\right)^{0.5}\left(\sec\theta\right)^{0.75}$$

$$\mathrm{X}_{tt} = \left(\frac{1-x}{x}\right)^{0.9}\left(\frac{\rho_v}{\rho_l}\right)^{0.5}\left(\frac{\mu_l}{\mu_v}\right)^{0.1}$$

$$Bo = \frac{gd^2\left(\rho_l-\rho_v\right)}{\sigma},\ \mathrm{Re}_L = \frac{G\left(1-x\right)d}{\mu_L},\ Ga = \frac{g\rho_L^{\,2}d^3}{\mu_L^{\,3}},\ Ph_L = \frac{Cp_L\left(T_{sat}-T_{wi}\right)}{\Delta h_{vl}}$$

$$Fr_{so} = 0.025\,\mathrm{Re}_L^{1.59}\left(\frac{1+1.09X_{tt}^{\,0.039}}{X_{tt}}\right)^{1.5}\frac{1}{Ga^{0.5}},\ \text{For } \left(\mathrm{Re}_L \le 1250\right)$$

$$Fr_{so} = 1.26\,\mathrm{Re}_L^{1.04}\left(\frac{1+1.09X_{tt}^{\,0.039}}{X_{tt}}\right)^{1.5}\frac{1}{Ga^{0.5}},\ \text{For } \left(\mathrm{Re}_L > 1250\right)$$

Fig. 4.11 shows the comparison between the new correlations and the measured data for microfin tubes. From the figure, it is observed that the new correlation agrees well with the measured data with average deviation and mean absolute deviation is 0.19% and 13.34%, respectively and 90.74 data points are within 30%.

Fig 4.12 (a) and (b) show the the comparison between the experimental data of (Diani et al., 2017) using microfin tube 3.4 mm ID and the present correlation. The figure shows that the trends of Diani et al.'s data well predicted using proposed correlation. However in mass velocity 200 $kgm^{-2}s^{-1}$ in low vapor quality (high wetness) region slightly overestimated.

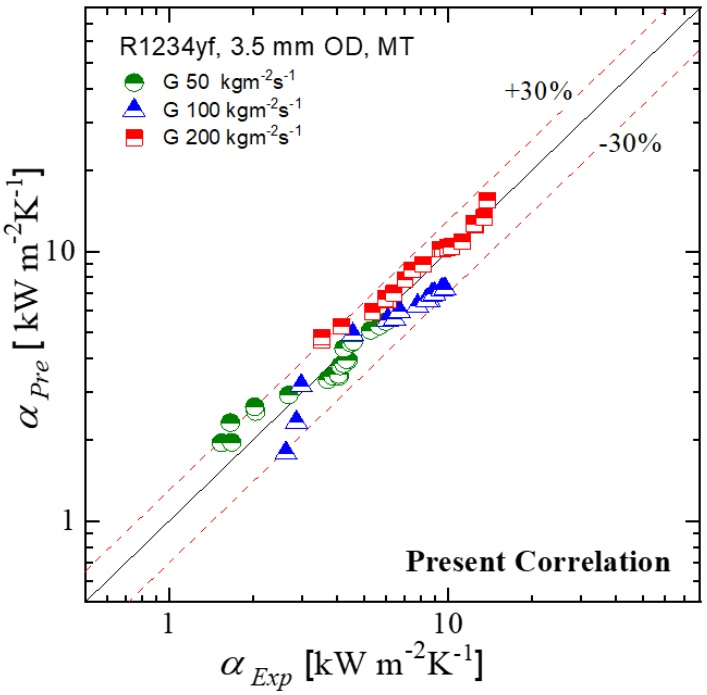

Fig. 4.11. Comparison of heat transfer coefficient between predicted by the present correlation and measured data.

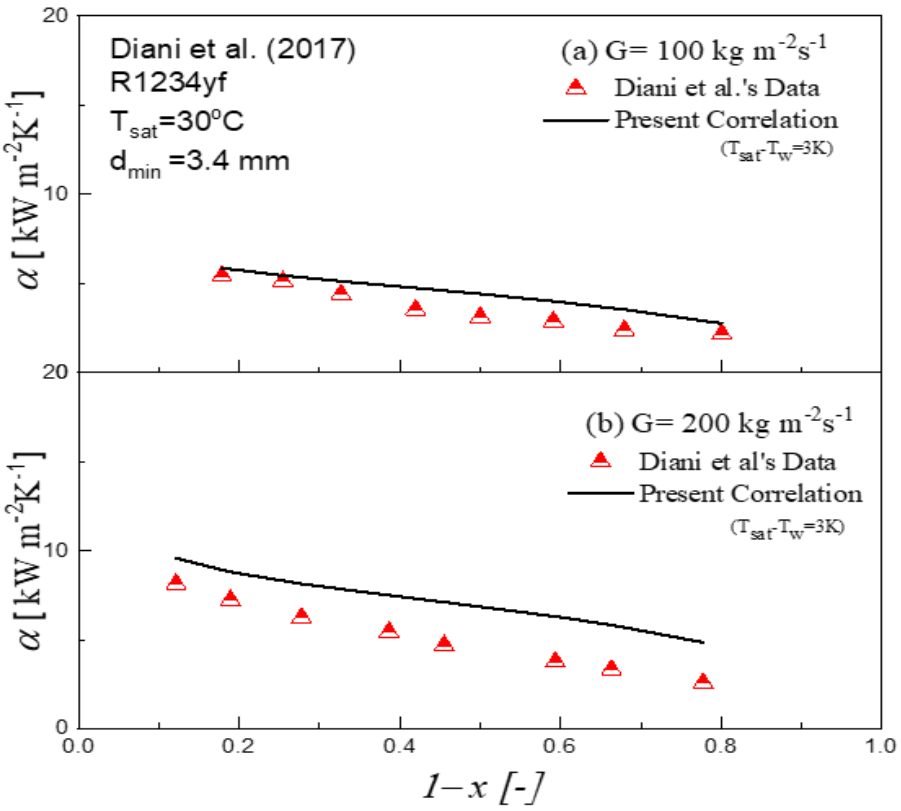

Fig. 4.12. Comparison of heat transfer coefficient between the present correlation and Diani et al. (2017)'s data

4.6Conclusion

Experimental study of condensation heat transfer coefficient of refrigerant R1234yf inside 3.5 OD horizontal microfin tube has been carried out. The effect of mass velocity, vapor quality, tube diameter, and saturation on condensation heat transfer coefficient was investigated. The results show the heat transfer coefficient decreases as the wetness increases for mass velocities of 3.18 mm and 2.17 mm equivalent diameter of the test tube. Also, the findings show that as the microfin tube's diameter is decreased, the heat transfer coefficient increases. The increase of saturation temperatures resulted in decreased heat transfer coefficient due to the refrigerant's changing thermal properties. Four correlations of the heat transfer coefficients for microfin tubes from the literature were used to predict the heat transfer coefficient. Hirose et al., 2018 correlation has good agreement with experimental data than other correlation. However, slightly overestimated, especially at low mass velocity. Therefore, the development of a new correlation of microfin tubes is required.

The new correlation for heat transfer condensation was developed. The proposed correlation agrees well with the measured data with average deviation and mean absolute deviation is 0.19% and 13.34%, respectively and 90.74% data points are within 30%.

References

Bashar, M.K., Nakamura, K., Kariya, K., Miyara, A., 2020. Condensation heat transfer of R1234yf in a small diameter smooth and microfin tube and development of correlation. Int. J. Refrig. 120, 331–339. https://doi.org/10.1016/j.ijrefrig.2020.09.002

Belman-Flores, J.M., Rodríguez-Muñoz, A.P., Pérez-Reguera, C.G., Mota-Babiloni, A., 2017. Experimental study of R1234yf as a drop-in replacement for R134a in a domestic refrigerator J.M. Int. J. Refrig. 81, 1–11. https://doi.org/10.1016/j.ijrefrig.2017.05.003

Carnavos, T.C., 1980. Heat Transfer Performance of Internal Finned Tubes in Turbulent Flow. Heat Transf. Eng. 1, 32–37.

Carnavos, T. C., 1980. Heat transfer performance of internally finned tubes in turbulent

flow. Heat Transf. Eng. 1, 32–37. https://doi.org/10.1080/01457638008939566

Diani, A., Campanale, M., Cavallini, A., Rossetto, L., 2018a. Low GWP refrigerants condensation inside a 2.4 mm ID microfin tube. Int. J. Refrig. 86, 312–321. https://doi.org/10.1016/j.ijrefrig.2017.11.011

Diani, A., Campanale, M., Rossetto, L., 2018b. Experimental study on heat transfer condensation of R1234ze(E) and R134a inside a 4.0 mm OD horizontal microfin tube. Int. J. Heat Mass Transf. 126, 1316–1325. https://doi.org/10.1016/j.ijheatmasstransfer.2018.06.047

Diani, A., Cavallini, A., Rossetto, L., 2017. R1234yf condensation inside a 3.4 mm ID horizontal microfin tube. Int. J. Refrig. 75, 178–189. https://doi.org/10.1016/j.ijrefrig.2016.12.014

Dobson, M.K., Chato, J.C., 1998. Condensation in smooth horizontal tubes. J. Heat Transfer 120, 193–213. https://doi.org/10.1115/1.2830043

Hirose, M., Ichinose, J., Inoue, N., 2018. Development of the general correlation for condensation heat transfer and pressure drop inside horizontal 4 mm small-diameter smooth and microfin tubes. Int. J. Refrig. 90, 238–248. https://doi.org/10.1016/j.ijrefrig.2018.04.014

Ichinose, J., Inoue, N., 2011. The condensation heat transfer and pressure drop of R410A and R32 inside horizontal small-diameter tubes – 2nd report: empirical correlation for condensation heat transfer and pressure drop. Trans. JSRAE 28, 479–490.

Inoue, N., Aono, J., Goto, M., Sato, M., Kiyotani, A., Sasaki, N., 2008. Evaluation of prediction method for pressure drop and condensation heat transfer coefficient inside internally helical-groove horizontal tubes. J. Japan Res. Inst. Adv. Copper-Base Mater. Technol. (In Japanese) 47, 232–237.

Inoue, N., Ichinose, J., 2012. Singel-Phase Heat Transfer And Pressure Drop Inside Internally Helical-Grooved Horizontal Small-Diameter Tubes 20, 1–13. https://doi.org/10.1142/S2010132512500228

JCGM 100, 2008. Evaluation of Measurement Data-Guide to the Expression of Uncertainty in Measurement.

Kedzierski, M.A., Goncalves, J.M., 1999. Horizontal convective condensation of alternative refrigerants within a micro-fin tube. J. Enhanc. Heat Transf. 6, 161–178. https://doi.org/10.1615/JEnhHeatTransf.v6.i2-4.90

Koyama, S., Chen, Y., Kitano, R., Kuwahara, K., 2001. Experimental Study on Void

Fraction of Two-Phase Flow Inside a Micro-Fin Tube. reports IAMS. Kyushu Univ. 15–1, 79–85.

Koyama, S., Yonemoto, R., 2006. Experimental Study on Condensation of Pure Refrigerants in Horizontal Microfin Tubes - Proposal of Correlations for Heat TRansfer Coefficient and Frictional Pressure Drop. Proceddings Int. Refrig. Air Cond. Conf. Purdue USA R133 1–8.

Lee, Y., Jung, D., 2012. A brief performance comparison of R1234yf and R134a in a bench tester for automobile applications. Appl. Therm. Eng. 35, 240–242. https://doi.org/10.1016/j.applthermaleng.2011.09.004

Lemmon, E.W., Bell, I.H., Huber, M.L., McLinden, M.O., 2018. NIST Standard Reference Database 23: Reference Fluid Thermodynamic Properties-REFPROP (DLL Version 10.0a). NIST, USA.

Li, G.Q., Wu, Z., Li, W., Wang, Z.K., Wang, X., Li, H.X., Yao, S.C., 2012. Experimental investigation of condensation in micro-fin tubes of different geometries. Exp. Therm. Fluid Sci. 37, 19–28. https://doi.org/10.1016/j.expthermflusci.2011.09.008

Qi, Z., 2015. Performance improvement potentials of R1234yf mobile air conditioning system. Int. J. Refrig. 58, 35–40. https://doi.org/10.1016/j.ijrefrig.2015.03.019

Qi, Z., 2013. Experimental study on evaporator performance in mobile air conditioning system using HFO-1234yf as working fluid. Appl. Therm. Eng. 53, 124–130. https://doi.org/10.1016/j.applthermaleng.2013.01.019

Rahman, M.M., Kariya, K., Miyara, A., 2018. An experimental study and development of new correlation for condensation heat transfer coefficient of refrigerant inside a multiport minichannel with and without fins. Int. J. Heat Mass Transf. 116, 50–60. https://doi.org/10.1016/j.ijheatmasstransfer.2017.09.010

Smith, S.L., 1969. Void fractions in two-phase flow: A correlation based upon an equal velocity head model. Proc. Inst. Mech. Eng. 184, 647–664.

Son, C.H., Oh, H.K., 2012. Condensation heat transfer characteristics of CO 2 in a horizontal smooth- and microfin-tube at high saturation temperatures. Appl. Therm. Eng. 36, 51–62. https://doi.org/10.1016/j.applthermaleng.2011.12.017

UNEP, 2016. The Kigali Amendment to the Montreal Protocol: HFC Phase-down. OzonAction Fact Sheet 1–7.

Yang, Y., Li, M., Wu, W., Zhang, H., Ma, Y., 2019. Condensation heat transfer

characteristics of R1234ze(E) and R32 in a minihorizontal smooth tube. Sci. Technol. Built Environ. 25, 889–904. https://doi.org/10.1080/23744731.2019.1581014

Yu, J., Koyama, S., 1998. Condensation heat transfer of pure refrigerant in microfin tubes, Procedings International Refrigeration Conference at Purdue. pp. 325–330.

Yu, J., Koyama, S., 1996. Condensation of Pure Refrigerants in Microfin Tubes - A Correlation for Local Heat Transfer Coefficient. (In Japanese). reports IAMS. Kyushu Univ. 10, 145–150.

Zhang, J., Zhou, N., Li, W., Luo, Y., Li, S., 2018. An experimental study of R410A condensation heat transfer and pressure drops characteristics in microfin and smooth tubes with 5 mm OD. Int. J. Heat Mass Transf. 125, 1284–1295. https://doi.org/10.1016/j.ijheatmasstransfer.2018.04.128

CHAPTER

5

EXPERIMENTAL INVESTIGATION ON FLOW BOILING HEAT TRANSFER OF R1234YF INSIDE HORIZONTAL MICROFIN TUBE

5.1 Introduction

In the acceleration of low GWP refrigerant implementation has caused the search for a new type of refrigerants such as R1234yf, a kind of hydro fluoro olefins (HFOs). R1234yf is promoted as a drop-in solution for replacing R134a in mobile air conditioning as both refrigerants have similar thermophysical properties (Lee and Jung, 2012; Qi, 2015).

The use of microfin tubes in automotive and HVAC systems is passing the new trend indicated by promoting the recent design of AC systems by some manufacturers. The study on microfin tubes with outer diameter lower than 5 or 4 mm draw the researcher's interest since the down-sizing of the heat exchanger of the AC system is continued. Moreover, the use of microfin as a heat exchanger has benefits in several aspects. For instance, it leads to high heat transfer characteristics, which improve the system efficiencies. Besides, the reduction of the refrigerant charge is beneficial in solving environmental issues.

Several investigations of boiling heat transfer using small diameter microfin tubes have been carried out. To investigate the influence of tube diameter, Jige and Inoue (Jige and Inoue, 2019) employed three horizontal small-diameter microfin tubes with equivalent diameters of 2.1 mm, 2.6 mm, and 3.1 mm with the same fin height, helix angle, and the number of fins. The flow boiling heat transfer and frictional pressure drop of R32 were investigated experimentally. In addition, our research group (Bashar et al., 2018) investigated smooth and microfin tube inside 2.5 mm outer diameter tubes on boiling heat transfer for R134a.

However, for microfin tube using R1234yf is very limited, Diani et al. (Diani et al., 2015) employed a 3.4 mm inner diameter of microfin tube to study the heat transfer coefficient of flow boiling of R1234yf. Therefore, this study investigates the flow boiling of heat transfer of R1234yf in 3.5 mm OD of microfin tube. Different mass velocity and heat flux effects on the two-phase heat transfer behavior are highlighted. Then, experimental data were compared with a model available in the literature.

5.2 Experimental Apparatus and Data Reduction

5.2.1 Experimental Apparatsus

The test equipment is shown in Fig 2.1 This facility consisted of two pumps, a coriolis flowmeter, two preheaters, three mixing chambers, a test section, several water loops, an accumulator, and a cooler. The two pumps are used to run the refrigerant; the difference between the two pumps is in the experimental conditions, for mass velocities of 50 $kgm^{-2}s^{-1}$ and below using the first pump and more than 50 $kgm^{-2}s^{-1}$ using the second pump. The preheaters regulate the quality of the refrigerant before it enters the test section. Three mixing chambers are fitted at the input of the first preheater and the inlet and outflow of the test section to measure pressure and the bulk temperature of the refrigerant. The accumulator regulates the test apparatus's system pressure, and a cooler functions to cool the refrigerant and ensure it is in liquid form to be circulated as a cycle. In test section, a tube-in-tube was used to transfer heat from the water to the refrigerant.

In addition to this apparatus, it is also equipped with several K-type thermocouples placed in specific positions to observe the refrigerant temperature, a sight glass to visualize the refrigerant, and a data logger to record all measuring instruments. The test equipment is also well insulated to maintain the system temperature.

5.2.2 Data Reduction

The local heat transfer coefficient during boiling is calculated by the Eq. (5.1).

$$\alpha = \frac{Q_{\mathrm{wat(i)}}}{\pi d_{\mathrm{eq}} Z_{\mathrm{(i)}} (T_{\mathrm{wi(i)}} - T_{\mathrm{r(i)}})} \tag{5.1}$$

Where Q_{wat} is the heat transfer rate of water side of each sub-section, $d_{eq\ is}$ the equivalent diameter of the test tube (microfin), $Z_{(i)}$ the length of each sub section, T_r is refrigerant temperature that estimated from the measure refrigerant pressure, and T_{wi} is temperature of the inner wall of the test tube. The heat transfer rate amount of water side of each sub section can be calculated by Eq. (5.2).

$$Q_{wat(i)} = m_{wat}\left(h_{wat(i)} - h_{wat(i-1)}\right) \tag{5.2}$$

The inner wall temperature of the test tube is calculated from the measured temperature of the test tube's outside wall surface by one dimensional equation of heat conduction Eq. (5.3).

$$T_{wi(i)} = T_{wo(i)} - Q_{wat(i)}\left(\ln\left(\frac{d_o}{d_{eq}}\right)\Big/ 2\pi Z_{(i)}\lambda_{tube}\right) \tag{5.3}$$

Where $T_{wo,}$ d_o and λ are outside wall surface temperature of test tube, outer diameter of test tube and the thermal conductivity of test tube, respectively.

$$h_{(i)} = h_{(i-1)} + \left(\frac{Q_{wat(i)}}{m_r}\right) \tag{5.4}$$

$$x_{(i)} = \frac{h_{(i)} - h_l}{h_v - h_l} \tag{5.5}$$

Where $h_{(i)}$ is the local enthalpy of refrigerant at each wall thermocouple point of the test tube, h_l and h_v are the saturated liquid and vapor enthalpy of refrigerant, respectively.

5.3 Heat Transfer Coefficient Models Used in the Present Study

5.3.1 (Wu et al., 2013) Correlation

An experimental investigation was performed for convective vaporization of R22 and R410A inside five micro-fin tubes with the same outer diameter of 5 mm. Data are for mass fluxes ranging from 100 to 620 kg $m^{-2}s^{-1}$ at 279 K saturation temperature. A new general semi-empirical model has been developed based on the present data and recent data from literature.

For estimating heat transfer coefficient, (Wu et al., 2013) developed correlation

by using asymptotic model as following formula :

$$h=\left(\left[\left(h_{cv}\right)^3+\left(h_{nb}\right)^3\right]\right)^{1/3}=\left(\left[\left(E_{RB}h_{cb,l}\right)^3+\left(S\,h_{pb}\right)^3\right]\right)^{1/3} \tag{5.6}$$

$h_{\mathrm{cb,l}}$ is the convective heat transfer coefficient occurring during evaporation at the current vapor quality, and at the most advantageous location in the liquid cross section. In micro-fin tubes, the liquid film will be distributed evenly around the tube wall in annular flow.

$$h_{cb,l}=C\mathrm{Re}_{\delta}^{m}\,\mathrm{Pr}_{l}^{0.4}\frac{k_l}{\delta} \tag{5.7}$$

$$\mathrm{Re}_{\delta}=\frac{4G(1-x)\delta}{(1-\varepsilon)\mu_l} \tag{5.8}$$

Where δ is the liquid film thickness calculated by follow equation.

$$\delta=\sqrt{A_c/\pi}\cdot\left(1-\sqrt{\varepsilon}\right) \tag{5.9}$$

In the above equation, the void fraction ε is determined by following Equation.

$$\varepsilon=\frac{x}{\rho_v}\left[\left(1+0.12(1-x)\right)\left(\frac{x}{\rho_v}+\frac{1-x}{\rho_l}\right)+\frac{1.18(1-x)\left[g\sigma\left(\rho_l-\rho_v\right)^{0.25}\right]}{G\rho_l^{0.5}}\right]^{-1} \tag{5.10}$$

The enhancement factor E_{RB} for single-phase turbulent flow correlation of (Ravigururajan and Bergles, 1985) was introduced to include the enhancement effect of the microfins on the convective boiling coefficient by using the film Reynolds number

$$E_{RB}=\left\{1+\left[2.64\,\mathrm{Re}_{\delta}^{0.036}\,\mathrm{Pr}^{-0.024}\left(\frac{e}{d_i}\right)^{0.212}\left(\frac{p}{d_i}\right)^{-0.21}\left(\frac{\beta}{90}\right)^{0.29}\right]^7\right\}^{1/7} \tag{5.11}$$

Heat transfer coefficient of Pool Boliling, h_{pb} estimated by following equation.

$$h_{pb} = 2.8 \times 207 \frac{k_l}{D_b} \left[\frac{(q - q_{ONB}) D_b}{k_l T_{sat}} \right]^{0.745} \left(\frac{\rho_v}{\rho_l} \right)^{0.581} \Pr^{0.533} \quad (5.12)$$

Where D_b is the departure bubble diameter:

$$D_b = 0.51 \left[\frac{2\sigma}{g(\rho_l - \rho_v)} \right]^{0.5} \quad (5.13)$$

q_{onb} is the minimum heat flux for the onset of nucleate boiling (ONB) during evaporation developed by (Zürcher et al., 2000), proposed to be:

$$q_{ONB} = \frac{2\sigma T_{sat} h_{cb,l}}{r_{crit} \rho_v h_{lv}} \quad (5.14)$$

Boiling suppression factor is not required in an asymptotic model. Dimensionless parameter S in Eq (5.6) is a nucleate boiling correction factor:

$$S = \frac{1}{\xi}\left(1 - e^{-\xi}\right) \quad (5.15)$$

$$\xi = 1.96 \times 10^{-5} \times \left(\frac{\rho_l}{\rho_v} \frac{C_{pl}}{h_{lv}} T_{sat} \right)^{1.25} \left(E_{RB} h_{cb,l} \right) D_b / k_l \quad (5.16)$$

The critical bubble radius r_{crit} in Eq. (5.14), is assume to be 0.38×10^{-6} m (Zürcher et al., 2000). $h_{cb,l}$ in Eq. (5.14) is replaced by $E_{RB}h_{cb,l}$ for micro-fin tubes. The two constants C = 0.014 and m = 0.68.

5.3.2 (Saitoh et al., 2007) Correlation

(Saitoh et al., 2007) modified Chen correlation (Chen, 1966) for flow boiling heat transfer of R-134a in horizontal tubes with taking taking into account the effect of tube diameter. The effect of tube diameter on flow boiling heat transfer coefficient was characterized by the Weber number in gas phase. This correlation could be applied to a wide range of tube diameters (0.5–11-mm-ID).

The heat transfer coefficient consists of a convective boiling contribution (Fh_l)

and a nucleate boiling contribution (Sh_{pool}) as follows :

$$h_{TP,Pre} = Fh_l + Sh_{pool} \tag{5.17}$$

where h_l is the heat transfer coefficient based on the Dittus– Boelter's equation only for liquid flow in a tube and h_{pool} is the heat transfer coefficient based on the Forster and Zuber relation for nucleate pool boiling. The factor F related to the Martinelli parameter X represents the enhancement of forced convection heat transfer, and the factor S related to the two-phase Reynolds number Re_{Tp} represents the suppression of boiling heat transfer due to decrease in superheat of the liquid film on a tube wall with increasing forced convection effect.

Where F, S as follows:

$$F = 1 + \frac{\left(\frac{1}{X}\right)^l}{1 + We_g^m} \tag{5.18}$$

$$S = \frac{1}{1 + a\left(\mathrm{Re}_{TP} \times 10^{-4}\right)^n} \tag{5.19}$$

The effect of tube diameter D on the fluid flow conditions is expressed by using the Weber number, as follows:

$$We_g = \frac{G_g^2 D}{\sigma \rho_g} \tag{5.20}$$

In summary, F is expressed as a function of X and We_g, F= f(X,We_g), whereas S for suppression of nucleate boiling is expressed as a function of Re_{TP} defined as:

$$Re_{TP} = \mathrm{Re}_l \, F^{1.25} \tag{5.21}$$

The h_{pool} in Eq. (5.17) is calculated by (Stephan and Abdelsalam, 1980) correlation for organic refrigerants, as follows:

$$h_{pool} = 207 \frac{\lambda_l}{d_b} \left(\frac{q d_b}{\lambda_l T_l}\right)^{0.745} \left(\frac{\rho_g}{\rho_l}\right)^{0.581} Pr_l^{0.533} \tag{5.22}$$

where d_b is the bubble departure diameter of nucleate boiling and given by :

$$d_b = 0.51\left[\frac{2\sigma}{g\left(\rho_l - \rho_g\right)}\right]^{0.5} \tag{5.23}$$

The parameters *a*, *l*, *m*, and *n* were determined by fitting data. The resulting values in the fitting are $a = 0.4$, $l = 1.05$, $m = -0.4$ and $n = 1.4$.

For estimated Lochart-Martinelli parameter use two equations based on Re_l, as follows:

$$X = \left(\frac{1-x}{x}\right)^{0.9}\left(\frac{\rho_g}{\rho_l}\right)^{0.5}\left(\frac{\mu_l}{\mu_g}\right)^{0.1} \text{ for } Re_l > 1000, Re_g > 1000 \tag{5.24}$$

$$X = \left(\frac{C_l}{C_g}\right)^{0.5} Re_g\left(\frac{G_l}{G_g}\right)^{0.5}\left(\frac{\rho_g}{\rho_l}\right)^{0.5}\left(\frac{\mu_l}{\mu_g}\right)^{0.5}, \text{For } Re_l < 1000, Re_g > 1000 \tag{5.25}$$

Whrere C_l is friction factor for liquid, $C_l = 16$ and C_g is friction factor for gas, $C_g = 0.046$.

Liquid-phase heat transfer, h_l, calculated by using two correlation based on Re_l as follows :

$$h_l = 0.023\frac{\lambda_l}{D}\left(\frac{G_l}{\mu_l}\right)^{0.8}\left(\frac{C_{pl}\mu_l}{\lambda_l}\right)^{1/3} \text{ for } Re_l > 1000 \tag{5.26}$$

$$h_l = \frac{4.36\lambda_l}{D}, \text{For } Re_l < 1000 \tag{5.27}$$

5.3.3 (Kim and Mudawar, 2013) **Correlation**

(Kim and Mudawar, 2013) correlation was developed using the pre-dryout database that consist of 18 working fluids, hydraulic diameters of 0.19 - 6.5 mm, mass velocities of 19 - 1608 $kgm^{-2}s^{-1}$, liquid-only Reynolds numbers of 57 - 49820, qualities of 0 - 1, and reduced pressures of 0.005 - 0.69. Prior correlations for both macro-channels and mini/micro-channels are evaluated using this pre-dryout database.

The heat transfer coefficient is estimated by using eq. (5.28) – (5.30)

$$h_{tp} = \left(\left(h_{nb} \right)^2 + \left(h_{cb} \right)^2 \right)^{0.5} \tag{5.28}$$

$$h_{\mathrm{nb}} = \left[2345 \left(Bo \frac{P_H}{P_F} \right)^{0.7} P_{\mathrm{R}}^{\ 0.38} \left(1 - x\right)^{-0.51} \right] \left(0.023 \mathrm{Re}_{\mathrm{l}}^{\ 0.8} \mathrm{Pr}_{\mathrm{l}}^{0.4} \frac{\lambda_{\mathrm{l}}}{D_{\mathrm{h}}} \right) \tag{5.29}$$

$$h_{\mathrm{cb}} = \left[5.2 \left(Bo \frac{P_H}{P_F} \right)^{0.08} We_{\mathrm{lo}}^{\ -0.54} + 3.5 \left(\frac{1}{X_{tt}} \right)^{0.94} \left(\frac{\rho_{\mathrm{g}}}{\rho_{\mathrm{l}}} \right)^{0.25} \right] \left(0.023 \mathrm{Re}_{\mathrm{l}}^{\ 0.8} \mathrm{Pr}_{\mathrm{l}}^{0.4} \frac{\lambda_{\mathrm{l}}}{D_{\mathrm{h}}} \right) \tag{5.30}$$

Where, Bo, P_{R}, We_{lo}, and Re_{l} are boiling number, reduced pressure, liquid-only Weber number, and liquid Reynolds number, respectively as follows:

$$Bo = \frac{q}{G h_{fg}} \tag{5.31}$$

$$\mathrm{P}_R = \frac{P}{P_{crit}} \tag{5.32}$$

$$We_{lo} = \frac{G^2 D_h}{\rho_l \sigma} \tag{5.33}$$

$$\mathrm{Re}_l = \frac{G\left(1 - x\right) D_h}{\mu_l} \tag{5.34}$$

5.4 Result and Discussion

5.4.1 Effect of experimental Parameter to Heat transfer coefficient

Fig 5.1 describes how mass velocity affects the heat transfer coefficient as a function of the vapor quality. In these operating test conditions, the vapor quality differences are from 0.12 to 0.93. Since this heat transfer coefficient remains constant at around 5 kW m^{-2} K^{-1} up to vapor quality of 0.40, in the low vapor quality region, the effect of mass velocity is not so remarkable and the nucleate boiling dominates the heat transfer. However, at the high-quality region, the increase in vapor quality increases, the heat transfer coefficient increases, and two-phase forced convection plays a role in the flow boiling mechanism. Because the heat transfer coefficient does not plateau as the mass velocity rises, forced convection presents and is dominant in the heat transfer process. Generally, the heat transfer coefficient rises slightly with vapor quality at low

mass velocity and it rises with vapor quality at high mass velocity, reaches a peak, and then drops at around 0.89 of vapor quality due to dry-out phenomena.

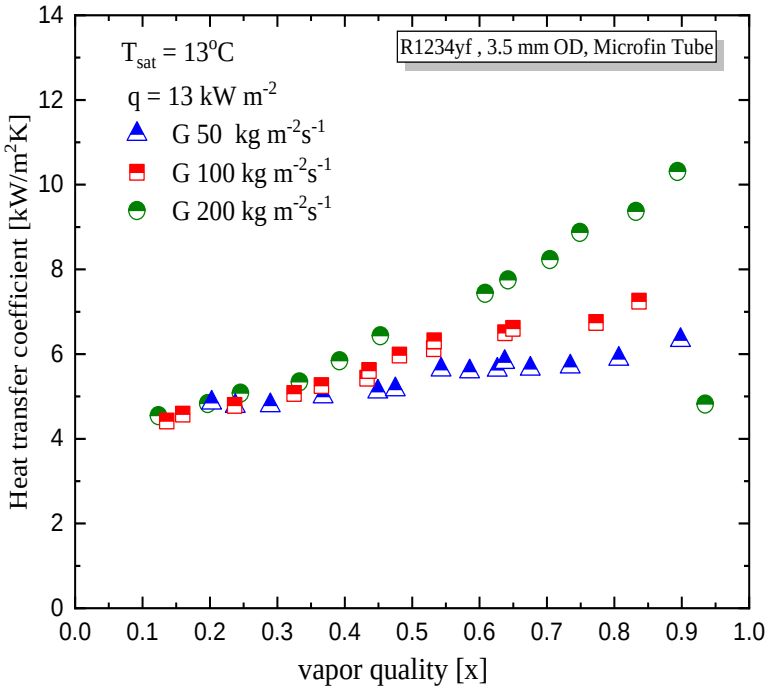

Fig. 5.1 Effect of mass velocity and vapor quality to heat transfer coefficient

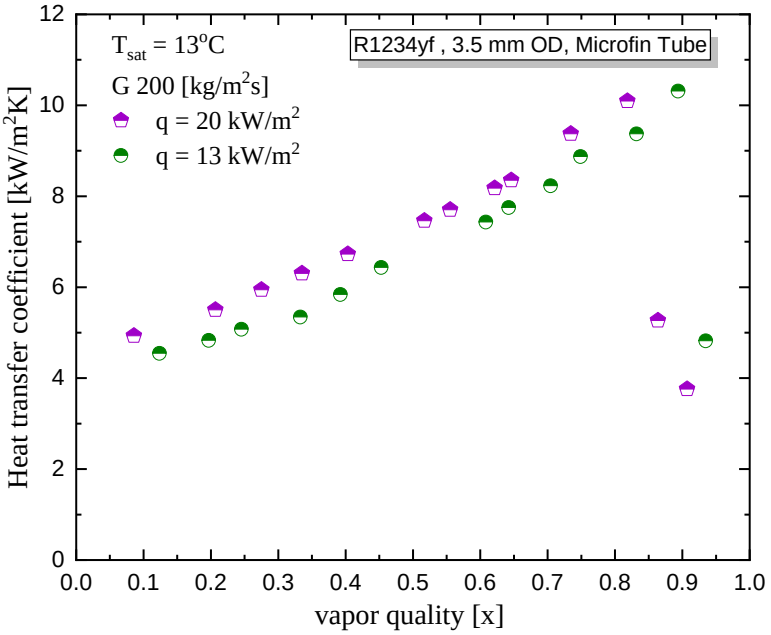

Fig. 5.2. Effect of heat flux on boiling heat transfer

In Fig. 5.2, the effect of heat flux was observed in the mass velocity 200 kg $m^{-2}s^{-1}$ and the impacts of heat flux are readily visible: nucleate boiling is the most crucial heat transfer mechanism.

5.4.2 Comparison with existing boling heat transfer coefficient correlations

Fig. 5.3 shows the comparison between experimental and predicted heat transfer coefficients with correlation by (Wu et al., 2013). It has been observed that experimental data were predicted 71% within ± 30% deviation. (Wu et al., 2013) correlation is well predicted to majority experimental data with the average deviation (AD) and mean deviation (MD) are -12.2% and 22.6%, respectively. The result of deviation using existing correlation shown in table 5.1. (Wu et al., 2013) correlation was developed using microfin tube.

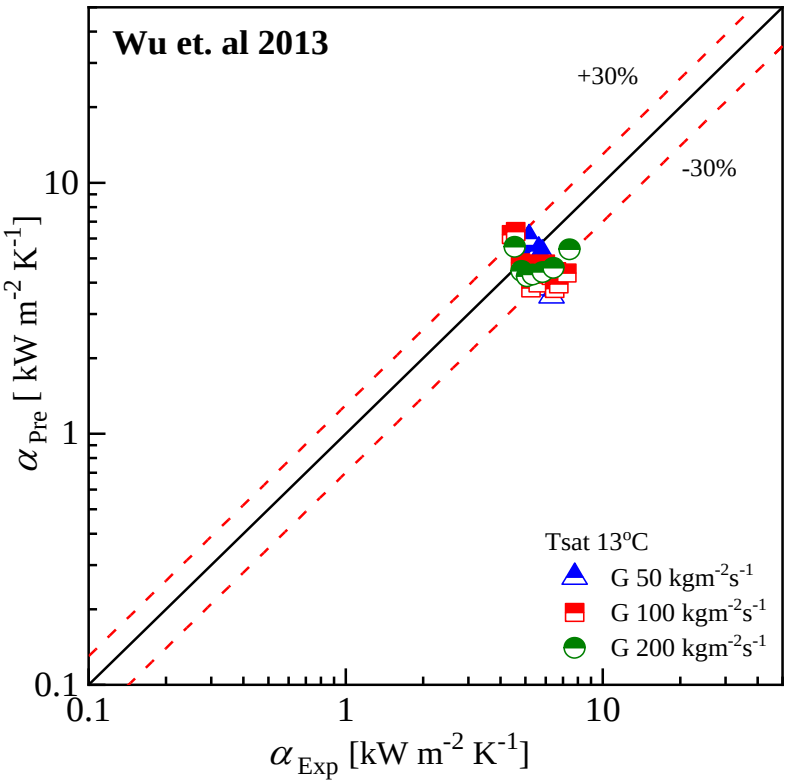

Fig. 5.3. Comparison of measured and predicted flow boiling heat transfer coefficient values for the microfin tube by (Wu et al., 2013) correlation

Fig. 5.4 shows the comparison between experimental and predicted heat transfer coefficients with correlation (Saitoh et al., 2007). It has been observed that experimental data were not well predicted, with the average deviation (AD) and the mean deviation (MD) being -47.78% and 47.78%, respectively. The experimental data points are 2.78% within ± 30% deviation. The result of deviation using existing correlation is also shown in table 5.1. (Saitoh et al., 2007) correlation is underestimated with experimental data. It means experimental data is larger than the predicted value. The reason is that the correlation was developed using the smooth tube.

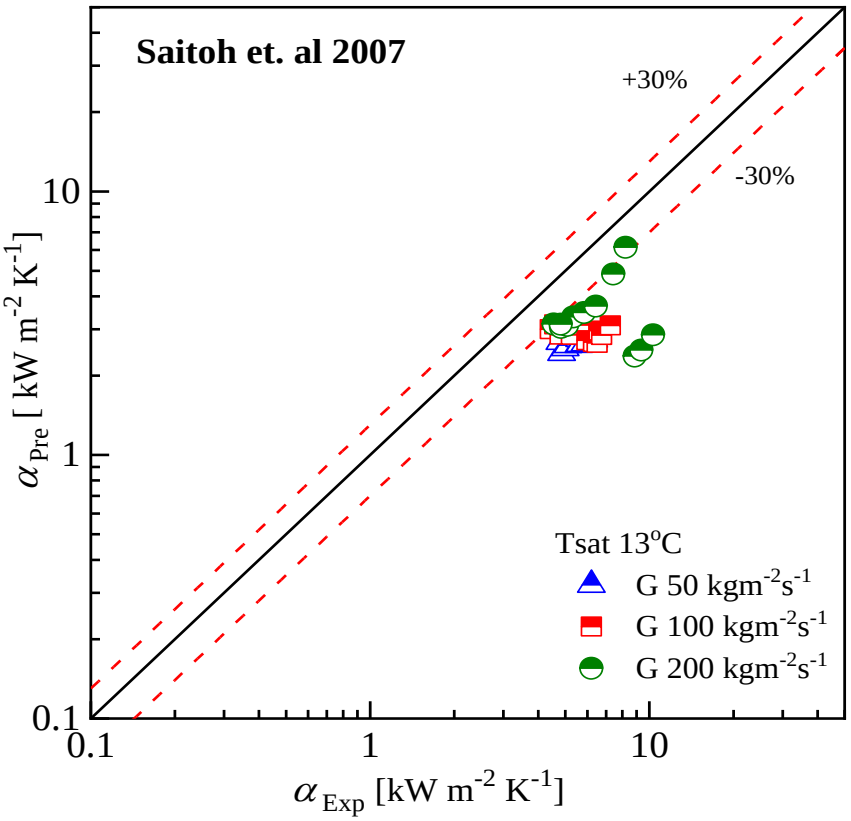

Fig. 5.4. Comparison of measured and predicted flow boiling heat transfer coefficient values for the microfin tube by (Saitoh et al., 2007) correlation

A similar trend with (Saitoh et al., 2007) correlation, (Kim and Mudawar, 2013) was also not well predicted with experimental data, as shown Fig. 5.4. The figure compares between experimental and predicted heat transfer coefficients, with the average deviation (AD) and the mean deviation (MD) being -57.99% and 57.99%, respectively.

The experimental data points are 2.78% within ± 30% deviation. The result of deviation using existing correlation is also shown in table 5.1. (Kim and Mudawar, 2013) correlation is underestimated with experimental data. It means experimental data is larger than the predicted value. The reason is that the correlation was developed using the smooth tube.

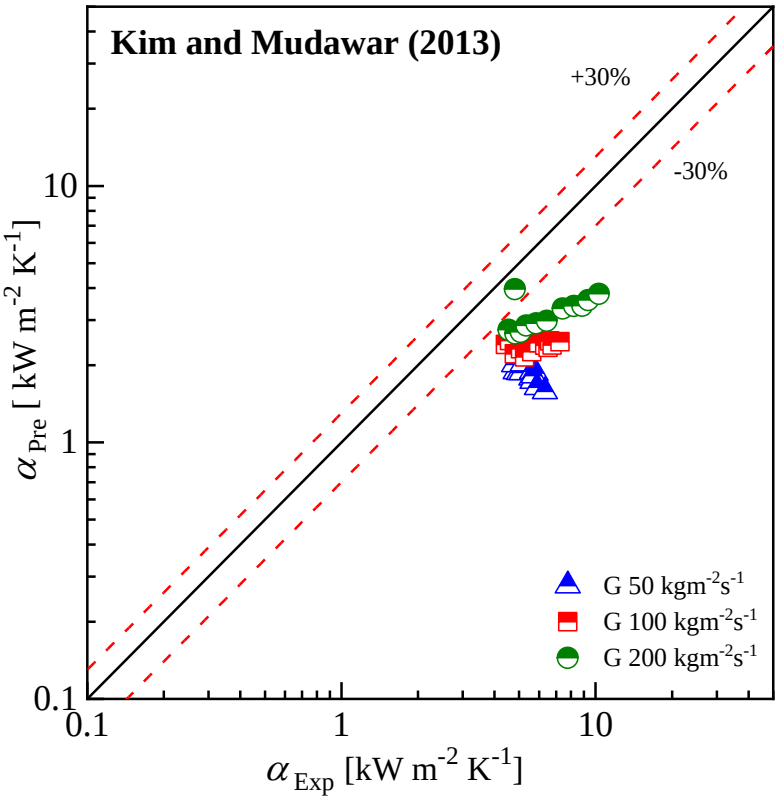

Fig. 5.5. Comparison of measured and predicted flow boiling heat transfer coefficient values for the microfin tube by (Kim and Mudawar, 2013) correlation

Table 5.1. Deviation of flow boiling heat transfer coefficient of R1234yf inside 3.5 OD microfin tube using existing correlations

Correlation	R454C			R454B		
	AD (%)	MD (%)	R30 (%)	AD (%)	MD (%)	R30 (%)
Goto et al. 2001	-39.7	39.7	28.6	-31	31	46.2
Proposed Correlation	-3.3	9.5	97.6	12.6	16.3	84.6

5.5 Conclusion

This paper presents experimental flow boiling heat transfer coefficients of R1234yf inside a microfin tube with equivalent inner diameter of 3.18 mm. The mass velocity varied from 50 to 200 kg $m^{-2}s^{-1}$, the heat fluxes from 13 to 20 kWm^{-2}, with a saturation temperature of 13 °C. Generally, the heat transfer coefficient rises slightly with vapor quality at low mass velocity. It rises with vapor quality at high mass velocity, reaches a peak, and drops at around 0.9 of vapor quality due to dry-out phenomena.

In the low vapor quality region, the effect of mass velocity is not so remarkable, and the nucleate boiling dominates the heat transfer. On the other hand, forced convection is present and dominant in the heat transfer process in the high-quality region. The heat transfer coefficient reaches 10.8 kW m^{-2} K^{-1} at vapor quality 0.89 in a condition of the mass velocity 200 kg $m^{-2}s^{-1}$ and the heat flux 13 kWm^{-2}. The effect of heat flux was observed in the mass velocity 200 kg $m^{-2}s^{-1}$ and the impacts of heat flux are readily visible: nucleate boiling is the most crucial heat transfer mechanism.

The existing correlation (Wu et al., 2013) is a good prediction of experimental data with the mean deviation of 22.6%.

References

Bashar, K., Ichinose, Y., Tuhin, A.R., Kariya, K., Miyara, A., 2018. Boiling Heat Transfer Of R134a Flowing Inside A Small Diameter Microfin And Smooth Tube Boiling Heat Transfer Of R134a Flowing Inside A Small Diameter Microfin And Smooth Tube. Mech. Eng. Res. J. 11, 32–37.

Chen, J.C., 1966. Correlation for Boiling Heat Transfer to Saturated Fluids in Convective Flow. Ind. Eng. Chem. Process Des. Dev. 5, 322–329. https://doi.org/10.1021/i260019a023

Diani, A., Mancin, S., Rossetto, L., 2015. Flow boiling heat transfer of R1234yf inside a 3.4mm ID microfin tube. Exp. Therm. Fluid Sci. 66, 127–136. https://doi.org/10.1016/j.expthermflusci.2015.03.019

Jige, D., Inoue, N., 2019. Flow boiling heat transfer and pressure drop of R32 inside 2.1 mm, 2.6 mm and 3.1 mm microfin tubes. Int. J. Heat Mass Transf. 134, 566–573. https://doi.org/10.1016/j.ijheatmasstransfer.2019.01.027

Kim, S.M., Mudawar, I., 2013. Universal approach to predicting two-phase frictional

pressure drop for mini/micro-channel saturated flow boiling. Int. J. Heat Mass Transf. 58, 718–734. https://doi.org/10.1016/j.ijheatmasstransfer.2012.11.045

Lee, Y., Jung, D., 2012. A brief performance comparison of R1234yf and R134a in a bench tester for automobile applications. Appl. Therm. Eng. 35, 240–242. https://doi.org/10.1016/j.applthermaleng.2011.09.004

Qi, Z., 2015. Performance improvement potentials of R1234yf mobile air conditioning system. Int. J. Refrig. 58, 35–40. https://doi.org/10.1016/j.ijrefrig.2015.03.019

Ravigururajan, T.S., Bergles, A.E., 1985. General correlations for pressure drop and heat transfer for single-phase turbulent flow in internally ribbed tubes.

Saitoh, S., Daiguji, H., Hihara, E., 2007. Correlation for boiling heat transfer of R-134a in horizontal tubes including effect of tube diameter. Int. J. Heat Mass Transf. 50, 5215–5225. https://doi.org/10.1016/j.ijheatmasstransfer.2007.06.019

Stephan, K., Abdelsalam, M., 1980. Heat-transfer correlations for natural convection boiling. Int. J. Heat Mass Transf. 23, 73–87. https://doi.org/10.1016/0017-9310(80)90140-4

Wu, Z., Wu, Y., Sundén, B., Li, W., 2013. Convective vaporization in micro-fin tubes of different geometries. Exp. Therm. Fluid Sci. 44, 398–408. https://doi.org/10.1016/j.expthermflusci.2012.07.012

Zürcher, O., Thome, J.R., Favrat, D., 2000. An onset of nucleate boiling criterion for horizontal flow boiling. Int. J. Therm. Sci. 39, 909–918. https://doi.org/10.1016/S1290-0729(00)01188-1

CHAPTER

6

EXPERIMENTAL STUDY ON PRESSURE DROP AND TWO-PHASE HEAT TRANSFER OF MIXTURE REFRIGERANT (R454B and R454C) INSIDE MICROFIN TUBE

Publications of this chapter

(1) Mainil, A.K.; Hakimatul, U.; Sakamoto, N,; Kariya, K.; Miyara, A. Experimental study on condensation Heat Transfer of R454B inside small Diameter microfin tube, Herrick Conferences, Purdue University, USA, 2022.

(2) Hakimatul, U.; Mainil, A.K.; Sadakata , K,; Kariya, K.; Miyara, A. Pressure Drop of Low GWP Refrigerant Mixture of R1234yf and R32 inside small Diameter microfin tube, Herrick Conferences, Purdue University, USA, 2022.

6.1 Introduction

Nowadays, refrigerant mixture are frequently employed and widely studied in refrigeration and heat pump systems (Mohanraj et al., 2011; Radermacher and Hwang, 2005). The latest trend in refrigeration is to employ zeotropic mixtures as refrigerants. Different behaviors and complications are observed when these mixtures are used. When two or more pure refrigerants are mixed to produce zeotropic refrigerant, the resulting combination can display distinct properties from the components. The refrigerant compositions in the liquid and vapor phases alter as a refrigerant combination transitions from all liquid to all vapor. This shift in composition results in fascinating behavior in zeotropic refrigerant mixes and numerous factors must be considered when experimenting with refrigerant combinations. Two-phase phenomena, temperature glides, and property fluctuations are examples of these.

6.1.1 Two-Phase Phenomena of mixture refrigerant

Refrigerant mixtures are frequently divided into two categories based on their vapor-liquid equilibrium properties: azeotropic mixtures and zeotropic mixtures. At particular temperatures and pressures, azeotropic mixtures have similar mass fraction compositions of the liquid and vapor phases, and the temperature glide, T_g, (the difference between the bubble and dew temperatures of the bulk mixture) is zero (Radermacher and Hwang, 2005). On the other hand, the composition of the vapor and liquid phases of the zeotropic mixture refrigerant changes with temperature, pressure, and vapor quality and shows temperature glide that tends to increase with the difference in boiling temperatures of the mixture components. This behavior is visible in temperature–composition (T-X) diagrams, where the upper and lower lines reflect the dew and bubble temperature lines, respectively, as functions of the molar composition of the mixture (see Fig. 6.1 and 6.2).

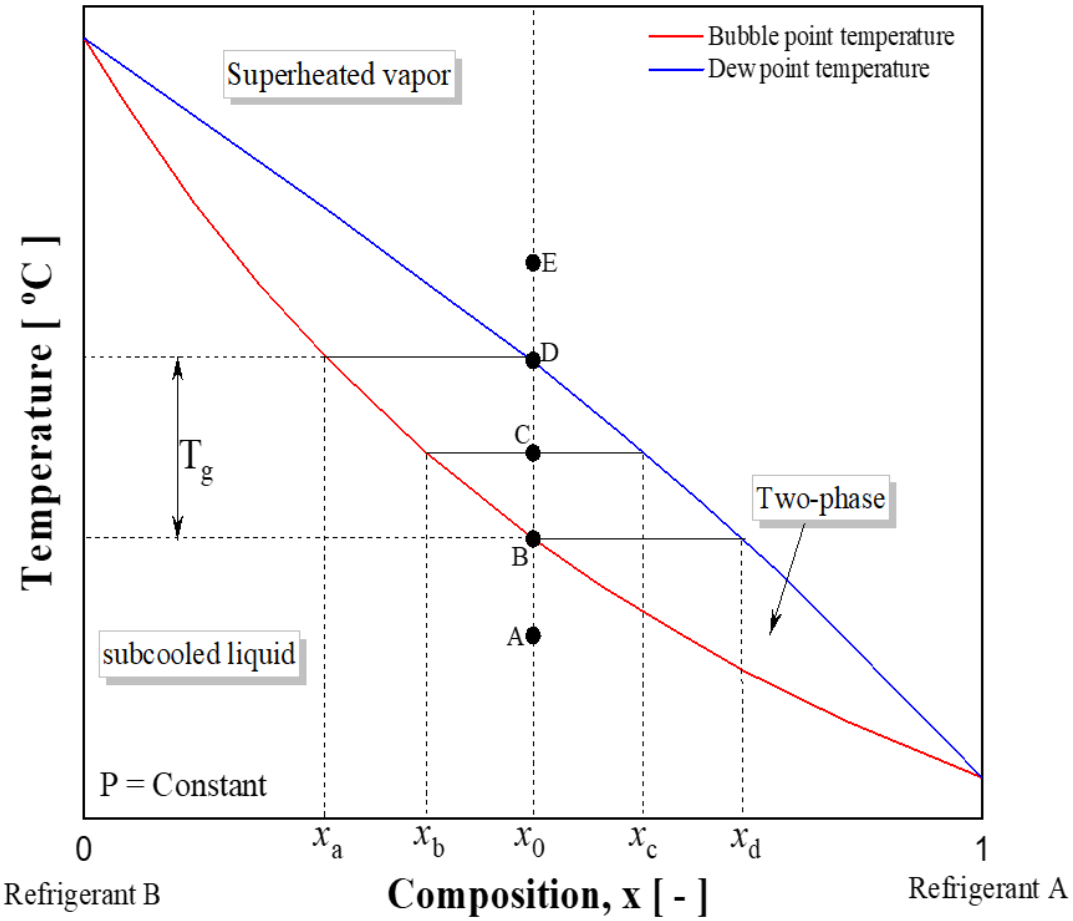

Fig. 6.1. Diagram of temperature-composition of zeotropic refrigerant

Fig. 6.1 shows an example T-x diagram for binary mixtures with zeotropic behavior. Zeotropic refers to a fluid in which the temperature glides is not equal to zero during the phase transition process in the figure, refrigerant mixture A/B is a zeotropic working fluid when the composition of Refrigerant A is not equal to x_{az}. In Fig. 6.1, Refrigerant A/B is a zeotropic working fluid regardless of composition. The compositions of the gas phase and liquid phase keep changing and different during the phase change process. The phenomenon is because different components have different boiling temperatures at the same pressure. The more volatile component with the lower boiling temperature gasifies first in the evaporation process. The component with the higher boiling temperature liquefies first in the condensation process.

For the explanation, in figure 1, x0 is the mass fraction of the refrigerant mixture. The zeotropic refrigerant evaporates from super-cooled liquid to superheated vapor from A to E. At point B (bubble point), zeotropic refrigerant is in a saturated liquid state, two-phase states at point C, and saturated vapor state at point D (dew point). When the zeotropic working fluid is in the saturated liquid at the start of the phase change process, the composition of the liquid phase of the refrigerant at point B approximately equals the initial composition x0, and that of the vapor phase equals x_d. Refrigerant A has a lower boiling temperature and more volatile component than Refrigerant B. more Refrigerant A is gasified first at the evaporative phase change process. When the zeotropic refrigerant is at point C, the liquid phase of the refrigerant's composition equals x_b, and the vapor phase refrigerant's composition equals x_d. The liquid phase working fluid composition at point D equals x_a at the end of the phase change process. The composition of the vapor phase refrigerant almost equals the initial composition x0. When the working fluid is entirely gaseous, the composition returns to its initial value. According to the changing composition trend in the phase change process of the zeotropic refrigerant, it was discovered that the composition change range that could be obtained by simple phase separation is (xa, xd).

Figure 6.2 shows an example binary mixture with an azeotropic point at molar fraction x_{az}. Temperature of bubble point (Td) coincides with temperature of dew points (Tb) for the azeotropic mixture of composition x_{az}.

Additionally, there is also a type of zeotropic mixtures known as near-azeotropic mixtures, which are zeotropic mixtures with a small enough temperature glide to be ignored. The temperature glide limit for defining a near-azeotropic mixture, however, is

unclear, ranging from 0.6 K according to (Mohanraj et al., 2011) to 10 °F (or 5.55 K) according to the Environmental Protection Agency (United States Environmental Protection Agency (EPA), n.d.). In Fig. 6.2, the compositions in the shaded area show compositions that could be classified as near-azeotropic.

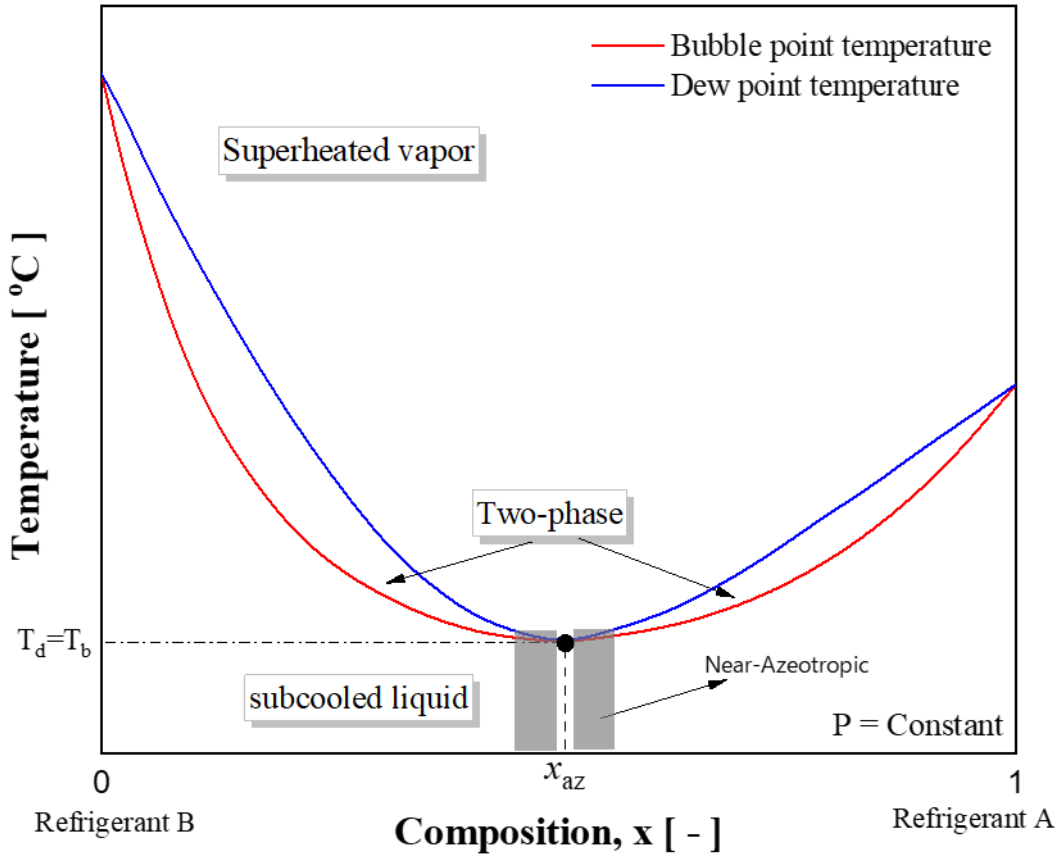

Fig. 6.2. Diagram of temperature-composition of azeotropic and zeotropic refrigerant

6.1.2 Zeotropic refrigerant of R454B and R454C

The heating, ventilation, air conditioning, and refrigeration (HVAC&R) sector are currently evolving as it transitions away from hydrofluorocarbons (HFCs) as working fluids and continues to encourage environmentally friendly refrigerants with lower global warming potential (GWP). Some replacement candidates include hydro-fluoro-olefins (HFOs), and mixtures of HFCs/HFOs hope to mitigate the high GWP, as the requirements by international regulation. Nowadays, R410A is one of the most widely used refrigerants for air conditioning applications in worldwide (Zhao et al., 2015). It has a high GWP (2088(IPCC, 2007)); therefore, it will be phased out shortly by replacing it with the low

GWP refrigerant (Mota-Babiloni et al., 2017). One promising candidate to replace R410A are R454B with a GWP of 466 (IPCC, 2007) (78 % reduction from R410A) with properties nearly identical to R410A (Devecioğlu, 2017; Shen et al., 2022; Tran et al., 2021).

The summary of several alternative refrigerants to the current refrigerant, where there are many mixed refrigerants as an alternative to pure refrigerants, is shown in table 6.1 below.

Table 6.1. Alternatives to Existing refrigerant (ASHRAE, 2019; Miyara et al., 2021)

Current (GWP)	**Non-flammable candidates [A1]**	**Mildly flammable candidates [A2L]**	**Flammable candidates [A3]**
R134a (1430)	R450A, R513A , R515B R744	R516A R1234yf R1234ze(E)	R290 R600a
R404A (3920) R507 (3990)	R448A, R449A/B R452A, R452C R744	R465A R457A, R454C R455A R717	N/A
R410A (2090)	R466A (HFC/CF3I) R463A	R32 (HFC) R459A, R447A, R452B, **R454C**, **R454B**	R443A R1270
R123 (77)	R1233zd(E) R514A R1336mzz(Z) R1224yd(Z)	N/A	N/A
R22 (1810)	R448A R449A, R449B	R457A, R444B, R454C	R290 (propane) R443A (R1270/290/600a)
R23 (14800)	R469A	N/A	N/A

Table 6.1 present the alternative refrigerant to the existing refrigerant. It can be seen that the pure refrigerant substitute for R134a is in the mildly flammable category. This table shows there is no pure refrigerant to substitute for R410A, R22, and R404A except for R32 for a substitute for R410A, which GWP is still above 500, in the sense that only mixed refrigerant is an alternative to their replacement.

These alternative mixed refrigerants make R32 a mixed component in the expected of increasing heat transfer and HFO, CO2, HC, and other HFCs to achieve the desired flammability, properties, and cycle performance.

R454B is a zeotropic mixture refrigerant made of R32 and R32 (68.9% and 31.1% in mass) and R454C is also made of R32 and R1234yf (21.5 and 78.5% in mass). R454B has a relatively small temperature glide (around 1.5°C) compared to other mixture refrigerants that have same constituent components, such as R454C (approximately 7 °C) and R454A (approximately 5°C), as shown in fig. 6.3 and fig. 6.4. Fig 6.4 is also show the comparison of GWP value of R454 B, C and A. However, the current concern is that R454B and R454C are categorized as A2L (ASHRAE, 2019), which is mildly flammable. In applying a heat exchanger that uses tubes, one potential option is to use a small diameter microfin tube that enhances heat transfer and reduces the amount of refrigerant charge.

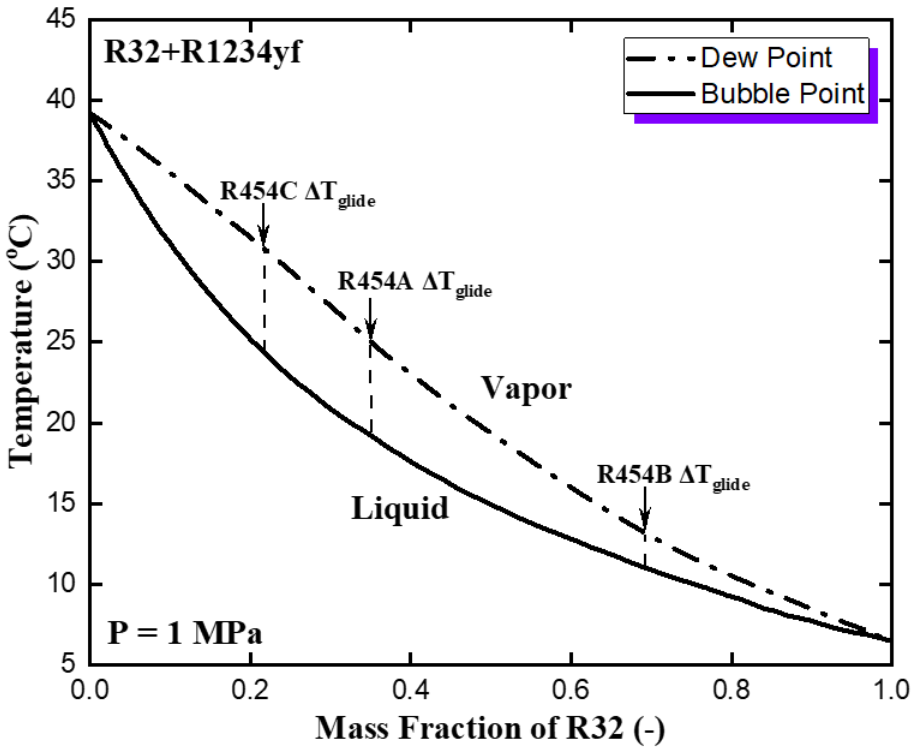

Fig. 6.3. R32/R1234yf equilibrium diagram at a constant pressure equal to 1 MPa

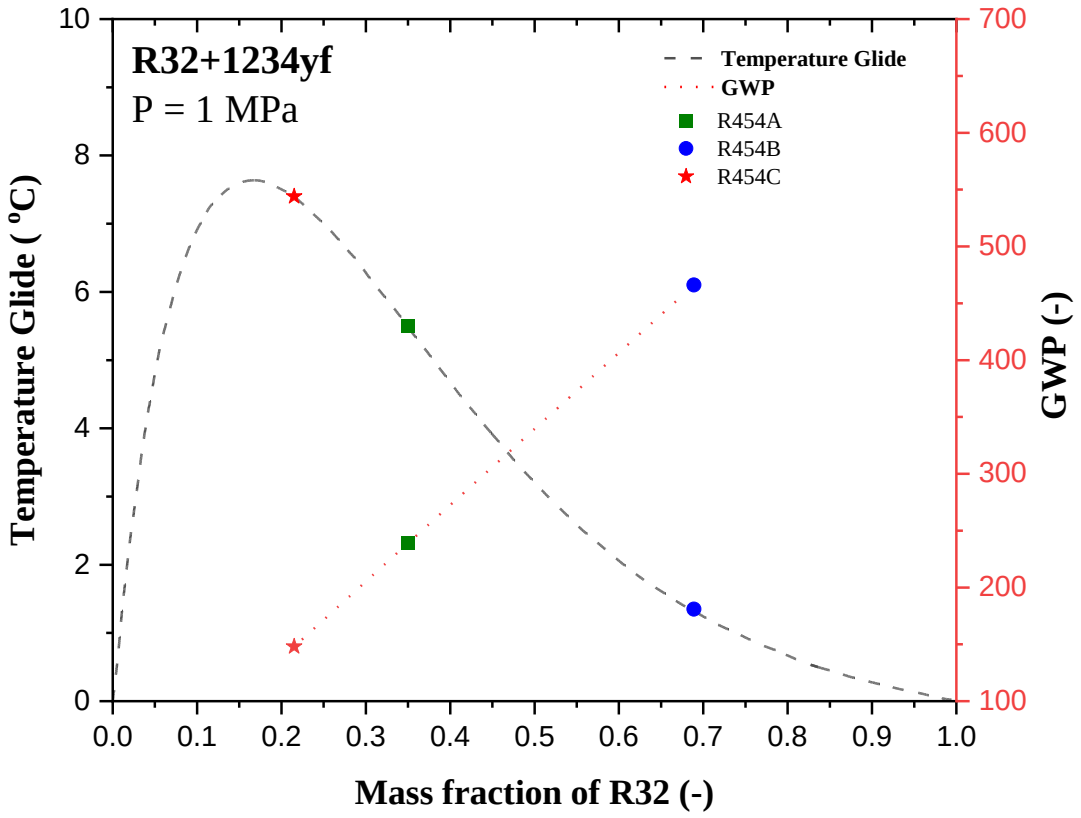

Fig. 6.4 Temperature glide R32/R1234yf mixture for various mass fraction and value of GWP of Refrigerant R454 A, B and C

This study investigated the two-phase flow condensation and boiling heat transfer as well as adiabatic pressure drop of R454B and R454C inside a 3.5 mm OD microfin tube. The effects of mass velocity and vapor quality, heat flux (just for flow boiling) were analyzed and discussed. The heat transfer coefficient is measured for mass velocity ranging between 50 kg $m^{-2}s^{-1}$and 200 kg $m^{-2}s^{-1}$, vapor quality from 0.1 to 0.9.

6.2 Data Reduction for Mixture refrigerant

Experimental apparatus and specification of tube are similar with the pure refrigerant in chapter 3, 4 and 5. Data reduction of mixture refrigerant in general for two-phase flow heat transfer and frictional pressure drop used equation (3.1) to equation (3.10) for adiabatic pressure drop, equation (4.1) to equation (4.7) for Condensation heat transfer and equation (5.1) to (5.5) for flow boiling heat transfer.

However for two-phase heat transfer in the case of mixture refrigerant, have additional calculation and estimating formula**.** Since R454B and R454C are a binary mixture of R32 and R1234yf, the local refrigerant temperatures are calculated by the mixture component mass balance from equation 6.1, 6.2, and 6.3. The value of $\dot{m}_b$, $\dot{m}_l$ and $\dot{m}_v$ represents the total mass flow rate, liquid-phase mass flow rate and the vapor-phase mass flow rate, respectively. w_b , w_l , and w_v are the bulk mass fraction, liquid phase, and vapor phase mass fractions of the binary mixture, respectively. The application of gas chromatography can know the bulk concentration of the binary temperature at the operating condition.

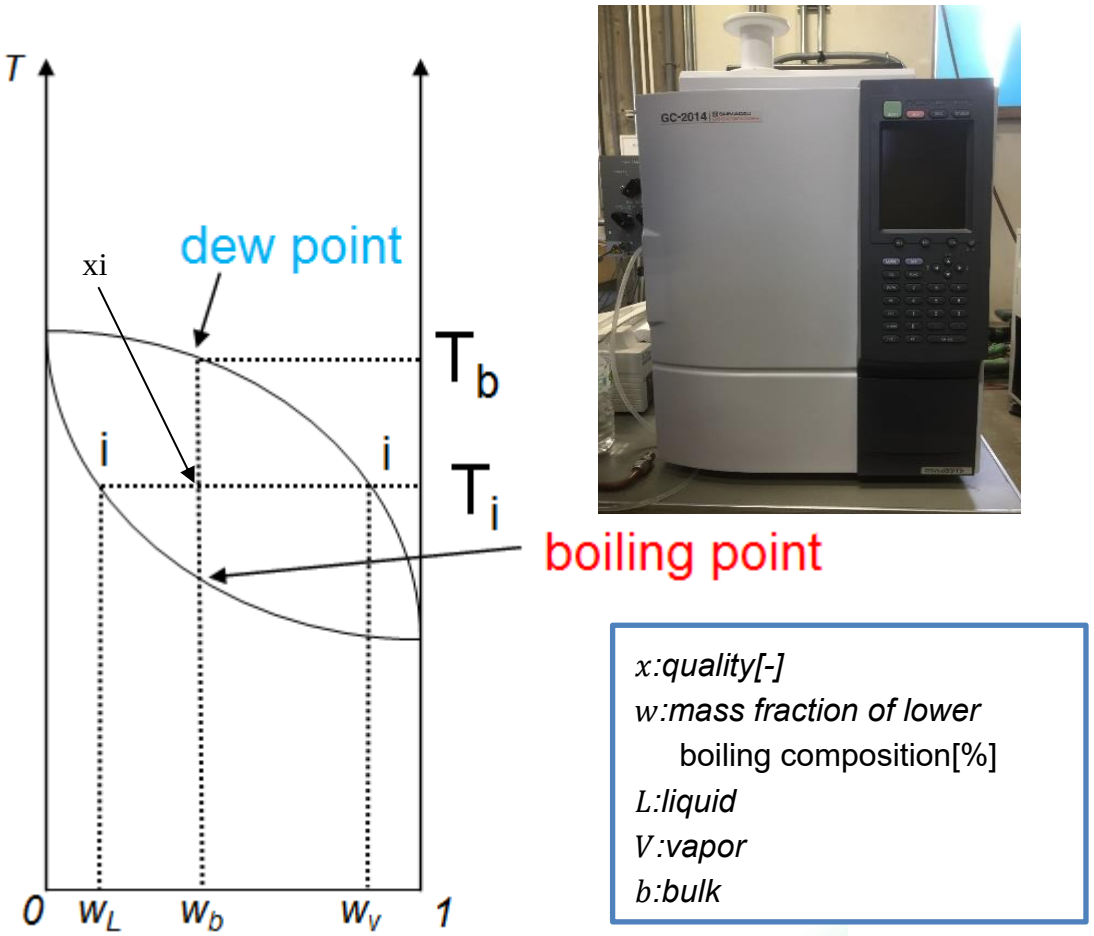

Fig. 6.5. Photography of the gas chromatography and the composition vs temperature graph.

Saturation temperature of mixture in the test section is not constant because of changing its component composition (Kariya et al., 2018). In order to derive local heat

transfer coefficient of mixture, we calculate saturation temperature considering the change of component composition during evaporation and condensation. From the relationship with conservation of mass and conservation of energy, we obtain the equation as follows.

$$\dot{m}_{\mathrm{b}} w_{\mathrm{b}} = \dot{m}_{\mathrm{v}} w_{\mathrm{v}} + \dot{m}_{\mathrm{l}} w_{\mathrm{l}} \tag{6.1}$$

$$x = \frac{\dot{m}_{\mathrm{v}}}{\dot{m}} \tag{6.2}$$

$$w_l = \frac{w_{\mathrm{b}}}{1 + x\left(\frac{w_{\mathrm{v}}}{w_{\mathrm{l}}} - 1\right)} \tag{6.3}$$

The refrigerant temperature, T_r, were obtained from REFPROP 10.0a (Lemmon et al., 2018) with the function follows:

$$w_{\mathrm{v}} = f\left(w_{\mathrm{l}}, P\right) \tag{6.4}$$

$$T_r = f\left(w_{\mathrm{l}}, P\right) \tag{6.5}$$

The corresponding enthalpy for liquid and vapour phase is also evaluated from REFPROP 10.0a (Lemmon et al., 2018) by the function of the concentration and the pressures at the measurement point.

$$h_{\mathrm{l}} = f\left(w_{\mathrm{l}}, P\right) \tag{6.6}$$

$$h_{\mathrm{v}} = f\left(w_{\mathrm{v}}, P\right) \tag{6.7}$$

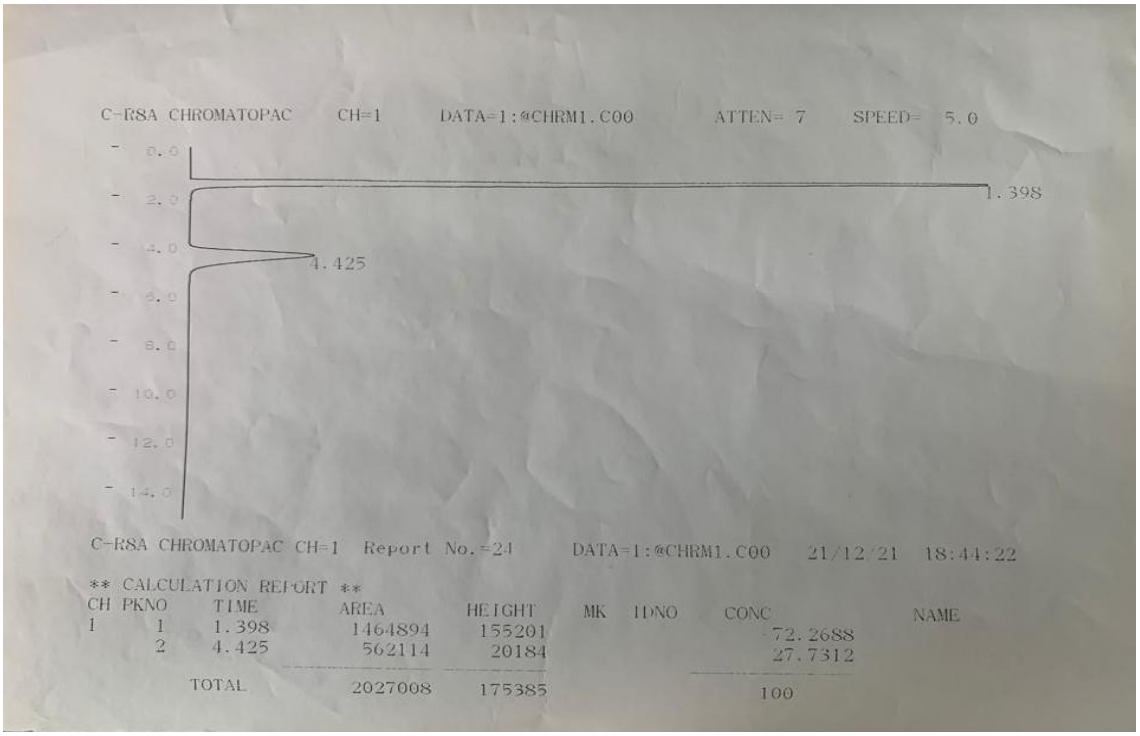

Fig.6.6. Measured mass concentration of the mixture by gas chromatography

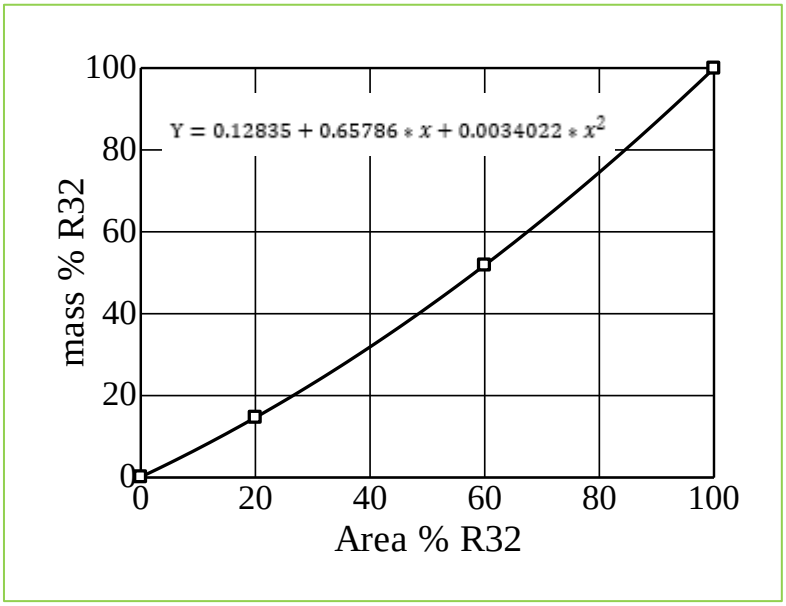

Fig.6.7. Relationship between the area percentage and mass percentage.

$$Y = 0.12835 + 0.65786x + 0.0034022x^2 \tag{6.8}$$

$$w_b = \frac{Y}{100} \tag{6.9}$$

A schematic flow chart for the data reduction method to obtained the saturation temperatures for mixture refrigerant are as follow.

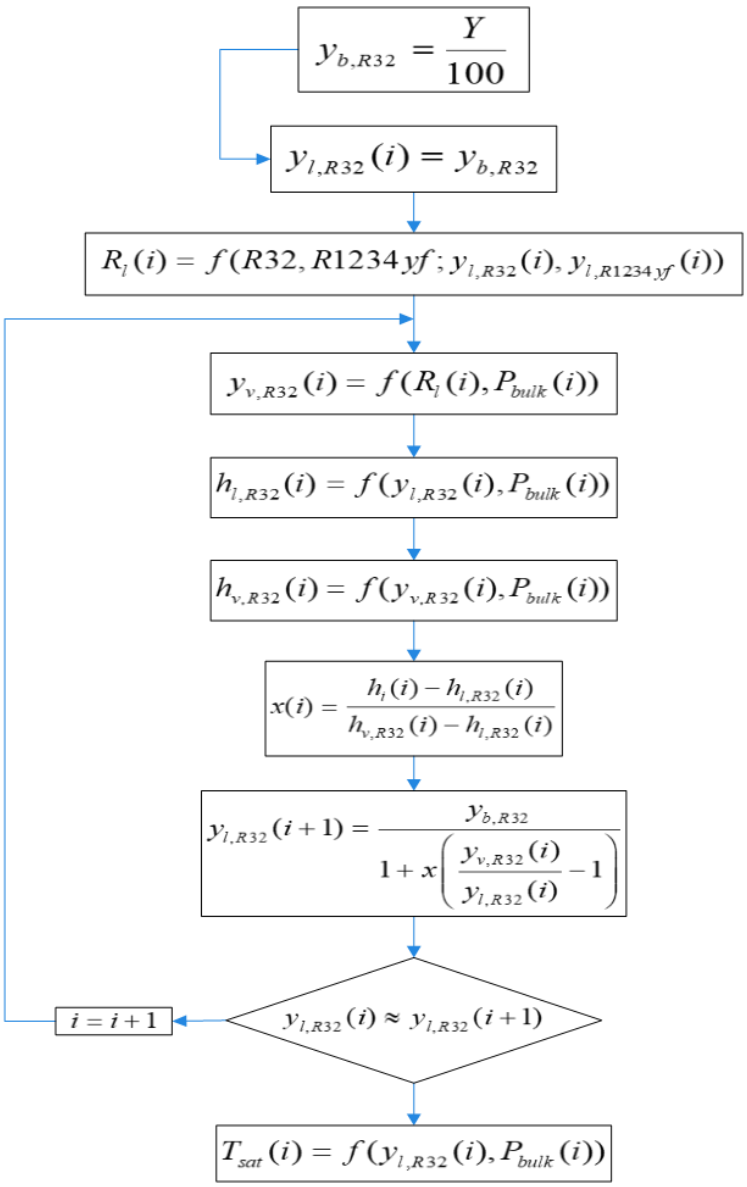

Fig. 6.8. Flow chart diagram showing the iteration process to estimate the saturation temperatures in Boiling Process.

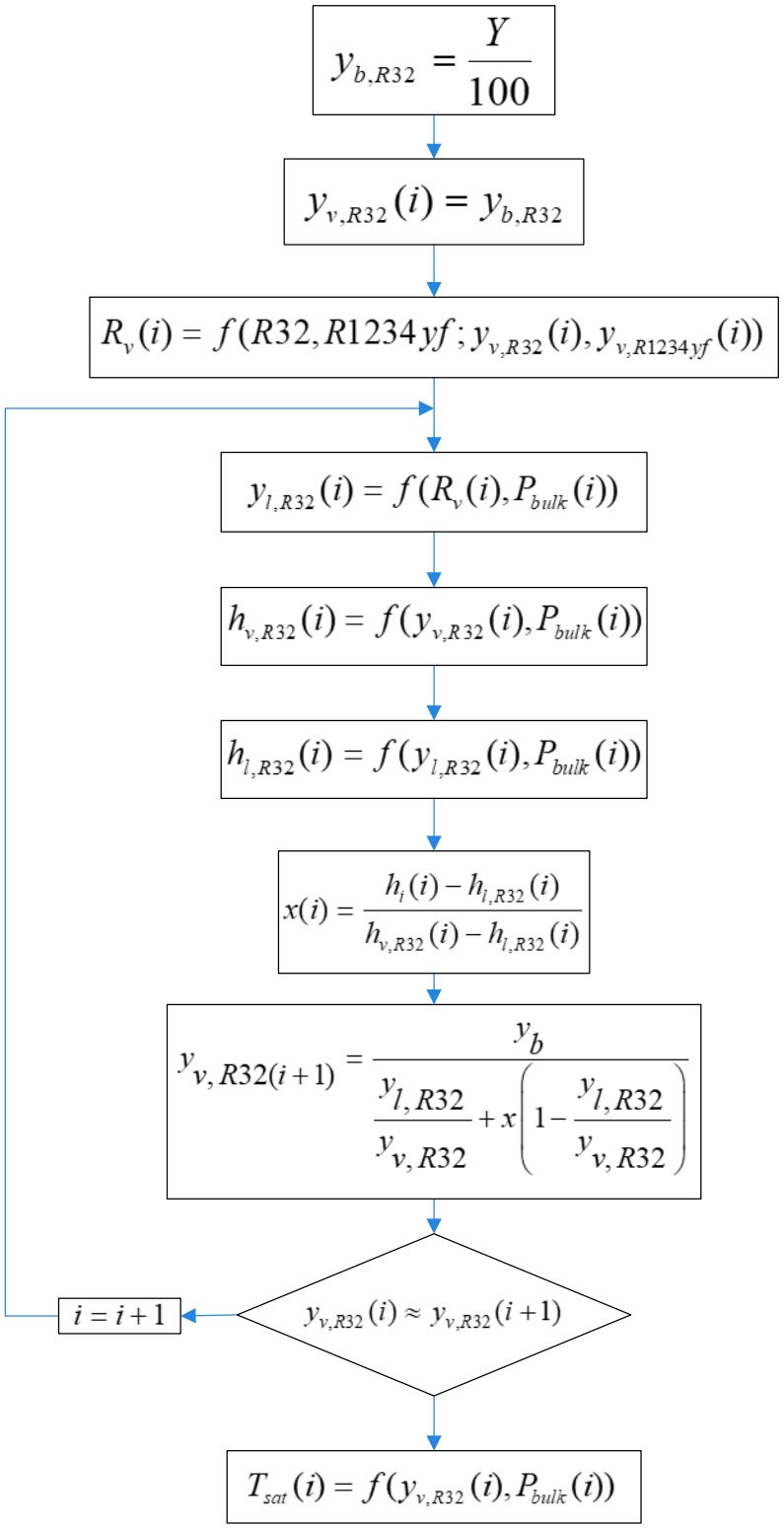

Fig.6.9. Flow chart diagram showing the iteration process to estimate the saturation temperatures for condensation Process.

6.3 Result of Pressure Drop

6.3.1 Frictional Pressure Drop of R454B and R454C

Fig. 6.10 shows the plot of experimental frictional pressure drop against the vapor quality at saturation temperature of 20 ºC for the mass velocity of 50 – 300 kg m^2s^{-1} in 3.5 mm outer diameter of microfin tube using refrigerant R454B. The higher pressure drop is at the mass velocity of 300 kg $m^{-2}s^{-1}$ with the value of frictional pressure drop reach of around 10 kPa m^{-1}. Here, the frictional pressure of R454B increased with increasing mass velocity and vapor quality. The effect of mass velocity and vapor quality on the increase of pressure drop due to increasing vapor shear stress and increased interfacial friction between vapor-liquid two-phase flow in the tube.

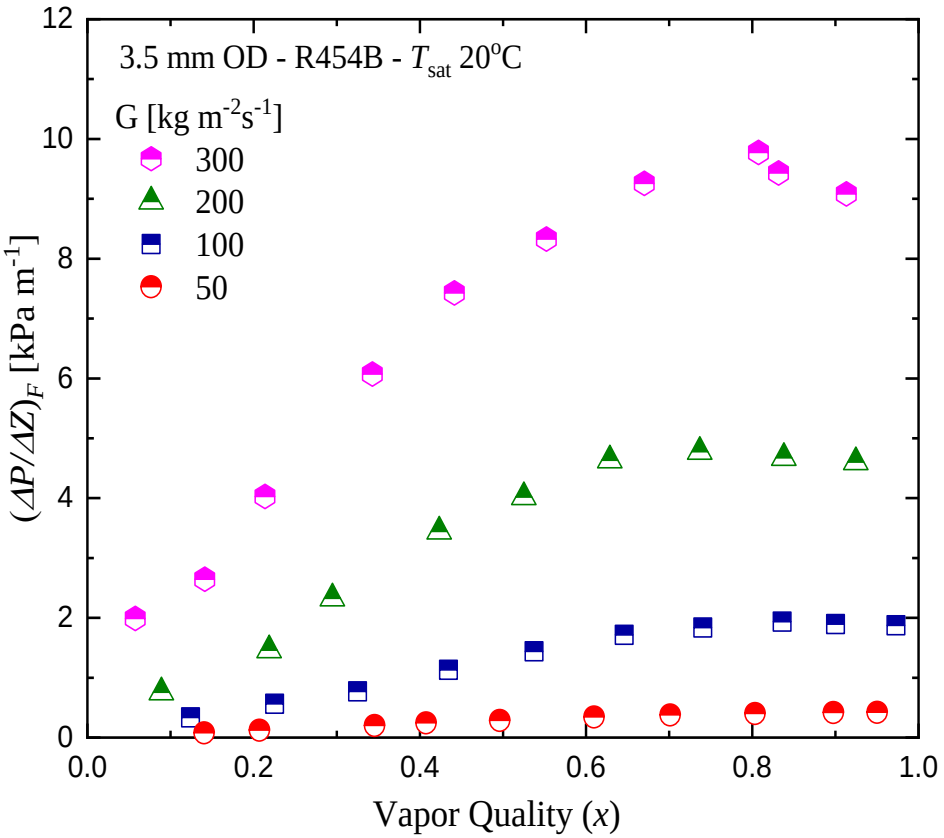

Fig. 6.10. Effect of mass velocity and vapor quality on frictional pressure drop of R454B

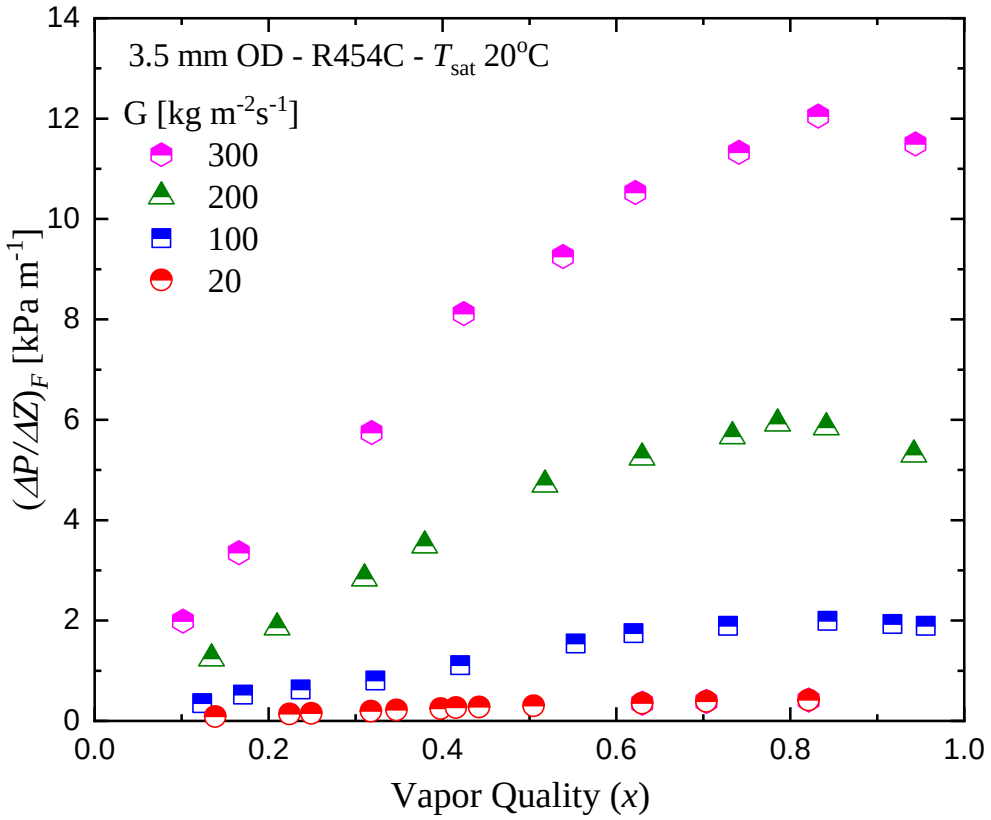

Fig. 6.11. Effect of mass velocity and vapor quality on frictional pressure drop of R454C

Fig. 6.11 depicts the result of experimental frictional pressure drop against the vapor quality at saturation temperature of 20 ºC for the mass velocity of 50 - 300 kg m^2s^1 in 3.5 mm outer diameter of microfin tube using refrigerant R454C. The same trend with figure 6.10 before, the higher pressure drop is at the mass velocity of 300 kg $m^{-2}s^{-1}$ with the value of frictional pressure drop reach of around 12 kPa m^{-1}. Here, the frictional pressure of R454C increased with increasing mass velocity and vapor quality. The effect of mass velocity and vapor quality on the increase of pressure drop due to increasing vapor shear stress and increased interfacial friction between vapor-liquid two-phase flow in the tube.

6.3.2 Comparison experimental result of frictional pressure drop of R454B, R454C and Pure refrigerant (R1234yf)

To compare the difference in frictional pressure drop between R454C and R454B and a comparison with pure refrigerant R1234yf, Figure 6.12 shows the comparison between the three refrigerants for each mass velocity.

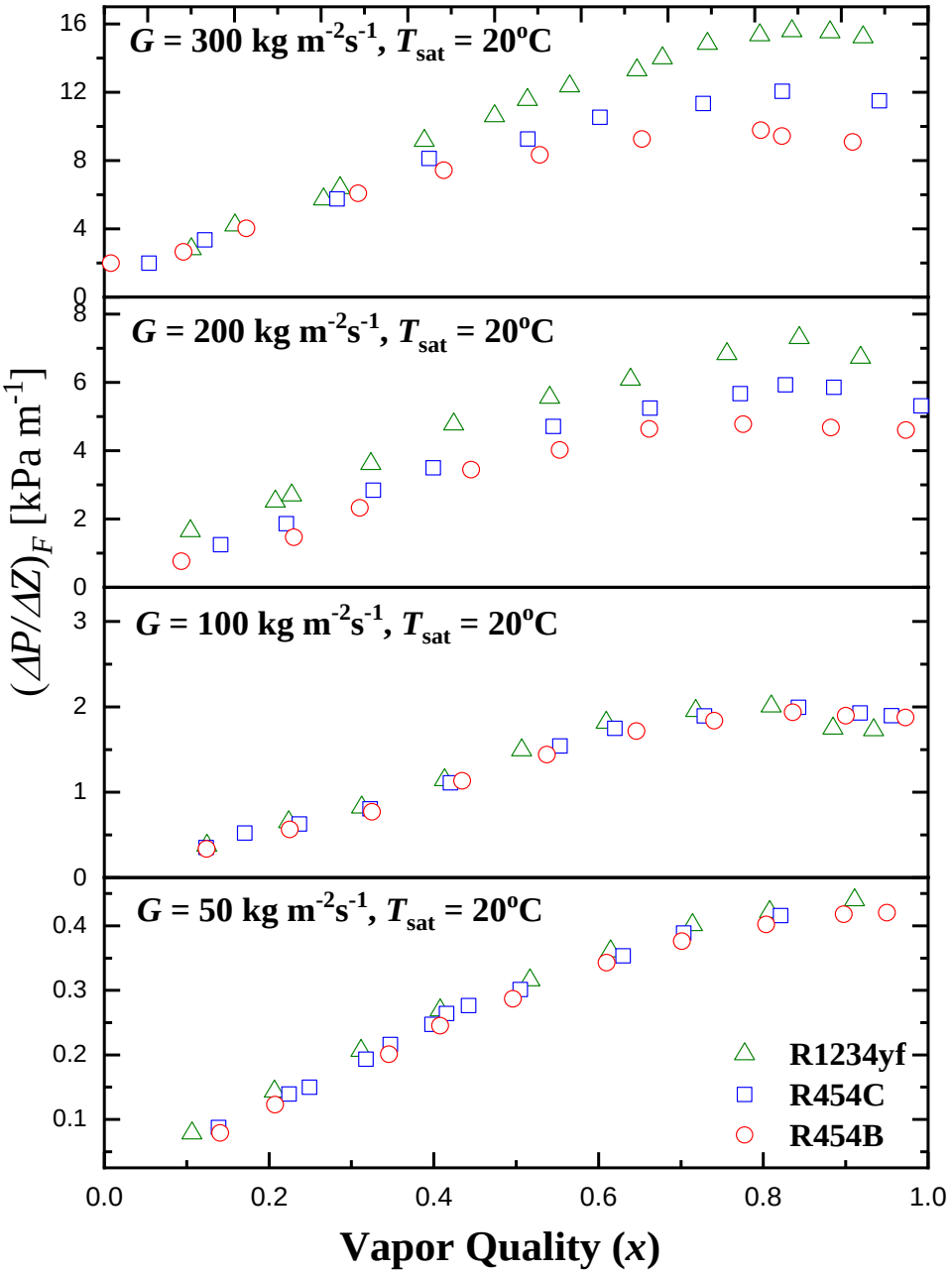

Fig. 6.12. Comparison frictional Pressure drop R454B, R454C and pure refrigerant (R1234yf)

Figure 6.12 shows that the frictional pressure drop of R454B is the lowest for each mass velocity, and R1234yf is the highest using the same microfin tube, where the results show that R1234yf has a frictional pressure drop value of 1.05 to 2.17 times greater than R454B and 1.06 to 1.32 times greater than 454C. A comparison between R454C and R454B shows that R454C is 1.01 to 1.64 times greater than R454B in the mass velocity

range of 50 kg $m^{-2}s^{-1}$ to 300 kg $m^{-2}s^{-1}$. This phenomenon is caused by the thermophysical difference between the three refrigerants, shown in table 6.2.

Table 6.2 comparison thermophisical properties of R454B, R454C and R1234yf at T_{sat}=20$_o$C (Lemmon et al., 2018)

T_{sat} [^oC]	ρ_l [kg m^{-3}]	ρ_v [kg m^{-3}]	μ_l [μPa-s]	μ_v [μPa-s]	σ [mN m^{-1}]
R454B	1005.6	43.80	121.6	12.5	6.87
R454C	1062.6	42.0	137.52	12.16	6.34
R1234yf	1109.9	32.80	162.26	11.17	6.80

Table 6.2 shows that the liquid viscosity and liquid density of R454B is lower than R454C and R1234yf, while the vapor density of R454B is higher than the others.

6.3.3 Comparison with Existing frictional pressure drop Correlation

Fig. 6.13 compares the experimental result of two-phase frictional pressure drop using R454B and R454C inside a 3.5 OD microfin tube and the predicted value using Existing correlation. One of existing correlation that used is (Goto et al., 2001) model.

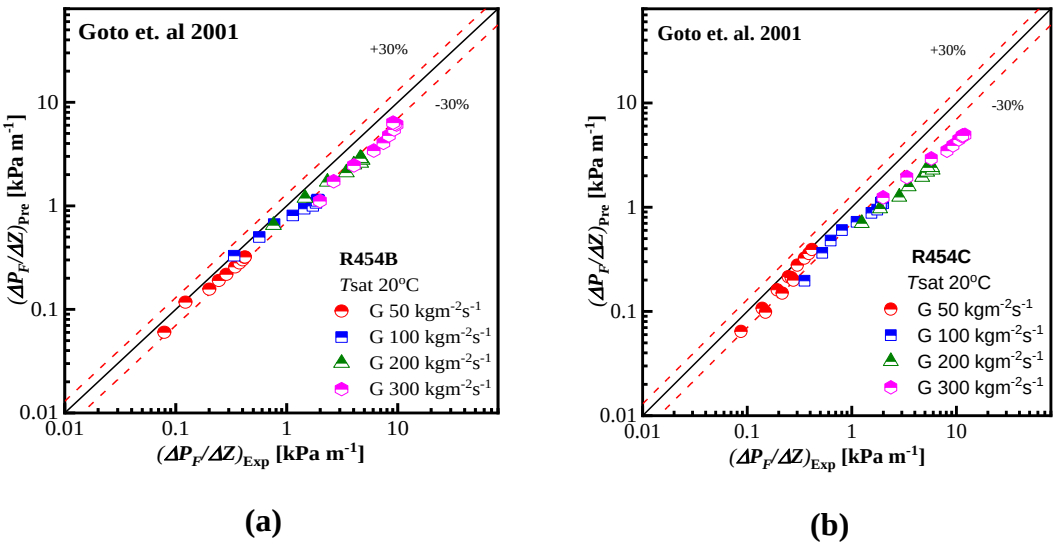

(a) **(b)**

Fig. 6.13. Comparison Experimental frictional Pressure drop and Predicted value using (Goto et al., 2001) correlation. (a) R454B (b) R454C

Figure 6.13 shows that (Goto et al., 2001) correlation majority underestimated with experimental data, especially in high mass velocity and well predicted in low mass velocity. The evaluation of the comparison model is seen in table 6.14. For R454B, the average deviation (AD) and the mean absolute deviation (MD) is 31% and 32%, respectively. While, for R45C, AD and MD are 32% and 34%, respectively.

Frictional pressure drop experimental data of R454B and R454C also compare with predicted data using the proposed correlation in chapter 3 as shown in Fig. 6.14. The result is well predicted for all mass velocities and refrigerants, with the average deviation and mean absolute deviation for R454C being -3.3% and 9.5%, respectively, and 97.6% of data points are within 30%. While, for R454B, AD and MD is 12.6% and 16.3%, respectively, and 84.6% of data points predicted by the proposed correlation are within 30%. The result can be seen in table 6.3.

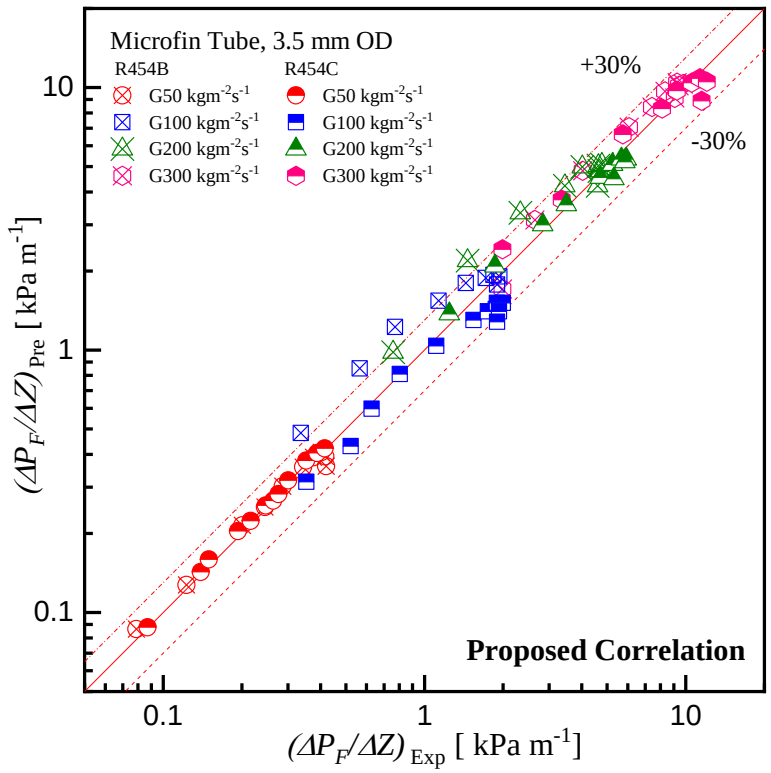

Fig. 6.14. Comparison Experimental frictional Pressure drop and Predicted value of R454B and R454C proposed correlation

Table 6.3. Deviation of frictional pressure drop R454B and R454C inside 3.5 OD microfin tube using (Goto et al., 2001) and proposed correlation

Correlation	R454C			R454B		
	AD (%)	MD (%)	R30 (%)	AD (%)	MD (%)	R30 (%)
Goto et al. 2001	-39.7	39.7	28.6	-31	31	46.2
Proposed Correlation	-3.3	9.5	97.6	12.6	16.3	84.6

6.4Result of Condensation Heat Transfer

6.4.1 Condensation Heat Transfer Coefficient of R454B and R454C

Fig. 6.15 shows the effect of mass velocity and vapor quality on condensation heat transfer coefficient at the saturation temperature of around 20 °C using refrigerant R454B inside 3.5 OD microfin tube. Three different mass velocities of 50, 100, and 200 kg $m^{-2}s^{-1}$ were varied. It was shown that the heat transfer coefficient increases with increased vapor quality and mass velocity. The velocity of vapor and liquid phases have been shown to be high at high vapor quality, resulting in high shear stress at the interface between vapor and liquid film relative to low vapor quality. There is a related rise in the heat transfer coefficient due to the increased interfacial shear stress. It is found that the heat transfer coefficient increases as vapor quality changes from 0.07 to 0.98. The heat transfer coefficient of R454B over the given vapor quality range increases from 2.1 to 14.9 kW m^{-2} K^{-1} with the increase in mass velocity from 50 to 200 kg m^{-2} s^{-1}.

For condensation heat transfer coefficient experimental data result of R454C also was conducted in three different mass velocities of 50, 100, and 200 kg $m^{-2}s^{-1}$ at the saturation temperature of around 20 °C. Fig. 6.16 depicts the effect of mass velocity and vapor quality on condensation heat transfer coefficient using refrigerant R454C inside 3.5 OD microfin tube. It was shown that the heat transfer coefficient increases with increased vapor quality and mass velocity and same trend with previous one. The velocity of vapor and liquid phases have been shown to be high at high vapor quality, resulting in high shear stress at the interface between vapor and liquid film relative to low vapor quality. There is a related rise in the heat transfer coefficient due to the increased interfacial shear stress. The heat transfer coefficient of R454C increases from 1.6 to 10.6 kW m^{-2} K^{-1} with the increase in mass velocity from 50 to 200 kg m^{-2} s^{-1}.

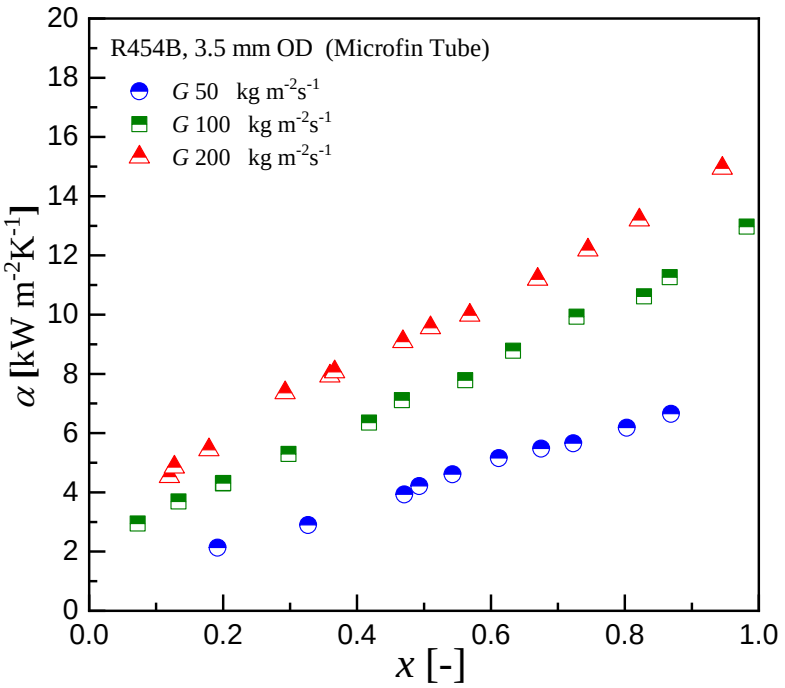

Fig. 6.15. Relation between condensation heat transfer coefficient and vapor quality at different mass velocity of R454B inside microfin tube

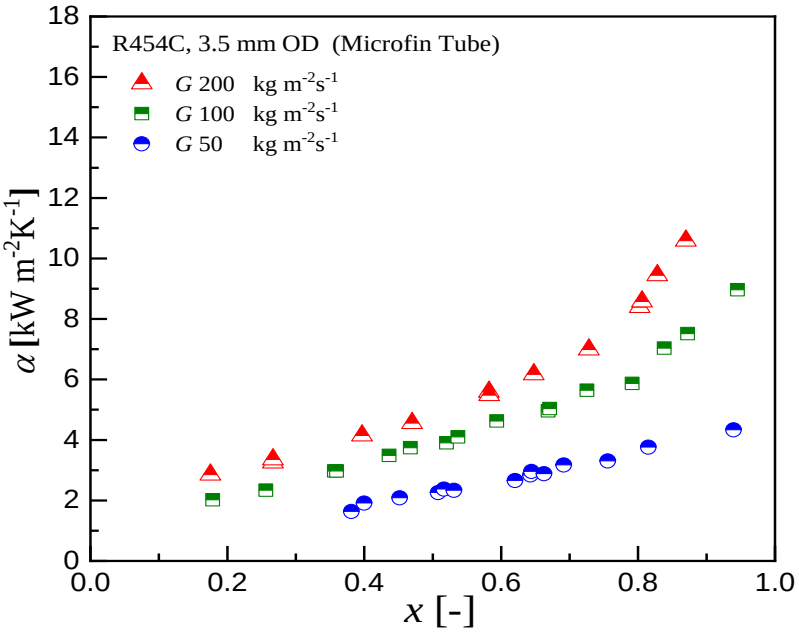

Fig. 6.16. Relation between condensation heat transfer coefficient and vapor quality at different mass velocity of R454C inside microfin tube

Figure 6.17 is an example of a combined graphic of refrigerant temperature distribution, wall, and water and is equipped with local heat transfer coefficient values, local heat flux, and vapor quality along the test tube during the condensation process.

This figure also includes the temperature at the inlet and outlet of the test section. It can be seen that the inlet and outlet temperatures, which are the refrigerant measurement temperatures, have a value close to the refrigerant temperature obtained using the iteration described previously, which is also estimated by supported by the Refrop program. Additionally, checking for measured refrigerant temperature inlet and outlet is also one of the procedures for clarifying the results of the iteration of the refrigerant temperature, where the refrigerant temperature must be close to its value with the inlet and outlet temperature of the test section in every experiment.

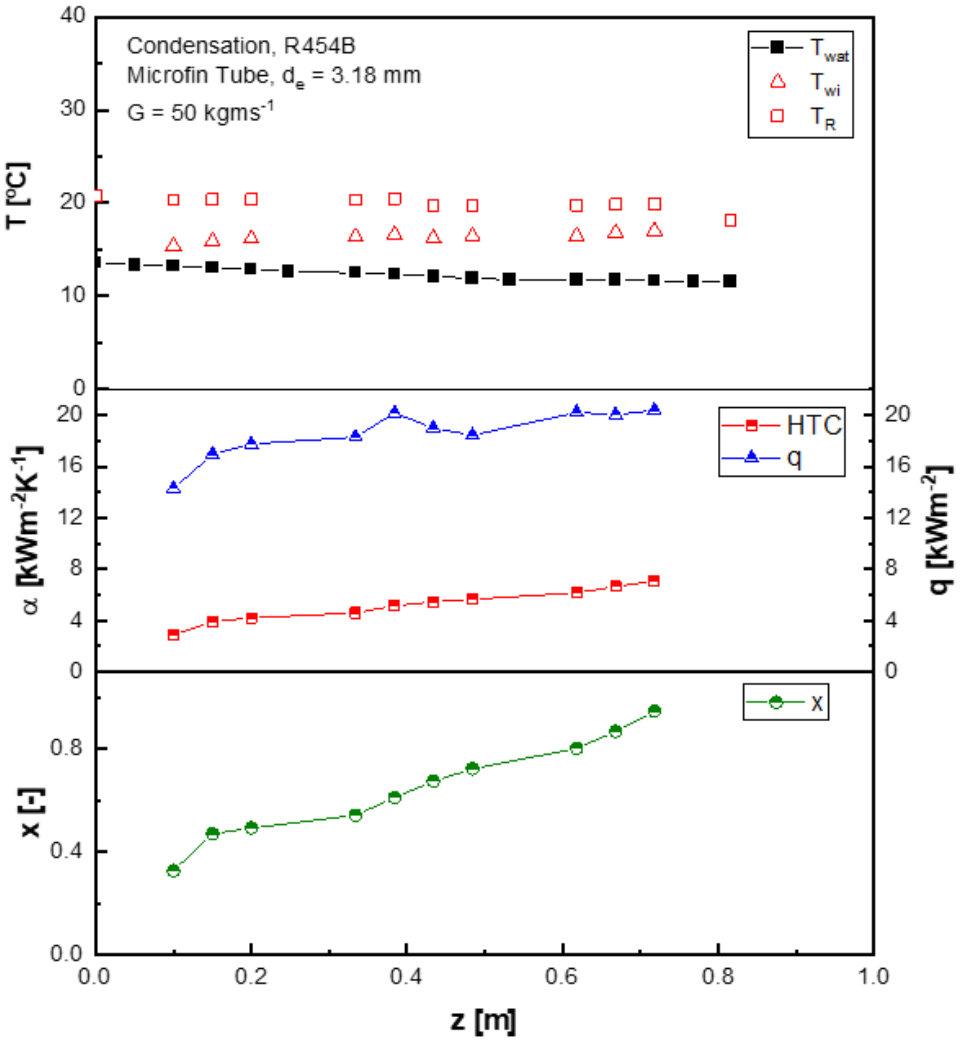

Fig. 6.17 Distribution temperature of refrigerant, wall, water in the test tube in condensation process.

6.4.2 Comparison experimental result of condensation heat transfer coefficient of R454B, R454C and Pure refrigerant (R1234yf)

To compare the difference in condensation heat transfer coefficient between R454C and R454B and a comparison with pure refrigerant R1234yf, Figure 6.17 shows the comparison between the three refrigerants for each mass velocity.

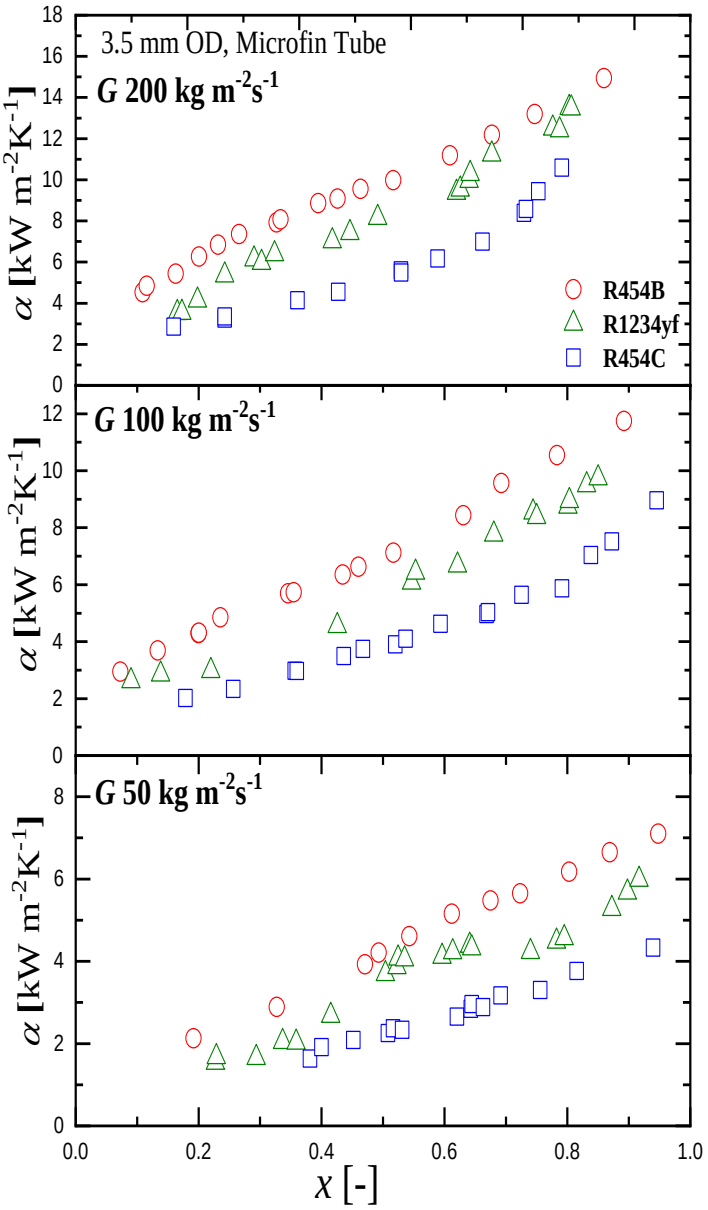

Fig. 6.18. Comparison condensation heat transfer coefficient of R454B, R454C and pure refrigerant (R1234yf) inside 3.5 mm OD microfin tube

Figure 6.18 compares the heat transfer coefficient of R454B and R454C with pure refrigerant R1234yf with the same mass velocity and tube specifications. The figure

shows that HTC's R454B is slightly larger than R1234yf, increasing 1.1 to 1.5 times enhancement in all mass velocities from 50 to 200 $kgm^{-2}s^{-1}$. With a sizeable R32 composition of about 68.9% in R454B, HTC's increase is relatively small. The condition is because of the degradation of HTC due to mass transfer resistance due to the presence of a temperature glide of zeotropic mixture refrigerant.

HTC's R454C is lower than R1234yf for all mass velocities with 1.2 to 1.7 degradation from R1234yf. The Degradation of heat transfer coefficient from this zeotropic mixture refrigerant due to mass transfer resistance during the condensation process due to the presence of a temperature glide of zeotropic mixture refrigerant.

6.4.3 Comparison with Existing of condensation heat transfer coefficient Correlation

Figure 6.19 shows the comparison between the experimental heat transfer coefficient and heat transfer coefficient from the correlation using the condensation heat transfer model developed by (Hirose et al., 2018).

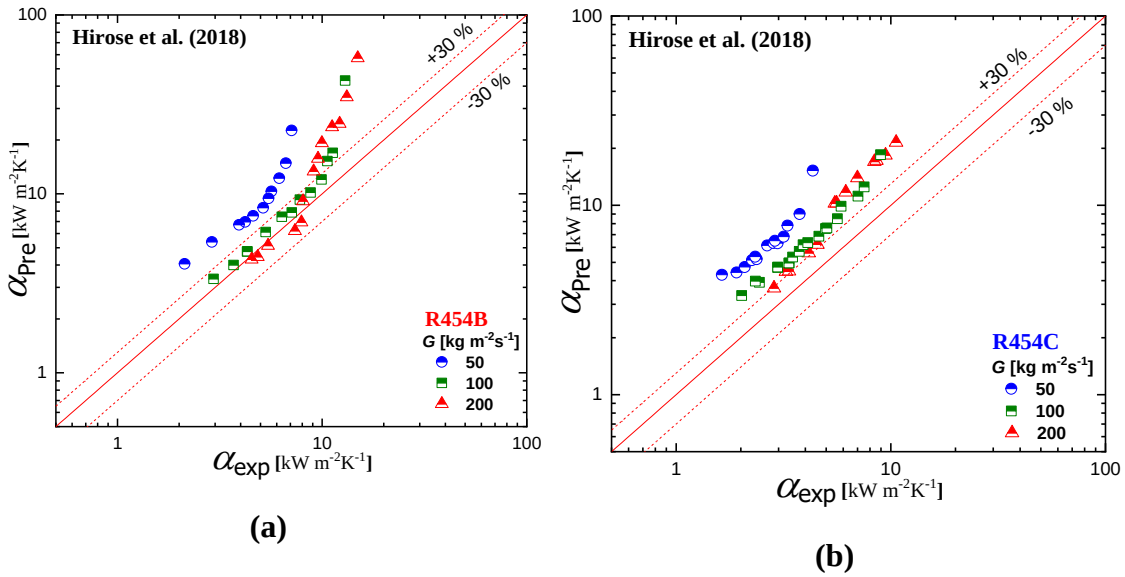

Fig. 6.19. Comparison Experimental condensation heat transfer coefficient and Predicted value of using (Hirose et al., 2018) correlation (a) R454B (b) R454C

Fig 6.19 show that for experimental data of R454C, the correlation majority is not well predicted and majority overestimated with average deviation (AD), and the mean absolute deviation (MD) is 86.6% and 86.6%, respectively and 2.2% of data point are within 30%. While, for R454B have similar trend with R454C with AD and MD is 64% and 67% and 43.2% of data point are within 30%. The result of deviation can be seen in

table

Figure 6.20 shows the comparison between the experimental heat transfer coefficient and heat transfer coefficient from the correlation using the proposed correlation for pure refrigerant in chapter 4.

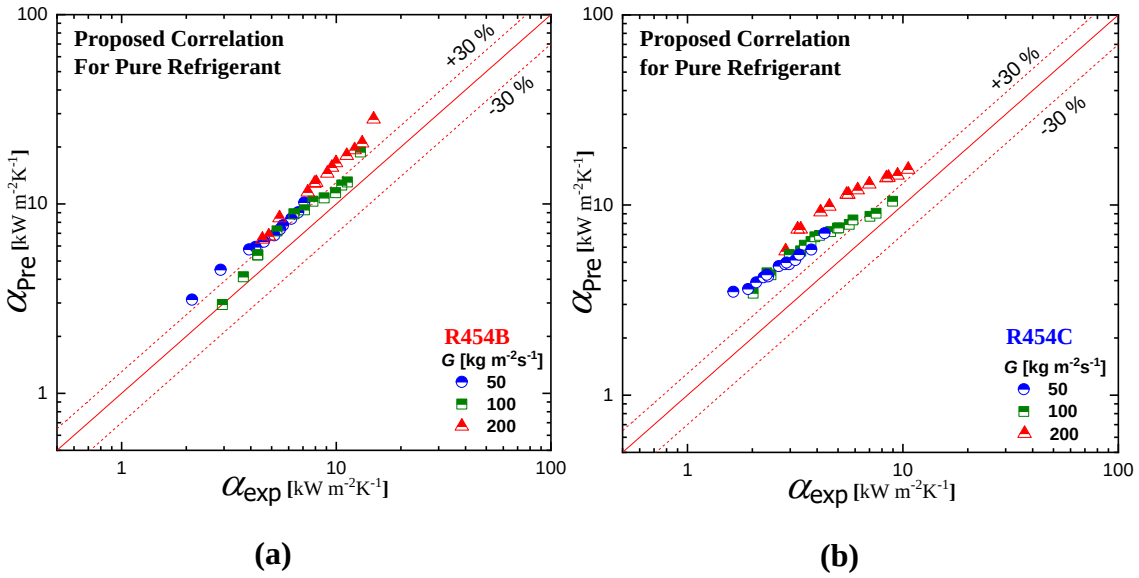

Fig. 6.20. Comparison Experimental condensation heat transfer coefficient and Predicted value of proposed correlation for pure Refrigerant (a) R454B (b) R454C

Fig 6.20 show that for experimental data of R454C, the correlation majority is not well predicted and majority overestimated with average deviation (AD), and the mean absolute deviation (MD) is 74.19% and 74.19%, respectively and 6.52.2% of data point are within 30%. While, for R454B have similar trend with R454C with AD and MD is 41.79% and 41.80% and 21.62% of data point are within 30%. The result of deviation can be seen in table 6.4.

The predictive model of (Hirose et al., 2018) and proposed correlation were developed using experimental data using microfin tube, where the Hirose diameter is close to this study, where the equivalent diameter is 3.48 mm, and proposed correlation using same tube in experiment to obtained data. However, the estimation results show that the majority of the prediction results are larger than the experimental results. The condition is because the prediction model was developed using pure refrigerants. Therefore, it can be concluded that there is a degradation of this heat transfer coefficient compared to a pure refrigerant. This degradation is caused by the mass transfer resistance of the zeotropic refrigerant.

Table 6.4. Deviation of Condensation heat transfer R454B and R454C inside 3.5 OD microfin tube using (Hirose et al., 2018) correlation and Proposed correlation for Pure Refrigerant

Correlation	R454B			R454C		
	AD (%)	MD (%)	R30 (%)	AD (%)	MD (%)	R30 (%)
(Hirose et al., 2018) correlation	64	67	43.2	86.6	86.6	2.2
Proposed Correlation for Pure Refrigerant	41.79	41.80	21.62	74.19	74.19	6.52

6.5 Result of Boiling Heat transfer

6.5.1 Boiling Heat Transfer Coefficient of R454B and R454C

The heat transfer coefficient is affected by mass velocity as a function of vapor quality, as shown in Fig 6.20. The vapor quality variances between the inlet and outlet of the test section range from 0.1 to 0.9 in these experimental conditions. Nucleate boiling appears to dominate the phase-change process, the mass velocity effect is not as noticeable as the heat transfer coefficient remains constant at around 7 kW m^{-2} K^{-1} in low vapor quality region up to vapor quality of 0.35. However, in the region of high vapor quality, as the mass velocity increases, the heat transfer coefficient increases, meaning that two-phase forced convection plays a dominant role in the flow boiling mechanism. Two-phase forced convection is always present and dominant in the phase change process because the heat transfer coefficient becomes unstable as the mass velocity increases.

Generally, the heat transfer coefficient increases slightly with vapor quality at low mass velocities, and no dry-out occurs. On the other hand, it rises with vapor quality at high mass velocities, reaches a peak, and then drops suddenly due to dry-out phenomena. In Fig. 6.21, it can be seen that the highest heat transfer coefficient is obtained at a mass velocity of 200 kg m^2s^{-1} with a vapor quality of 0.86 with a value of 12 kW m^{-2} K^{-1}.

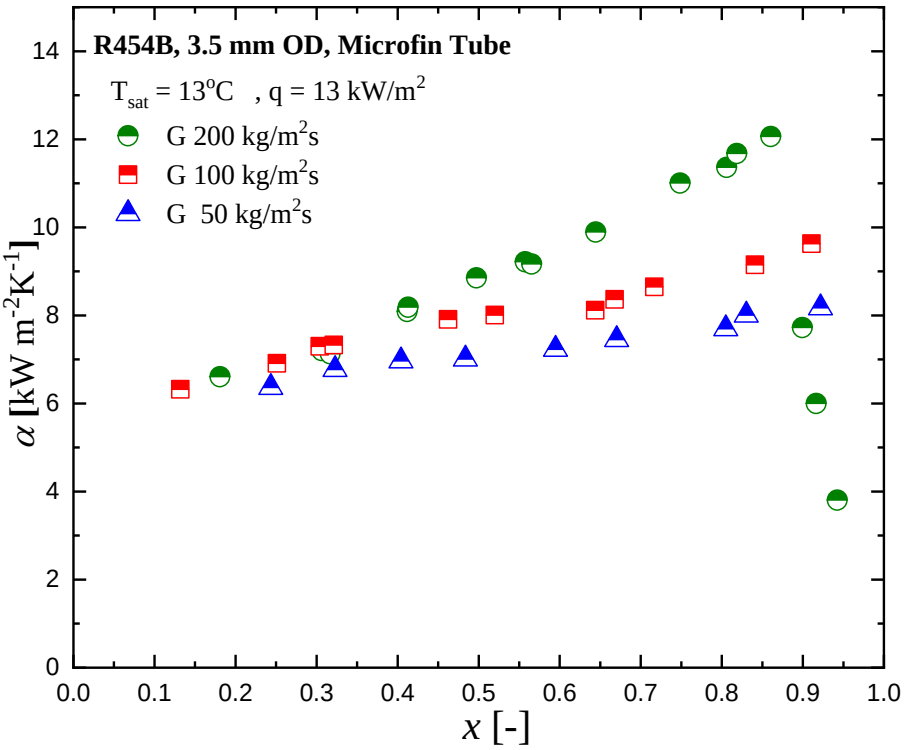

Fig. 6.21. Effect of mass velocity and vapor qaulity on boiling heat transfer using R454B inside 3.5 OD microfin tube

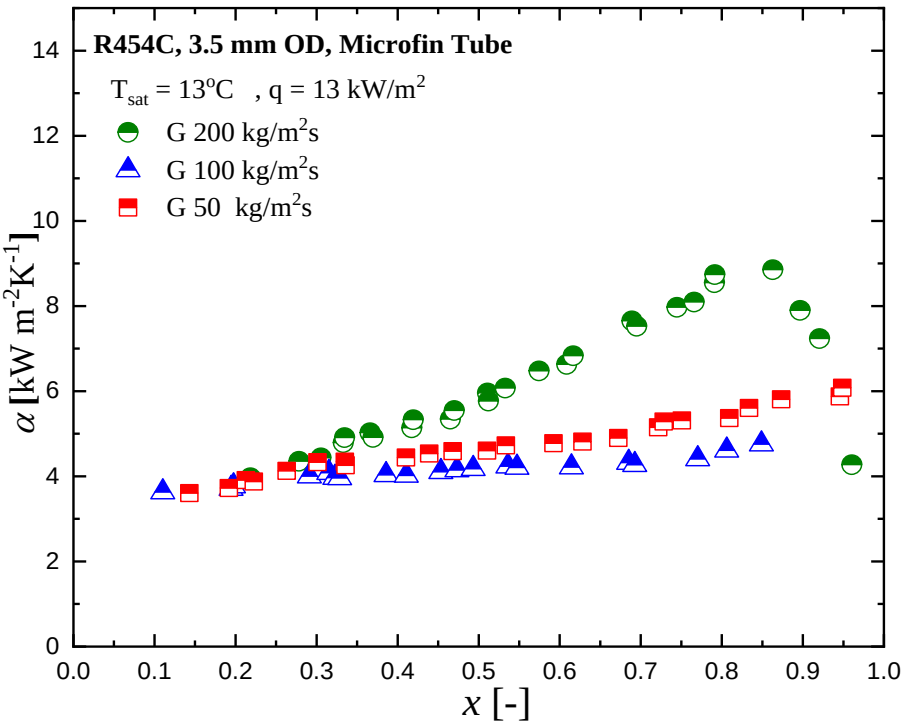

Fig. 6.22. Effect of mass velocity and vapor quality on boiling heat transfer using R454C inside 3.5 OD microfin tube

Fig 6.22 show the same trend with before. It show the Effect of mass velocity and vapor quality on boiling heat transfer using R454C inside 3.5 OD microfin tube. Nucleate boiling also appears to dominate the phase-change process, the mass velocity effect is not as noticeable as the heat transfer coefficient remains constant at around 4 kW m^{-2} K^{-1} in low vapor quality region up to vapor quality of 0.3. However, in the region of high vapor quality, as the mass velocity increases, the heat transfer coefficient increases, meaning that two-phase forced convection plays a dominant role in the flow boiling mechanism. Two-phase forced convection is always present and dominant in the phase change process because the heat transfer coefficient becomes unstable as the mass velocity increases.

Fig. 6.23 shows the effect of heat flux at the same mass velocity. In mass velocity 200 $kgm^{-2}s^{-1}$, two kind of heat flux for experimental condition is conducted in experiment to clarify the effect of heat flux for both R45CB and R454C. The heat transfer coefficient increased with increasing heat flux due to the enhancement of nucleate boiling in the low vapor quality region. The impact of heat flux are readily visible: nucleate boiling is the most crucial heat transfer mechanism.

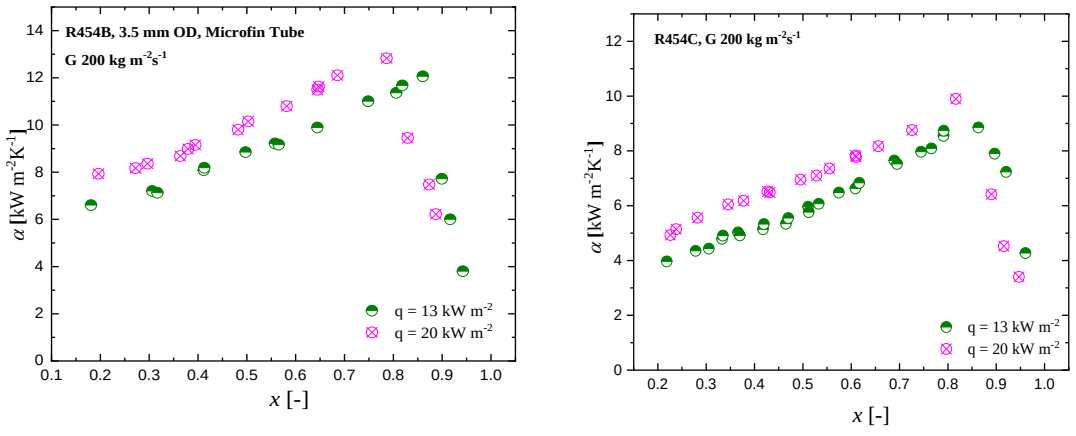

(a) (b)

Fig. 6.23. Effect of heat flux on boiling heat transfer inside 3.5 OD microfin tube.
(a) R545B, (b) R454C

Figure 6.24 is an example of a combined graphic of refrigerant temperature distribution, wall, and water and is equipped with local heat transfer coefficient values, local heat flux, and vapor quality along the test tube during flow boiling process. This figure also includes the temperature at the inlet and oulet of the test section. It can be seen

that the inlet and outlet temperatures, which are the refrigerant measurement temperatures, have a value close to the refrigerant temperature obtained using the iteration described previously, which is also estimated by supported the Refrop program. Additionally, checking for measured refrigerant temperature inlet and outlet is also one of the procedures for clarifying the results of the iteration of the refrigerant temperature, where the refrigerant temperature must be close to its value with the inlet and outlet temperature of the test section every experiment.

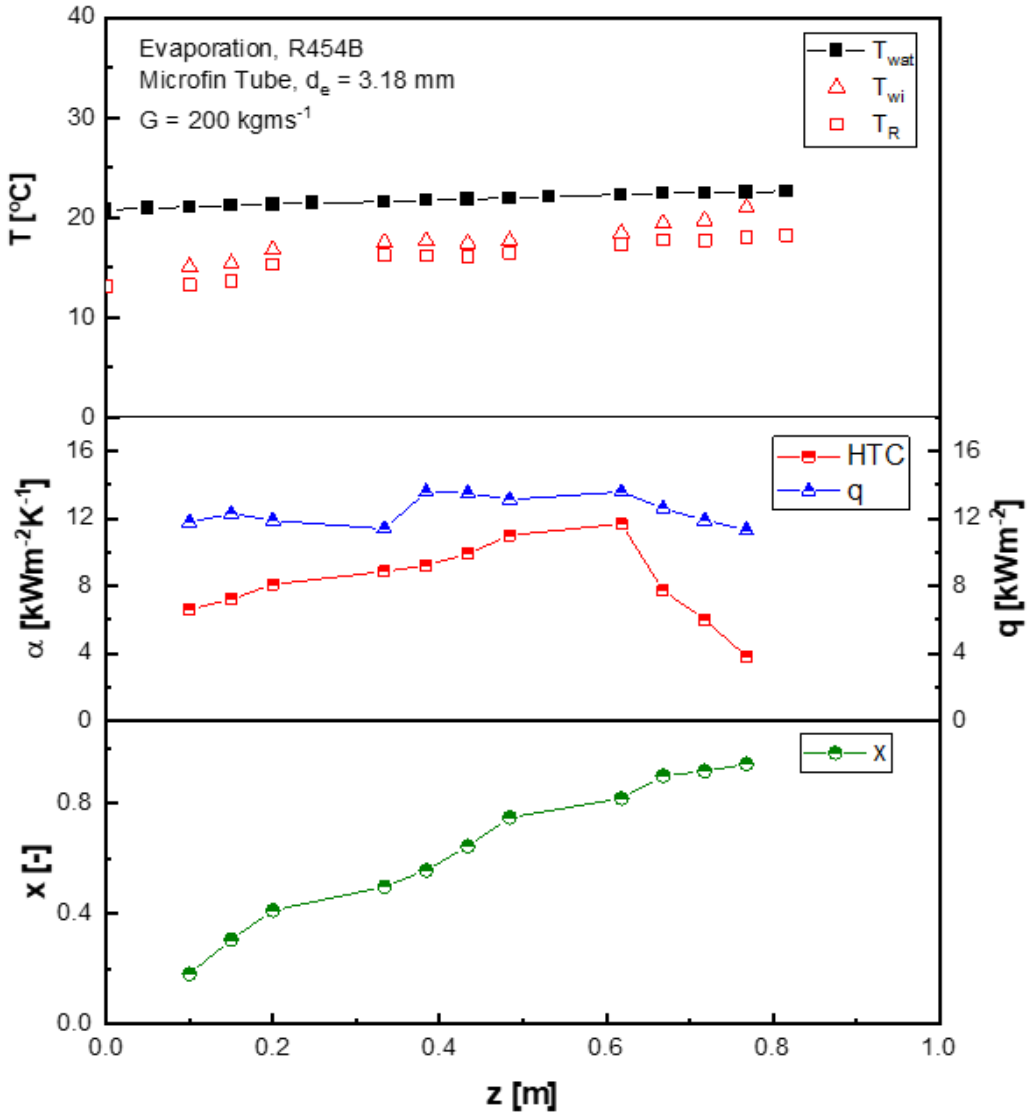

Fig. 6.24 Distribution temperature of refrigerant, wall, water in the test tube in evaporation process.

6.5.2 Comparison experimental result of flow boiling heat transfer coefficient of R454B, R454C and Pure refrigerant (R1234yf)

Figure 6.25 compares the Boiling heat transfer coefficient of R454B and R454C with pure refrigerant R1234yf with the same mass velocity and tube specifications. The figure shows that HTC's R454B is slightly larger than R1234yf, increasing 1.2 to 1.4 times enhancement in all mass velocities from 50 to 200 $kgm^{-2}s^{-1}$. With a sizeable R32 composition of about 68.9% in R454B, HTC's increase is relatively small. The condition is because of the degradation of HTC due to mass transfer resistance due to the presence of a temperature glide of zeotropic mixture refrigerant.

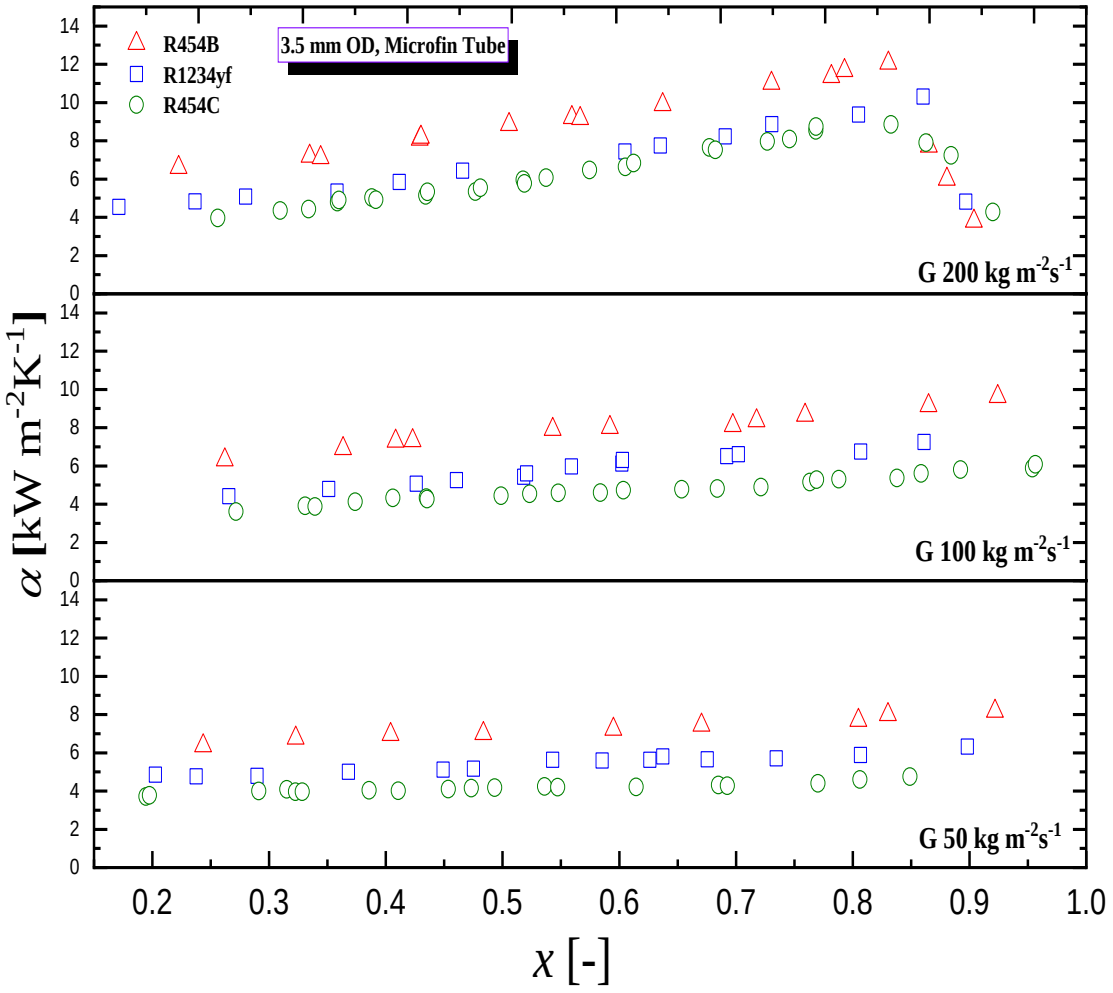

Fig. 6.25. Comparison Boiling heat transfer coefficient of R454B, R454C and pure refrigerant (R1234yf) inside 3.5 mm OD microfin tube

HTC's R454C is lower than R1234yf for all mass velocities with 1.1 to 1.4 degradation from R1234yf. The Degradation of heat transfer coefficient from this zeotropic mixture refrigerant due to mass transfer resistance during the evaporation process due to the presence of a temperature glide of zeotropic mixture refrigerant.

6.6 Conclusion

This study investigated the two-phase flow condensation and boiling heat transfer as well as adiabatic pressure drop of R454B and R454C inside a 3.5 mm OD microfin tube. The effects of mass velocity and vapor quality, heat flux (just for flow boiling) were analyzed and discussed. The heat transfer coefficient is measured for mass velocity ranging between 50 kg $m^{-2}s^{-1}$and 200 kg $m^{-2}s^{-1}$, vapor quality from 0.1 to 0.9 and compared with existing correlation with the following conclusions:

- The frictional pressure of R454B and R454C increased with increasing mass velocity and vapor quality. The effect of mass velocity and vapor quality on the increase of pressure drop due to increasing vapor shear stress and increased interfacial friction between vapor-liquid two-phase flow in the tube.
- The frictional pressure drop of R454B is the lowest for each mass velocity, and R1234yf is the highest using the same microfin tube, where the results show that R1234yf has a frictional pressure drop value of 1.05 to 2.17 times greater than R454B and 1.06 to 1.32 times greater than 454C. A comparison between R454C and R454B shows that R454C is 1.01 to 1.64 times greater than R454B in the mass velocity range of 50 kg $m^{-2}s^{-1}$ to 300 kg $m^{-2}s^{-1}$. This phenomenon is caused by the thermo-physical difference between the three refrigerants.
- (Goto et al., 2001) correlation majority underestimated with frictional pressure drop experimental data, especially in high mass velocity and well predicted in low mass velocity. For R454B, the average deviation (AD) and the mean absolute deviation (MD) is 31% and 32%, respectively. While, for R45C, AD and MD are 32% and 34%, respectively.
- Frictional pressure drop experimental data of R454B and R454C also compare with predicted data using the proposed correlation in chapter 3. The result is well predicted for all mass velocities and refrigerants, with the average deviation and mean absolute deviation for R454C being -3.3% and 9.5%, respectively, and

97.6% of data points are within 30%. While, for R454B, AD and MD is 12.6% and 16.3%, respectively, and 84.6% of data points predicted by the proposed correlation are within 30%.

- The condensation's HTC increases with increased vapor quality and mass velocity. There is a related rise in the heat transfer coefficient due to the increased interfacial shear stress. It is found that the heat transfer coefficient increases as vapor quality changes from 0.07 to 0.98. The heat transfer coefficient of R454B over the given vapor quality range increases from 2.1 to 14.9 kW m^{-2} K^{-1} with the increase in mass velocity from 50 to 200 kg m^{-2} s^{-1}.
- The heat transfer coefficient of R454C increases from 1.6 to 10.6 kW m^{-2} K^{-1} with the increase in mass velocity from 50 to 200 kg m^{-2} s^{-1}.
- HTC's R454B is slightly larger than R1234yf, increasing 1.1 to 1.5 times enhancement in all mass velocities from 50 to 200 $kgm^{-2}s^{-1}$. With a sizeable R32 composition of about 68.9% in R454B, HTC's increase is relatively small. The condition is because of the degradation of HTC due to mass transfer resistance due to the presence of a temperature glide of zeotropic mixture refrigerant.
- HTC's R454C is lower than R1234yf for all mass velocities with 1.2 to 1.7 degradation from R1234yf. The Degradation of heat transfer coefficient from this zeotropic mixture refrigerant due to mass transfer resistance during the condensation process due to the presence of a temperature glide of zeotropic mixture refrigerant.
- Condensation Heat transfer experimental data of R454B and R454C also compare with predicted data using the proposed correlation for pure refrigerant Fig 6.19 . The correlation majority is not well predicted for R454C and majority overestimated with average deviation (AD), and the mean absolute deviation (MD) is 74.19% and 74.19%, respectively and 6.52% of data point are within 30%. While, for R454B have similar trend with R454C with AD and MD is 41.79% and 41.80% and 21.62% of data point are within 30%. The condition is because the proposed correlation was developed using pure refrigerants. Therefore, it can be concluded that there is a degradation of this heat transfer coefficient compared to a pure refrigerant. This degradation is caused by the mass transfer resistance of the zeotropic refrigerant.

- For boiling process, generally, the heat transfer coefficient increases slightly with vapor quality at low mass velocities, and no dry-out occurs. On the other hand, it rises with vapor quality at high mass velocities, reaches a peak, and then drops suddenly due to dry-out phenomena. For R454B, the highest heat transfer coefficient is obtained at a mass velocity of 200 kg m^2s^{-1} with a vapor quality of 0.86 with a value of 12 kW m^{-2} K^{-1}. And for R454C, the highest heat transfer coefficient is obtained at a mass velocity of 200 kg m2s-1 with a vapor quality of 0.86 with a value of 8.8 kW m^{-2} K^{-1}.
- Nucleate boiling appears to dominate the phase-change process, the mass velocity effect is not as noticeable as the heat transfer coefficient remains constant at around 7 kW m^{-2} K^{-1} in low vapor quality region up to vapor quality of 0.35 for R454B and at around 4 kW m^{-2} K^{-1} in low vapor quality region up to vapor quality of 0.3 for R454C. However, in the region of high vapor quality, as the mass velocity increases, the heat transfer coefficient increases, meaning that two-phase forced convection plays a dominant role in the flow boiling mechanism. Two-phase forced convection is always present and dominant in the phase change process because the heat transfer coefficient becomes unstable as the mass velocity increases.
- Two kind of heat flux for experimental condition is conducted in experiment to clarify the effect of heat flux for both R45CB and R454C. The heat transfer coefficient increased with increasing heat flux due to the enhancement of nucleate boiling in the low vapor quality region. The impact of heat flux are readily visible: nucleate boiling is the most crucial heat transfer mechanism.

References

ASHRAE, 2019. Designation and Safety Classification of Refrigerants. ANSI/ASHRAE Stand. 34-2019 2019, 1–52.

Devecioğlu, A.G., 2017. Seasonal performance assessment of refrigerants with low GWP as substitutes for R410A in heat pump air conditioning devices. Appl. Therm. Eng. 125, 401–411. https://doi.org/10.1016/j.applthermaleng.2017.07.034

Goto, M., Inoue, N., Ishiwatari, N., 2001. Condensation and evaporation heat transfer of R410A inside internally grooved horizontal tubes. Int. J. Refrig. 24, 628–638.

https://doi.org/10.1016/S0140-7007(00)00087-6

Hirose, M., Ichinose, J., Inoue, N., 2018. Development of the general correlation for condensation heat transfer and pressure drop inside horizontal 4 mm small-diameter smooth and microfin tubes. Int. J. Refrig. 90, 238–248. https://doi.org/10.1016/j.ijrefrig.2018.04.014

IPCC 2007, 2007. Climate Change 2007: The Physical Science Basis. Contribution of Working Group I to the Fourth Assessment Report of the Intergovernmental Panel on Climate Change. Summary for Policymakers. (Edited by Solomon, S. DQin MManning ZChen MMarquis KAveryt MHL MS. p. 996.

Kariya, K., Sonoda, K., Miyara, A., 2018. Condensation and evaporation local heat transfer characteristics of the refrigerant mixture of R1123 and R32 inside a plate heat exchanger 1–9.

Lemmon, E.W., Bell, I.H., Huber, M.L., McLinden, M.O., 2018. NIST Standard Reference Database 23: Reference Fluid Thermodynamic Properties-REFPROP (DLL Version 10.0a). NIST, USA.

Miyara, A., Kariya, K., Inoue, N., Jige, D., 2021. Evaporation of Low GWP A2L Refrigerants in Small Diameter Tubes and Plate Heat Exchanger, in: Ashrae Virtual Annual Conference.

Mohanraj, M., Muraleedharan, C., Jayaraj, S., 2011. A review on recent developments in new refrigerant mixtures for vapour compression-based refrigeration, air-conditioning and heat pump units. Int. J. ENERGY Res. 35, 647–669. https://doi.org/10.1002/er.1736

Mota-Babiloni, A., Makhnatch, P., Khodabandeh, R., 2017. Recent investigations in HFCs substitution with lower GWP synthetic alternatives: Focus on energetic performance and environmental impact Adrián. Int. J. Refrig. 82, 288–301. https://doi.org/10.1016/j.ijrefrig.2017.06.026

Radermacher, R., Hwang, Y., 2005. Vapor Compression Heat Pumps with Refrigerant Mixtures, 1st ed. CRC Press, New York. https://doi.org/10.1201/9781420037579

Shen, B., Li, Z., Gluesenkamp, K.R., 2022. Experimental study of R452B and R454B as drop-in replacement for R410A in split heat pumps having tube-fin and microchannel heat exchangers. Appl. Therm. Eng. 204, 117930. https://doi.org/10.1016/j.applthermaleng.2021.117930

Tran, N., Kasireddy, R.V., Wang, C.C., 2021. An experimental investigation on convective boiling heat transfer of R-454B with lubricant oil of POE-32 or POE-68

mixture in a horizontal smooth tube. Int. J. Heat Mass Transf. 181, 121990. https://doi.org/10.1016/j.ijheatmasstransfer.2021.121990

United States Environmental Protection Agency (EPA), n.d. Section 608 Technician Certification.

Zhao, L., Zeng, W., Yuan, Z., 2015. Reduction of potential greenhouse gas emissions of room air-conditioner refrigerants: A life cycle carbon footprint analysis. J. Clean. Prod. 100, 262–268. https://doi.org/10.1016/j.jclepro.2015.03.063

CHAPTER

7

CONCLUSIONS AND RECOMMENDATIONS

7.1 Conclusions

In this current study, experimental data on pressure drop and heat transfer in two-phase flow in microfin tubes (*do* = 3.5 mm) for pure refrigerant, R1234yf and mixture refrigerants, R454 B and R454C are presented. Moreover, two-phase frictional pressure drop and condesantion heat transfer correlations are developed based on the experimental data and previous data.

7.1.1. Summary of Experimental Investigation And Development General Correlation For Frictional Pressure Drop of Two-Phase Flow Inside Microfin Tube

1) The two-phase frictional pressure drop experiments of R1234yf in microfin with outer diameter 3.5 mm have been conducted in this study at saturation temperature of 20 °C and 30°C, mass velocity from 50 kg $m^{-2}s^{-1}$ to 300 $kgm^{-2}s^{-1}$, and vapor quality 0.1-0.9. The previous data with the 2.5 mm outer diameter microfin tube was added for further analysis.

2) The effects of mass velocity, vapor quality, saturation temperature, and diameter of microfin were analyzed. As a whole, the increase of frictional pressure drop was observed with the decrease of microfin diameter. The smaller diameter of the microfin tube leads to the increase of shear stress due to the increase of velocity gradients. Further, the increasing vapor shear stress and friction between liquid and vapor phase at higher mass velocity and vapor quality increase the pressure drop.

3) Some existing correlations of microfin tubes were used to assess the two-phase frictional pressure drop of experimental data. The previous correlations cannot well predict the experimental data.

4) A new correlation was developed and the proposed correlation expressed the experimental data of 3.5 mm OD and 2.5 mm OD very well with a mean deviation of 12.2 %, average deviation of -0.6 %, and 92.3 % of the data points are within the deviation of 30%. Validation of the new correlation with 699 data points from other researchers gave good agreement with approximately 17.6 % of mean deviation. The newly developed correlation could broadly be applied to the microfin tube diameter of 2.5 mm to 9.52 mm and the wide range of mass velocity and several refrigerants.

7.1.2 Summary of Experimental Investigation on Condensation Heat Transfer of Refrigerant R1234yf in Horizontal Microfin Tube And Development

1) Experimental study of condensation heat transfer coefficient of refrigerant R1234yf inside 3.5 OD horizontal microfin tube has been carried out. The effect of mass velocity, vapor quality, tube diameter, and saturation on condensation heat transfer coefficient was investigated.
2) The results show the heat transfer coefficient decreases as the wetness increases for mass velocities of 3.18 mm and 2.17 mm equivalent diameter of the test tube. Also, the findings show that as the microfin tube's diameter is decreased, the heat transfer coefficient increases. The increase of saturation temperatures resulted in decreased heat transfer coefficient due to the refrigerant's changing thermal properties.
3) Four correlations of the heat transfer coefficients for microfin tubes from the literature were used to predict the heat transfer coefficient. Hirose et al., 2018 correlation has good agreement with experimental data than other correlation. However, slightly overestimated, especially at low mass velocity. Therefore, the development of a new correlation of microfin tubes is required.
4) The new correlation for heat transfer condensation was developed. The proposed correlation agrees well with the measured data with average deviation and mean

absolute deviation is 0.19% and 13.34%, respectively and 90.74% data points are within 30%.

7.1.3 Summary of Experimental study on flow boiling heat transfer of R1234yf inside a 3.5 mm OD horizontal microfin

1) This study presents experimental flow boiling heat transfer coefficients of R1234yf inside a microfin tube with equivalent inner diameter of 3.18 mm. The mass velocity varied from 50 to 200 kg $m^{-2}s^{-1}$, the heat fluxes from 13 to 20 kWm^{-2}, with a saturation temperature of 13 °C.
2) Generally, the heat transfer coefficient rises slightly with vapor quality at low mass velocity. It rises with vapor quality at high mass velocity, reaches a peak, and drops at around 0.9 of vapor quality due to dry-out phenomena.
3) In the low vapor quality region, the effect of mass velocity is not so remarkable, and the nucleate boiling dominates the heat transfer. On the other hand, forced convection is present and dominant in the heat transfer process in the high-quality region.
4) The heat transfer coefficient reaches 10.8 kW m^{-2} K^{-1} at vapor quality 0.89 in a condition of the mass velocity 200 kg $m^{-2}s^{-1}$ and the heat flux 13 kWm^{-2}. The effect of heat flux was observed in the mass velocity 200 kg $m^{-2}s^{-1}$ and the impacts of heat flux are readily visible: nucleate boiling is the most crucial heat transfer mechanism.
5) The existing correlation (Wu et al., 2013) is a good prediction of experimental data with the mean deviation of 22.6%.

7.1.4 Summary of Experimental Study On Pressure Drop And Two-phase Heat Transfer Of Mixture Refrigerant (R454B and R454C) Inside Microfin Tube

1) This study investigated the two-phase flow condensation and boiling heat transfer as well as adiabatic pressure drop of R454B and R454C inside a 3.5 mm OD microfin tube. The effects of mass velocity and vapor quality, heat flux (just for flow boiling) were analyzed and discussed. The heat transfer coefficient is measured for mass velocity ranging between 50 kg $m^{-2}s^{-1}$and 200 kg $m^{-2}s^{-1}$, vapor quality from 0.1 to 0.9 and compared with existing correlation.
2) The frictional pressure of R454B and R454C increased with increasing mass velocity and vapor quality. The effect of mass velocity and vapor quality on the

increase of pressure drop due to increasing vapor shear stress and increased interfacial friction between vapor-liquid two-phase flow in the tube.

3) The frictional pressure drop of R454B is the lowest for each mass velocity, and R1234yf is the highest using the same microfin tube, where the results show that R1234yf has a frictional pressure drop value of 1.05 to 2.17 times greater than R454B and 1.06 to 1.32 times greater than 454C. A comparison between R454C and R454B shows that R454C is 1.01 to 1.64 times greater than R454B in the mass velocity range of 50 kg $m^{-2}s^{-1}$ to 300 kg $m^{-2}s^{-1}$. This phenomenon is caused by the thermo-physical difference between the three refrigerants.
4) (Goto et al., 2001) correlation majority underestimated with frictional pressure drop experimental data, especially in high mass velocity and well predicted in low mass velocity. For R454B, the average deviation (AD) and the mean absolute deviation (MD) is 31% and 32%, respectively. While, for R45C, AD and MD are 32% and 34%, respectively.
5) Frictional pressure drop experimental data of R454B and R454C also compare with predicted data using the proposed correlation in chapter 3. The result is well predicted for all mass velocities and refrigerants, with the average deviation and mean absolute deviation for R454C being -3.3% and 9.5%, respectively, and 97.6% of data points are within 30%. While, for R454B, AD and MD is 12.6% and 16.3%, respectively, and 84.6% of data points predicted by the proposed correlation are within 30%.
6) The condensation's HTC increases with increased vapor quality and mass velocity.
7) HTC's R454B is slightly larger than R1234yf, increasing 1.1 to 1.5 times enhancement in all mass velocities from 50 to 200 $kgm^{-2}s^{-1}$. With a sizeable R32 composition of about 68.9% in R454B, HTC's increase is relatively small. The condition is because of the degradation of HTC due to mass transfer resistance due to the presence of a temperature glide of zeotropic mixture refrigerant.
8) HTC's R454C is lower than R1234yf for all mass velocities with 1.2 to 1.7 degradation from R1234yf. The Degradation of heat transfer coefficient from this zeotropic mixture refrigerant due to mass transfer resistance during the condensation process due to the presence of a temperature glide of zeotropic mixture refrigerant.

9) Condensation Heat transfer experimental data of R454B and R454C also compare with predicted data using the proposed correlation for pure refrigerant Fig 6.19 . The correlation majority is not well predicted for R454C and majority overestimated with average deviation (AD), and the mean absolute deviation (MD) is 74.19% and 74.19%, respectively and 6.52% of data point are within 30%. While, for R454B have similar trend with R454C with AD and MD is 41.79% and 41.80% and 21.62% of data point are within 30%. The condition is because the proposed correlation was developed using pure refrigerants. Therefore, it can be concluded that there is a degradation of this heat transfer coefficient compared to a pure refrigerant. This degradation is caused by the mass transfer resistance of the zeotropic refrigerant.
10) For boiling process, generally, the heat transfer coefficient increases slightly with vapor quality at low mass velocities, and no dry-out occurs. On the other hand, it rises with vapor quality at high mass velocities, reaches a peak, and then drops suddenly due to dry-out phenomena. For R454B, the highest heat transfer coefficient is obtained at a mass velocity of 200 kg m^2s^{-1} with a vapor quality of 0.86 with a value of 12 kW m^{-2} K^{-1}. And for R454C, the highest heat transfer coefficient is obtained at a mass velocity of 200 kg m2s-1 with a vapor quality of 0.86 with a value of 8.8 kW m^{-2} K^{-1}.
11) Nucleate boiling appears to dominate the phase-change process, the mass velocity effect is not as noticeable as the heat transfer coefficient remains constant at around 7 kW m^{-2} K^{-1} in low vapor quality region up to vapor quality of 0.35 for R454B and at around 4 kW m^{-2} K^{-1} in low vapor quality region up to vapor quality of 0.3 for R454C . However, in the region of high vapor quality, as the mass velocity increases, the heat transfer coefficient increases, meaning that two-phase forced convection plays a dominant role in the flow boiling mechanism. Two-phase forced convection is always present and dominant in the phase change process because the heat transfer coefficient becomes unstable as the mass velocity increases.
12) Two kind of heat flux for experimental condition is conducted in experiment to clarify the effect of heat flux for both R45CB and R454C. The heat transfer coefficient increased with increasing heat flux due to the enhancement of nucleate boiling in the low vapor quality region. The impact of heat flux are readily visible: nucleate boiling is the most crucial heat transfer mechanism.

7.2 Recommendation

1) Microfin tube with different specification geometry should be investigated to get the data to know the effect of helix angle, apex angle , fin height and number of fin.
2) It is better to visualize the flow pattern of the refrigerant inside the microfin tube
3) It is better to compare the experimental data by using simulation.
4) Development of two-phase heat transfer correlation of mixture refrigerant is necessary.